UNIVERSITY OF CAPE TOWN

COMPARATIVE ANALYSIS OF POLYMER ELECTROLYTE MEMBRANE (PEM) FUEL CELLS.

A Thesis

By

EMMANUEL O. BALOGUN

Department of Electrical Engineering

Submitted in fulfilment of the requirements

For the degree of

MASTER OF SCIENCE

(Electrical Engineering)

Supervised by: Prof. Paul Barendse *(Electrical Engineering)*

Co-Supervisor by: Dr. Jessica Chamier *(Chemical Engineering)*

August 2018

Declaration

This thesis is submitted to the Department of Electrical Engineering, University of Cape Town, in complete fulfilment of the requirements for the degree of Master of Science.

I know the meaning of plagiarism and declare that all the work in the document, save for that which is properly acknowledged, is my own. This thesis has been submitted to the Turnitin module (or equivalent similarity and originality checking software) and I confirm that my supervisor has seen my report and any concerns revealed by such have been resolved with my supervisor. Some part of this work have been submitted for publication in peer reviewed journals and at refereed international conferences

Emmanuel Balogun ..Signed by candidate

Date .....10/08/2018.....

Acknowledgements

Success is no accident. It is hardwork, perseverance, learning, studying, sacrifice and most of all, love of what you are doing or learning to do – ***Pele***

My unreserved gratitude goes to Almighty God who has guided me through the thick and thin of this journey. I have gotten this far by His grace, not of works, hence, I have no occasion for boasting in my abilities.

Special thanks to my supervisors Prof. Paul Barendse and Dr. Jessica Chamier for their guidance and leadership. Thank you for teaching me the importance of collaboration and joint effort. I am also very thankful to Mr. Nabeel Hussain and Mr. Francois Van Schalkwyk for their invaluable help and initiative.

To my dear friend, colleague and lab guide, Firdaus.Hendricks, thank you for believing in me and supporting me even when you have no reason to. Thank you for always being available, for the in-betweens that made the difficult times bearable. HySA Catalysis is lucky to have someone as dedicated and passionate like you in their team. To Tapiwa Chivengwa, words cannot describe how grateful I am for your support and guidance within and outside the lab. Your little words of wisdom are always on time to spur me on. I know you were the guardian angel God specifically sent to help me during the course of my lab work – your labour of love are never forgotten my brother.

Many thanks to the Mandela Rhodes Foundation for providing me with the scholarship that enable me fulfil the dream of obtaining an MSc degree. Thanks to my colleagues within the Advanced Machines and Energy Systems (AMES) Group who made the time spent enjoyable. Namely: Aroge Akindele, Olayiwola Olufemi, John Mushenya, Alao Olakunle, Omolola

Faloye, and Akionla Ajayi-Obe. Thank you all for your willingness to assist and also help have some fun.

To the woman who believed in me even when I doubted myself, my mum, Aderonke Unegbu, I say a big thank you. Thanks for the prayers and sacrifices, thanks for being my pillar of strength, thanks for understanding my not being always available and I am grateful for the unconditional love. This degree is especially dedicated to you. A big thanks to my friends and family members who always try to make things easier for me – you guys are the best!

Trust in the lord with all your heart and lean not on your own understanding; in all your ways submit to him, and he will make your paths straight. Prov 3:5-6

Abstract

Per-Fluoro-Sulphonic-Acid (PFSA) ionomers have been singled out as the preferable ionomers for use in Polymer Electrolyte Membrane Fuel Cells (PEMFC) owing to their extensive intrinsic chemical stability and super sulfonic acid strength which is core to the PEMFC proton conductivity. This thesis presents a deeper analysis into these PFSA ionomer membrane electrode assemblies (MEA), presenting an electrochemical-analytical comparative analysis of the two basic types, which are the Long-Side-Chain (LSC) Nafion® and the Short-Side-Chain (SSC) Aquivion® ionomer MEAs with emphasis on performance and durability. In particular, electrochemical circuit models and semi-empirical models were employed to enable distinguishable comparative analysis. Also, this thesis presents further probe into the effect of ionomer ink making processes, critically investigating the effect of the High Shear Dispersion (HSD) process on both the Nafion® and Aquivion® ionomer MEA.

The findings in this research provides a valuable insight into the performance and durability of PFSA ionomer MEAs under various application criteria. The effect of operating parameters and accelerated stress testing (AST) on the PFSA ionomers was determined using electrochemical impedance spectroscopy (EIS) and equivalent circuit model (ECM) analysis. The result of this study, shows that the ionomer ink making process for Nafion® and Aquivion® MEAs are not transferrable. Analysis of the PEMFC performance upon application of the high shear dispersion (HSD) process showed that Nafion® MEA had a 10.47% increase in voltage while the Aquivion® MEA had a 2.53% decrease in voltage at current density of 1.14 A/cm^2. Also, upon accelerated stress testing, the Nafion® showed a 10.49% increase in its voltage while the Aquivion® on the other hand had a 7.16% decrease in voltage at 0.66 A/cm^2. Thus indicating the HSD process enhances the performance of the Nafion® MEA and inhibits the performance of the Aquivion® MEA.

Table of Contents

List of Figures

List of Tables

Appendix

List of Symbols

a_a – Activity of anode

a_c – Activity of cathode

a_{H2O} – Activity of water

CPE – Constant phase element

D_b - Bolt nominal diameter

e^- - Electron

ε – Overall Efficiency

ε_v- Voltage efficiency

ε_f - Current efficiency

E_w - Working Electrode

E_r – Reference Electrode

E – Cell's Potential/ Voltage

F_{clamp} - Clamping force

F – Faraday's constant

ΔG – Gibbs free energy

i_o – Current density

k – Activity coefficient

K_b - Coefficient of friction.

L – Inductor

n – Number of electrons

η_s – Surface overpotential

q - Electronic charge

R - Universal gas constant

R_{corr} –Correlation co-efficient

T – Temperature

T_t - Applied Torque

T_o - Reference temperature

V_{ocv} – Open Circuit Voltage

V – Overall Cell Voltage

V_{rev} – Reversible Cell Voltage

V_{irev} – Irreversible Cell Voltage

V_{ohmic} - Voltage loss due to ohmic polarization

$V_{activation}$ - Voltage loss due to activation polarization

$V_{concentration}$ - Voltage loss due to concentration polarization

W – Warburg Impedance

W_e – Work done

W_{el} - Electrical Energy

1. INTRODUCTION

1.1 Background

The 21st century has propelled us into a world of tremendous technology advancement. However this modern world has created an insatiable demand for energy which is needed to drive growth and development. Current realities has shown that we now live in an extremely energy hungry world, one in which the quality of life is now directly dependent on amount of energy consumed. Research has shown that for a quality life, the energy consumption on a yearly basis should be about 9,000 kWh per capita [1]. This value equals the energy contained in about 1,000 litres of crude oil. Using less energy per year makes life more laborious, however above this limit, life quality is in essence independent of the energy consumption. For a good quality of life according to current standards in industrialised nations, a minimum yearly energy requirement of 10,000 kWh seems therefore to be a realistic assumption [1].

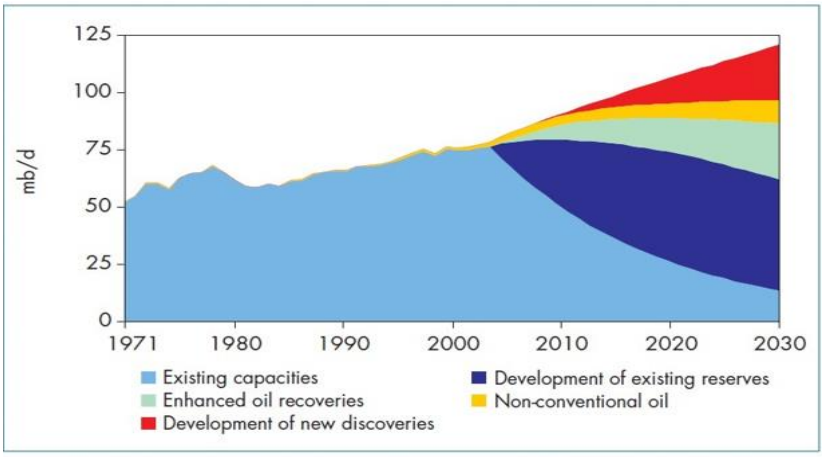

Figure 1.1: Oil production forecast according to WEO [2].

Almost all the energy demand of the modern world is being currently met by fossil fuels. Unfortunately, fossil fuels are also the primary culprit behind climate change. Fossil fuels are to blame for more than 80% of greenhouse gas emissions — and 98% of CO_2 emissions alone

[2]. While natural processes can absorb some of this CO_2, an estimated 4.1 billion metric tons of CO_2 is added to our atmosphere each year. Apart from the environmental concerns, there is also the challenge of sustainability, a report published by World Energy Outlook (WEO) confirmed that the crude oil production from currently producing fields have already reached their peaks in 2008 and is now depleting as shown in Figure 1.1 [2, 3].

For us to have a decarbonized and sustainable energy system, it is certain that we need to start looking beyond fossil fuels. Currently, effort is concentrated in finding and developing new fields on one hand and producing non-conventional oil on the other, in order to satisfy the continuously increasing world energy demand. As a mitigating technique, several new technologies have been developed to enhance generation, improve conversion of power and improve the efficiency of existing systems. Static generating systems which include wind turbines, solar panels, tidal generation systems, hydrogen fuel cells and super capacitors has been developed to replace fossil and nuclear based power stations. In addition to the development of static generating, small scale systems for electrical generation have become an area of interest, particularly the aspect of electrical generation, conversion and storage in transport applications. All these technologies have advantages and disadvantages, depending on the region and on the environmental conditions [4].

Efficient design and implementation of fuel cell technology has proven in recent times to be a great advantage in the portable, transportation and stationary sectors. Potentially, fuel cells could be a very suitable power source for remote places where electrical sources are unavailable. Vehicular transport systems are currently implementing fuel cells as viable power source to run cars, buses and other vehicular means of transportation [5]. Fuel cells show some strengths - comparing with the direct competitors such as easy recharging, compactness, low noise, easily scalable, and also able to produce different amounts of power. On the other hand, fuel cells are also expected to handle efficiently the environmental issues associated with

transportation, it lessens pollution, and it can operate effectively and efficiently to almost 50% capacity. All that it is needed is a good supply of hydrogen [4, 6].

By mode of operation, a fuel cell is similar to a battery which contains chemicals that produce electricity as a power source. The difference is that; the fuel cell can go on as long as chemicals which produce electricity actively flows inside it, the battery on the other hand ends up useless or dead as soon as all of its power is consumed. Hydrogen and oxygen (air) are the basic fuel used, and as long as these two chemicals are continuously flowing into the fuel cell, it will be assured of a very long life expectancy. Furthermore, fuel cells have been shown to be more efficient than other competing technologies – fuel cell's efficiency is not limited by the Carnot cycle as experienced when using combustion engines. For instance a hydrogen fed polymer electrolyte membrane (PEM) fuel cell has a maximum possible efficiency of 83% when operating at 25 ºC [7].

However, despite the considerable advantages related with the use of fuel cells, they also show serious drawbacks. In contrast to other available technologies, the fuel cell technology is more expensive and this high cost is the barrier to its widespread application. Additional limitations of fuel cells are related to their durability, room temperature compatibility and ability to produce good performances right after starting or restarting after a resting period. Therefore, the use of the fuel cell technology is intimately related with the ability to develop technological solutions that minimizes or solve these drawbacks [6, 8].

1.2. Purpose of Investigation

Polymer Electrolyte Membrane Fuel Cell (PEMFC) has been regarded overtime as the most promising of all the various types of fuel cells to be the substitute energy source for both mobile and portable applications, hence considerable research has gone into the process of optimizing the different components of the PEMFC. The parts of the PEMFC are broadly divided into two

sections, first being the Membrane Electrode Assembly (MEA) consisting of the gas diffusion layers, catalyst layers and most importantly the polymer electrolyte membrane. The other is the hardware, which is basically made up of the gaskets and bipolar plates. Until recently, Nafion® ionomer which is a long-side chain (LSC) ionomer has been the only reliable ionomer for use in PEMFC MEAs, however, in recent times, there have been several breakthroughs in designing several other substitute ionomers, one of which is the short-side chain (SSC) ionomer, popularly called Aquivion®. There have been some studies on the comparison of the Nafion® and Aquivion® PFSA. Postnov et al. [9] described the behaviour of nanocomposites upon doping with Nafion® and Aquivion® ionomers. They found that doping with Aquivion® results in an increase in proton conductivity of hybrid membranes with low relative humidity. Buto et al. [10] carried out a comparative study of composite based on Nafion® and Aquivion® Membrane as actuators, they observed that SSC Aquivion -IPMC provides larger force than LSC- Nafion-IPMC. Gebert et al. [11] and Arico et al. [12] had earlier investigated the performance of the Nafion® membrane in contrast to the Aquivion® membrane at a stack level under high temperature application above 100^{o}C. Following up on earlier works on high temperature fuel cells(HTFC 90–140 °C), Peron et al. [13] showed in their work that SSC ionomer MEAs performed better than the LSC ionomer MEAs in HTFC and at low RH (dry-20%) where there is no problem of flooding due to R.H and water management as observed in low temperature PEMFC. This hence serves as an indication that SSC Aquivion® ionomers during low RH operation, enhances water mobility, proton conductivity, and oxygen reduction reaction kinetics through self-humidification in HTFCs [13, 14].

This work serves to augment earlier research on the PFSA ionomers in the PEMFC space, by comparing the durability, performance, method and techniques of preparation of these ionomer types. The comparative analysis of the LSC Nafion® and SSC Aquivion® ionomer MEA performance and durability would be achieved by carrying out an accelerated stress test (AST)

using relative humidity (R.H) cycling and load cycling on the ionomers whereby they are analysed using Electrochemical Impedance Spectroscopy (EIS) and other analytical tools. EIS is a powerful tool that allows a deep in-situ kinetic analysis of catalytic phenomena as well as the separation of different processes contributing to overpotential and the polarization curves. These methods determine the trend of cell potential and of the output power density as a function of the current density.

Putting into consideration the difference in chemical structure and equivalent weight of both Nafion® and Aquivion® ionomers, this study hopes to investigate the effect of transferring existing Nafion® ionomer processing methods to the Aquivion® ionomer. Using the polarization curve and EIS as analytical tools, the impact of these preparation techniques on the performance and durability of the Nafion® and Aquivion® ionomers are analysed and quantified. Also, this thesis shall help in ascertaining the more durable and reliable ionomer type between the LSC Nafion® and SSC Aquivion® ionomers.

1.3. Aim and Objectives of this Thesis

The main objective of this thesis is to attain a comparative study of the Perfluorosulfonic acid (PFSA) LSC Nafion® and SSC Aquivion® ionomer MEAs in order to determine the better performing and more durable of the two for both portable and mobile applications. The specific objectives of this thesis include:

- A detailed literature survey on the polymer electrolyte membrane (PEM) fuel cell
- Optimization analysis of the PEMFC hardware and MEA components.
- Comparative study of the long side chain ionomer (Nafion®) and short side chain ionomer (Aquivion®) by critical evaluation of the degradation life cycle test of both ionomer MEAs.

- An analytical review of the various stages and techniques involved in the preparation of the PFSA ionomers, proposing afterwards, the best preparation technique for optimum performance of both LSC Nafion® and SSC Aquivion® ionomer.
- Polarization Curve and Electrochemical impedance spectroscopy (EIS) analysis to give detailed investigation of intrinsic activities within the cell to ascertain optimized condition and durability.

1.4. Scope of Work and Methodology

This research focuses on the application of the electrochemical impedance spectroscopy to characterize the PEMFC's MEA through detailed analysis of the long side chain (Nafion®) ionomer and the short side chain ionomer (Aquivion®) for practical application. The EIS system is interfaced with the PEMFC device under optimized hardware parameters for both tested ionomers. The different ionomers are allowed to degrade under the same conditions using an accelerated stress test based on cycling the relative humidity and applied current density. The EIS is then used to analyse the intrinsic occurrence within the PEMFC when using the Nafion® ionomer and Aquivion® ionomer MEA. The PEMFC cell is operated and controlled using an in-house FuelCon Elevator–C test station used for characterising fuel cells and the EIS signals are measured using the True-Data EIS device [15], the interface between both systems is through the Visual Basic software ran on the FuelCon Elevator–C test station which allows the condition to be controlled.

1.5. Outline of Thesis

Chapter 1: Introduces the topic by giving background to the study, identifies the purpose of investigation, followed by the objectives, scope of work and plan of development.

Chapter 2: Presents a literature survey of current PEMFC technology, and shows the knowledge gap this thesis hopes to address.

Chapter 3: Presents a detailed analysis of the optimized hardware and MEA conditions for efficient operation of the PEMFC.

Chapter 4: Comparative analysis and characterization of the long side chain (Nafion®) and short side chain (Aquivion®) ionomer MEAs using EIS as a diagnostic tool.

Chapter 5: MEA degradation –life cycle test of the Nafion® and Aquivion® ionomer using Accelerated Stress Test.

Chapter 6: Ionomer Preparation: Effect of High Shear Dispersion on Membrane Performance.

Chapter 7: Discusses major findings and observations.

Chapter 8: Presents the conclusions and recommendations for future work.

Chapter 1 and 2 introduces the concept under discussion with emphasis given to the theory behind the concept and set the background for subsequent chapters. Chapter 3 and 4 both speaks to the PEMFC parameters optimization and PFSA ionomer characterizations. Chapters 5 and 6 shows the effect of AST and by extension probes and compares the life cycle/ durability of the different PFSA ionomer MEAs under standard and revised ionomer preparation conditions. The major findings was presented in chapter 7 and chapter 8 states the conclusion and recommendation from the work done in this thesis.

1.6. Research Outputs

Parts of the work presented in this thesis were presented at refereed international conferences and submitted to peer reviewed journals.

Conference Publications:

1. E. Balogun, P. Barendse, J. Chamier, “Effect of Anode Stoichiometry and Back Pressure on the Performance of PEMFCs”, IEEE Power Africa, Cape Town 2018.

2. E. Balogun, P. Barendse, J. Chamier, "Effect of Anode and Cathode Relative Humidity Variance and Pressure Gradient on Polymer Electrolyte Membrane Fuel Cell (PEMFC) Performance", IEEE Energy Conversion Congress and Exposition (ECCE), Portland, OR. USA, 2018 (Accepted).

Journal and Transaction Publications:

1. E. Balogun, N. Hussain, J. Chamier , P. Barendse "Comparative analysis and characterization of LSC Nafion® and SSC Aquivion® ionomer MEA under AST using EIS-ECM" Journal of Power Sources 2018 (Submitted)

2. E. Balogun, N. Hussain, J. Chamier , P. Barendse "Effect of Catalyst Ink Mixing Techniques on LSC Nafion® and SSC Aquivion® ionomer MEA under AST using EIS-ECM" International Journal of Hydrogen Energy 2018 (In process of being submitted)

References

[1] Alan D. Pasternak (2000, Oct.), "Global Energy Futures and Human Development: A Framework for Analysis". Lawrence Livermore National Laboratory, U.S. Department of Energy

[2] DOE/EIA (2008), World Energy Outlook 2011. Available: https://www.nrc.gov/docs/

[3] Denis Bona, "Study on the key factors allowing the PEM fuel cell systems large commercialization: fuel cell degradation and components integration." Ph.D. dissertation, Applied Science and Technology Department, Politecnico di Torino, 2014

[4] C. S. Spiegel, "Designing & Building Fuel Cells" Mc Graw Hill, New York (2007)

[5] Larminie and A. Dicks, "Fuel Cell Systems Explained" J. Wiley & Sons (2003).

[6] R. O'Hyare, S. Cha, W. Colella and F. Prinz, "Fuel Cell Fundamentals" John Wiley & Sons, New York (2006)

[7] K. R. Cooper, V. Ramani, J. M. Fenton and H. R. Kunz, "Experimental Methods and Data Analysis for Polymer Electrolyte Fuel Cells, Scribner Associates" North Carolina (2005).

[8] Valter Bruno Reis e Silva, “Polymer Electrolyte Membrane Fuel Cells: Activation Analysis and Operating Conditions Optimization.” PhD. dissertation, Uni of Porto August 2009.

[9] V. N. Postnov, N. A. Mel’nikova*, G. A. Shul’meister, A. G. Novikov, I. V. Murin, and A. N. Zhukov “Nafion- and Aquivion-Based Nanocomposites Containing Detonation Nanodiamonds” Russian Journal of General Chemistry, 2017, Vol. 87, No. 11, pp. 2754–2755.

[10] B Luo, Z Chen “Comparative Experimental Study on Ionic Polymer Mental Composite based on Nafion and Aquivion Membrane as Actuators” IOP Conf. Series: Materials Science and Engineering 269 (2017).

[11] M. Gebert, A. Ghielmi, L. Merlo, M. Corasaniti, and V. Arcella “AQUIVION™ -- The short-side-chain and low-EW PFSA for next-generation PEFCs expands production and utilization” Solvay Solexis S.p.A., viale Lombardia 20, I-20021 Bollate (MI), Italy ECS Transactions, 26 (1) 279-283 (2010)

[12] A. S. Aricò*, A. Di Blasi, G. Brunaccini, F. Sergi, G. Dispenza, L. Andaloro, M. Ferraro, V. Antonucci, P. Asher, S. Buche, D. Fongalland, G. A. Hards, J. D. B. Sharman, A. Bayer, G. Heinz, N. Zandonà, R. Zuber, M. Gebert, M. Corasaniti, A. Ghielmi, D. J. Jones “High Temperature Operation of a Solid Polymer Electrolyte Fuel Cell Stack Based on a New Ionomer Membrane” WILEY-VCH Verlag GmbH & Co. KGaA, Weinheim 2010

[13] Peron, J.; Edwards, D.; Haldane, M.; Luo, X.; Zhang, Y.; Holdcroft, S.; Shi, Z. J. Power Sources 2011, 196, 179–181

[14] Park, Y.-C.; Kakinuma, K.; Uchida, H.; Watanabe, M. J. Power Sources 2015, 275, 384–391

[15] FuelCon True-Data EIS Impedance spectrum analyser for fuel cell device for fuel cell research and diagnostics – Operation Manual

2. Literature Review

2.0 Introduction

This chapter presents a literature survey on the Polymer Electrolyte Membrane Fuel Cell (PEMFC). The purpose of this section is to set the background for work presented in this thesis. The various types of fuel cells are discussed in brief and differences between them are identified. A detailed analysis of the PEMFC is then presented, its components and operating conditions are analysed as well as its process parameters. Furthermore, we highlight the ineluctability of PEMFC degradation with continuous use, finally this section is concluded with the discussion on PEMFC diagnostic techniques.

2.1 Understanding the Fuel Cell Technology

A fuel cell is an electrochemical device that directly converts the chemical energy embedded in a fuel into electrical energy. The fuel is often times an alcohol, hydrocarbon or any substance derivable from it, example is hydrogen, which can be supplied continuously. Fuel cells are made up of an anode site where electro-catalytic oxidation of the fuel takes place producing electrons and a cathode site where reduction of the oxygen occurs.

2.2 Development of Fuel Cell Technology

The idea of using electricity to break water was first explained by W. Nicholson and A. Carlisle in the 1800's, however it was W. R. Grove that has been widely credited to be the father of the "fuel cell". In 1839, while Grove was working on electrolysis of water using electrodes made of thin platinum foil immersed in dilute sulforic acid solution, he discovered that it may be possible to generate electricity by reversing the electrolysis of water. The term 'fuel cell' was coined by Mond and Langer in 1889. While working on the Grove's invention, they were able

to successfully translate the theory into a practical device, thus, leading to the birth of the first practical fuel cell that runs on air and coal gas. In 1896, W. Jacques suggested the possibility of a fuel cell powered train and identified the potential of fuel cells for household and marine applications. From the early 1930s, Bacon has researched fuel cells for potentials as energy storage devices. Francis Bacon successfully developed what was perhaps the first successful fuel cell device, building on the works of earlier researchers, with the aid of a hydrogen-oxygen cell using alkaline electrolytes and nickel electrodes - cheaper alternatives to the catalysts used by Mond and Langer. In 1939, Bacon and company first demonstrated a practical 5KW fuel cell system. Based on Bacon's development, United Technologies (UTC) produced fuel cells for Apollo Lunar Mission that served as power sources for on-board applications. As can be observed in Figure 2.1 showing the history of fuel cell, in early 1960s, General Electric (GE) started to work on fuel cells and developed the first fuel cell based on a proton-exchange membrane (PEM) [1-5].

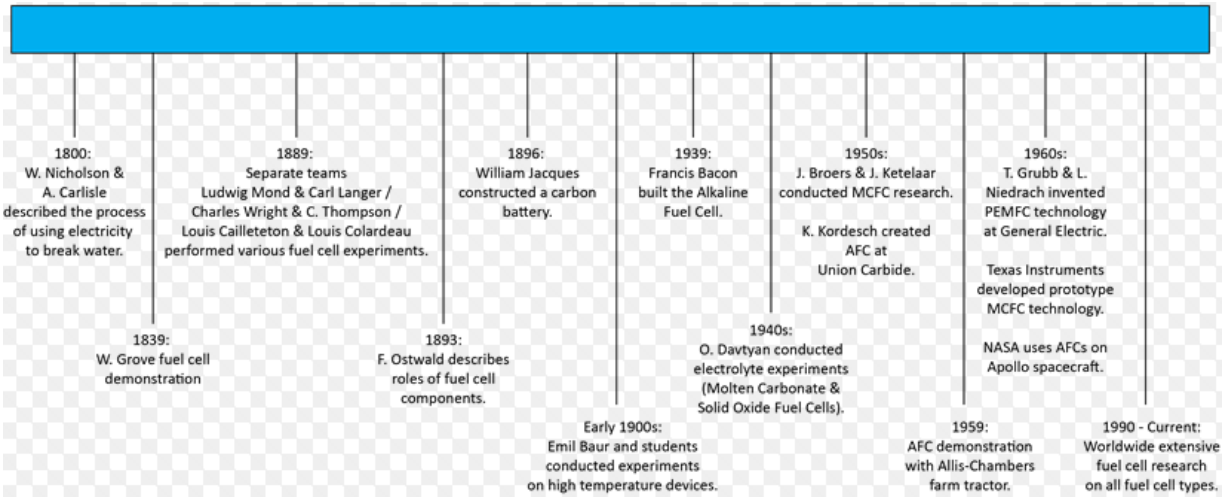

Figure 2.1 Historical view of fuel cell technology development [5].

Recent development in the fuel cell technology has afforded a number of manufacturers ranging from major auto makers to government establishment to play a leading role in supporting the research and development towards the development of fuel cell technology for

use in fuel cell vehicles (FCV) and other applications. The concentrated attention given to research and development (R&D) of the fuel cell technology has yielded quite meaningful results as the fuel cell technology is already adequately developed for commercialization but is limited due to cost and life expectancy of the technology. Of the diverse types of fuel cells, Polymer Electrolyte Membrane (PEM) Fuel Cells are considered the most promising energy converters especially for automobile applications.

The MEA, often tagged as the most important part of the Polymer Electrolyte Membrane Fuel Cell (PEMFC) is especially critical to the performance and life expectancy of the PEMFC. With over 80% of the fuel cell market, the PEMFC has been at the fore front of several investigative research projects and the MEA being the heart of the PEMFC has received primary attention. In order to ensure wider adaptation and ensure competitiveness with other related technologies, there is need to reduce the associated cost and ensure improved performance of the PEMFC. Optimizing the design and operation of the MEA is key to achieving this. Today, there are various types of ionomers for the MEA, but PFSA ionomer are commercially available, with the long side chain (LSC) PFSA ionomer, popularly referred to as Nafion® leading the pack, the other is the short-side chain (SSC) PFSA ionomer, also known as Aquivion®. Currently, there is a concentrated effort towards research and development activities which are majorly focused on addressing the challenges of improved conductivity, cost reduction, ease of manufacture, optimization for use in specific applications, operation under reduced or zero external humidification, high-temperature operation, and low fuel crossover [6]. The objectives of this thesis aligns with this global R&D trend with its focus on determining the most efficient and durable PFSA ionomer type for PEMFC applications.

2.3 Fuel cells and Batteries

Fuel cells and batteries are both electrochemical devices with very similar structure with each possessing a stack consisting of several elementary cells often connected in series. Each single cell is composed of an electrode-electrolyte-electrode assembly. Furthermore, both batteries and fuel cells undergo similar electrochemical processes of charging and discharging, hence it is not farfetched transferring some knowledge from one device into another. However, both batteries and fuel cells are completely distinct in terms of their constituent cells. Unlike batteries, fuel cells electrodes are often porous with gas transport. Also the operating conditions of both electrochemical cells are fundamentally different.

The electrochemical process in a battery is sort of a batch process and its storage energy is often limited by the active mass, whereas, the fuel cell needs a constant supply of reactants and removal of water for efficient performance. Also in the fuel cell, power production is separated from energy storage (energy storage is dependent on external gas storage), hence the performance characterization of both devices are different. In a battery, the performance is investigated by plotting the voltage against time whereas for the fuel cell, voltage is plotted against current density to give the polarization curve [6, 7].

Table 2.1: Comparing and contrasting Battery and Fuel Cell technologies [6].

	Function	**Output Current**	**Fuel**	**Advantages**	**Disadvantage**
Battery	Energy storage and conversion	DC	Stored Chemicals	High maturity rate	Low operational cycles
Fuel Cell	Energy Conversion	DC	Mostly pure Hydrogen	High Efficiency, reduced emission	High cost

Fuel cells have a faster refill rate and longer operating time compared to batteries, as doubling the operating time means only doubling the quantity of fuel and not the doubling of the capacity of the unit itself. Unlike batteries, fuel cells have no 'memory-effect' during their refuelling process, thus making them more efficient than batteries. PEMFC and DMFC have low heat transmission which makes them ideal for military applications. Higher temperature fuel cells produces high-grade process heat along with electricity making them well suited for cogeneration applications (such as combined heat and power for residential use) [8].

2.4 Types of Fuel Cells

Over the course of the 150 years of existence of the Fuel Cell technology, several types of fuel cells have been developed, each with its own advantages, limitations, and potential applications. These various types of fuel cells all obey the same electrochemical principle, however, they can be classified based on the type of electrolyte being used, system requirements, mode of operation and performance. Each of the classes of fuel cell operate on different temperature range, powered by different kinds of fuel, requires different kinds of catalyst and hence undergoes quite distinguished electro-chemical reactions. The most common types of fuel cells include:

2.4.1 Phosphoric Acid Fuel Cell (PAFC)

PAFC's belong to a class of fuel cell considered to be the "modernized" fuel-cells. Phosphoric acid fuel cells (PAFCs) use liquid phosphoric acid as an electrolyte. They are more tolerant of impurities, hence they can be fuelled by using reformed hydrogen. PAFCs operate at high temperatures between 190 - 200^{o}C, they are not easily corroded, and have low oxygen solubility [9]. PAFC's are often inhibited due to their large size. Because they are very bulky, they require a very high platinum catalyst loading compared to other fuel cells, hence making them considerably more expensive. PAFC have an energy generation efficiency 37%–42%

when used in a stand-alone mode, making them just a slightly more efficient than the conventional combustion-based power plants at 33% efficiency [10, 11].

2.4.2 Solid Oxide Fuel Cell (SOFC)

SOFC's are operated at very high temperatures of over 1,000°C (1,830°F). As a result of their high temperature, the electro-catalyst used in the SOFC is often ceramic instead of the very expensive precious-metal catalyst, thereby reducing cost and eliminates the possibility of flooding concerns. Also, their high temperature operation mode makes them more tolerant with impurities, making it possible to use internally reformed fuels, hence reducing the cost associated with adding a reformer to the system. However, on a stack level, there is an increased risk of contact loss due to its susceptible temperature changes thus creating a form of micro gap between the electrodes and adjacent contact layers [41]. The present challenge for developers is to produce robust, high-performance stack technologies based on suitable low-cost materials with similar expansion coefficient and fabrication methods. SOFCs have an efficiency of over 60% [11, 12].

2.4.3 Molten Carbonate Fuel Cell (MCFC)

MCFCs operate at high temperatures ranging between 600^{o}C and 700^{o}C. The electrolyte used at the anode and cathode is a molten carbonate salt mixture suspended in a porous, chemically inert ceramic lithium aluminium oxide ($LiAlO_2$) matrix. The absence of a precious metal catalyst makes them less expensive. Also, the MCFC's do not need an external reformer as it converts methane and other light hydrocarbons in natural gas and biogas to hydrogen within the fuel cell itself by a process called internal reforming. MCFC's are not susceptible to CO_2 poisoning. Therefore, the CO_2 produced at the anode in a MCFC can be utilized in a water-gas shift reaction as fuel. The major drawback of the MCFC is accelerated component breakdown and corrosion that occurs within the cell due to the presence of highly corrosive electrolyte and high temperature operation hence causing severe durability issues [12].

2.4.4 Alkaline Fuel Cell (AFC)

Alkaline fuel cells (AFCs) are typically low temperature fuel cells, operating at temperature values ranging from room temperature to as high as 70^{o}C. AFC uses a solution of potassium hydroxide (KOH) in water as the electrolyte and they have also been proven to use a variety of non-precious metals as catalyst at the anode and cathode. AFC's were one of the first fuel cell technologies developed and it was successfully deployed in the Apollo Space Program by NASA. It has an efficiency of over 60%. Several drawbacks have been associated with AFC, they include electrode poisoning, water removal issues and also tendency to form a by-product that would otherwise cause electrolyte dilution and reduce performance. There is also the challenge of formation of insoluble carbonates when operated in air as a result of presence of CO_2 which will end up affecting the reaction at the cathode [9].

2.4.5 Polymer Electrolyte Membrane Fuel Cell (PEMFC)

PEM fuel cells operate at relatively low temperatures, around 80°C (176°F). As a result of their low temperature, they have a very rapid start-up time and hence resulting in less wear on system components, therefore making them more durable. PEMFC relies on the use of a Platinum catalyst at both electrodes to facilitate the respective charge separation and reactions. The PEMFCs are not tolerant to impurities, and hence would be difficult to use hydrogen from reformer gas because the Platinum catalyst used at the electrodes are sensitive to CO poisoning. If for instance the hydrogen gas is obtained from a hydrocarbon fuel source, it is essential that an additional process be included to reduce the carbon monoxide present in the fuel gas. This increases the overall cost of the PEMFC. Of all the various types of fuel cells, PEMFC have been considered to possess the best viability for industrial application, especially in the auto industry.

2.4.6 Direct Methanol Fuel Cell (DMFC)

DMFCs share various similarities with the PEMFCs. Like PEMFC, the DMFC also uses a polymer electrolyte membrane. However, instead of hydrogen fuel, DMFCs are powered by pure methanol, which is usually mixed with water and fed directly to the fuel cell anode, this methanol dissociates into hydrogen protons, electrons and CO_2. The by-products of the electrochemical process are water and CO_2. The wide availability, ease of transportation as well as ability to be easily reformed from gasoline or biomass contributes to the reasons for using Methanol instead of hydrogen as fuel in the DMFC. [13]

Figure 2.2 and Tables 2.2-2.3 shows in summary, the various types of fuel cells and their distinguishing attributes, highlighting their strength, weaknesses and their historic or potential sector of application.

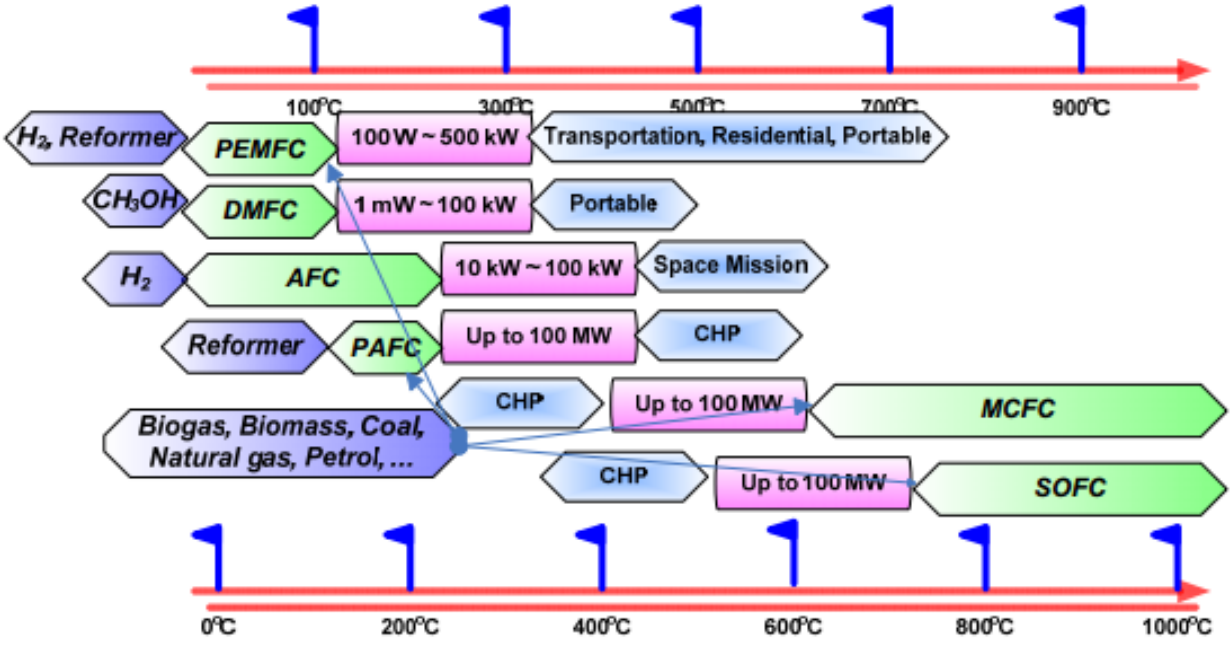

Figure 2.2 – Fuel cell comparison showing power, sources of energy and applications [13].

Table 2.2: Anodic (1) and Cathodic (2) reaction of the various fuel cell types [52].

AFC	(1) $H_2 + 2OH^- \rightarrow 2H_2O + 2e^-$	(2) $\frac{1}{2}O + HO + 2e^- \rightarrow 2OH^-$
MCFC	(1) $H_2 + CO_3^{2-} \rightarrow H_2O + CO_2 + 2e^-$	(2) $\frac{1}{2}O2 + CO_2 + 2e^- \rightarrow CO_3^{2-}$
DMFC	(1) $CH_3OH + H_2O \rightarrow CO_2 + 6H^+ + 6e^-$	(2) $\frac{3}{2}O2 + 6H + + 2e^- \rightarrow 3H2O$
PEMFC	(1) $H_2 \rightarrow 2H^+ + 2e^-$	(2) $\frac{1}{2}O2 + 2H + + 2e^- \rightarrow H2O$
PAFC	(1) $H_2 \rightarrow 2H^+ + 2e^-$	(2) $\frac{1}{2}O2 + 2H + + 2e \rightarrow H2O$

Table 2.3: Comparison of the five main types of fuel cells [10, 13, 14].

	PEMFC		PAFC	AFC	MCFC	SOFC
	DMFC	H_2 FC				
Operating Temperature (°C)	60 - 120	60 - 120	160 - 200	60 - 100	600 - 700	600 - 1000
Charge Carrier	H^+		H^+	OH^-	CO_3^{2-}	O^{2-}
Electrolyte	PEM		Liquid H_3PO_4 immobilized	Liquid KOH immobilized	Li_2CO_3/K_2CO_3 or Li_2CO_3/Na_2CO_3	Yttrium oxidedoped zirconia
Efficiency (%)	30 - 35	35 - 40	35-40	55-60	40-55	35-45
Application	Portable and Vehicles		Stationary (cogeneration)	Military and Spatial use	Stationary (cogeneration)	Stationary (Housing and cogeneration)
Catalyst	Pt and Ru	Pt	Pt	Pt	Ni	Perovskites (Ceramic)
Range	1 W - kW	50 W - 150 kW	25 kW - 250 kW	< 12 kW	10 kW - MW	200 kW - MW

2.5 PEM FUEL CELLS

This thesis is focused on the Polymer Electrolyte Membrane Fuel Cells (hereafter referred to as a PEMFC). PEMFCs are chosen as the core of this thesis over other forms of fuel cells because of their high energy conversion efficiency, zero emissions, and high-energy density at low operating temperatures, quick start-up, and system robustness.

The idea of PEMFC was first brought to practical use in 1960 when NASA used it for powering the Gemini Space program. However, the PEMFC was soon abandoned for Alkaline Fuel Cells due to the extreme water management difficulties, hydrogen storage and transport challenges, lack of performance, high cost, and insufficient lifetime that came with operating them. Despite the drawbacks encountered by the Gemini space program, PEMFC does have some interesting properties which stands out as a potential source of sustainable portable power supply especially in the automobile industry. Some of these properties include its low operating temperature, absence of harmful by-product, high energy efficiency, high power density and low start-up time. Over the past years, scientists as well as engineers mostly within the automobile industry have focused on developing and enhancing the performance of the PEMFC as well as reducing its cost through a variety of cutting edge research in order to aid its commercialization in the near future [15]. The PEMFC is divided into two sub-systems which includes:

- The Fuel Cell (Stack): A Fuel cell stack is composed of multiple single MEA cells connected in series.
- The control systems provides intelligence to the operation of the PEMFC and is essential to the proper functioning of the different components of the single cell or stack.

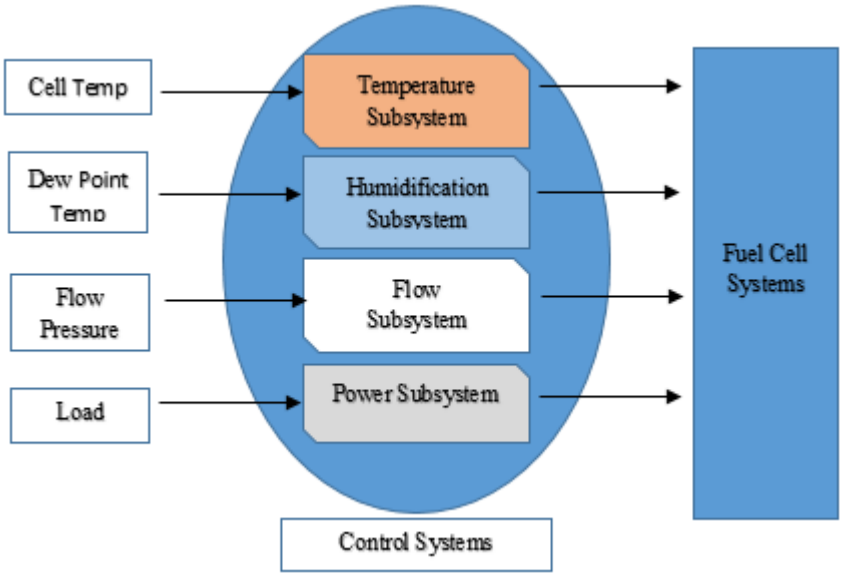

Figure 2.3: Fuel Cell Control System.

2.5.1 STRUCTURE OF PEMFC

The PEMFC structure is usually compact with all its components carefully aligned together. A single PEMFC unit is made up of bipolar current collector and an embedded graphite plate at either sides of its exterior. Moving inward, the next layer as shown in the Figure 2.4 is the Gas Diffusion Layer (GDL) which is also called the Porous Transport Layer (PTL). The GDL is isolated from the graphite plate by a gas gasket which serves as a seal at both sides of the cell.

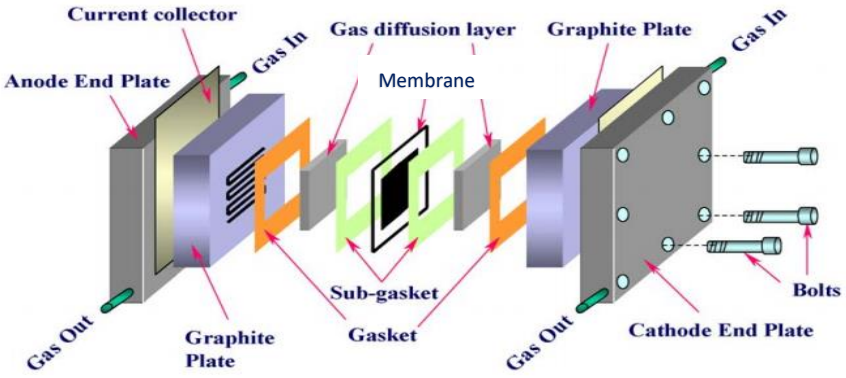

Figure 2.4: Schematics of the PEMFC.

At the core of the single PEMFC is the membrane. The membrane electrode assembly (MEA) comprises of the membrane, GDLs, catalyst layers and the gaskets. As depicted in Figure 2.4,

the different components are sealed with a gasket in order to prevent electron conduction within the cell and also ensure proper sealing.

2.5.2 GENERAL WORKING PRINCIPLE OF PEMFC

Typically, the PEMFC consists of five layers with characteristic functions, at the heart of the single cell PEMFC is the membrane electrolyte assembly (MEA) which is sandwiched between two gas diffusion layers (GDL) and two current collectors (one at either side of the electrodes) as depicted in Figure 2.4. A Fuel cell stack (combination of several single cells in series) has a bipolar plate housing each single cell and serving as a series connection between several single cells to produce a higher voltage value.

The PEMFC during operation follows the basic redox chemistry, with oxidation occurring at the anode and reduction reaction taking place at the cathode. At the anode, the hydrogen gas (H_2), the fuel, is oxidised to protons (H^+) liberating electrons upon coming in contact with the electrode in the MEA. The liberated electron transits through the external electric circuits where the current can be utilized while the protons flow through the MEA to the cathode side as depicted in the Figure 2.5. The MEA is made up of two thin porous electrodes (catalyst layers) housing a proton conducting membrane. This membrane allows the passage of protons (with water) through it to the cathode side and repels electrons and gases from passing through. At the cathode side, reduction of the oxygen (O_2) (or air) takes place as it recombines with the arriving protons and electrons from the anode side to form water (H_2O) in an exothermic reaction, releasing vast amount of heat.

As can be observed from Figure 2.5, water movement is essential to the operation of the PEMFC. The cathode and anode sub-system are connected to an external humidification system. The movement of water occurs in various ways through the system. Water is dragged by the protons while in transit through the MEA to the cathode side through a process of

electro-osmotic drag and the reverse process involves water moving from the cathode to the anode due to back diffusion occurring as a result of water concentration gradient existing because of the water generation at the cathode and the inlet humidified gas. For proper operation of the PEMFC there is a need to optimize every condition and pay close attention to the inter-relationship between the various processes that results in this movements.

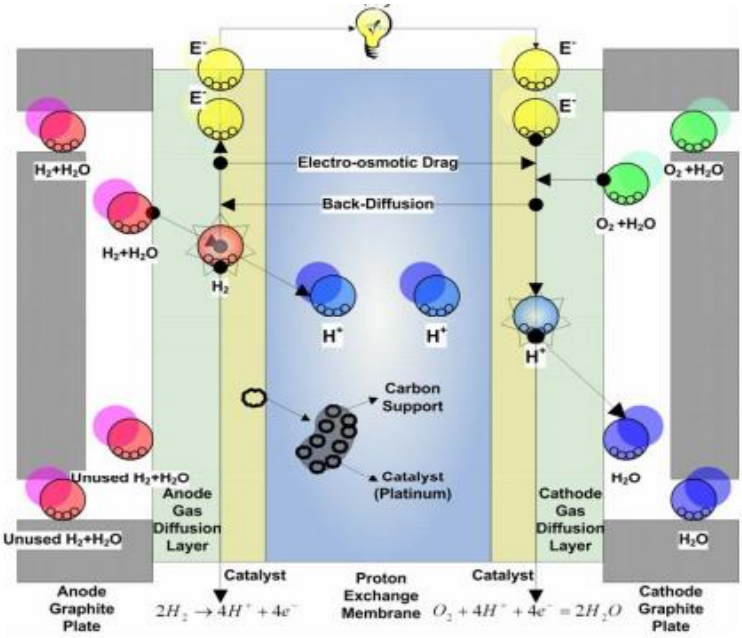

Figure 2.5: Basic operation principle of the PEMFC [16].

One cannot simply change a single parameter in a PEMFC, as a change in one parameter produces a chain effect resulting in a change in at least two other parameters, which may result in an unexpected outcome, hence the need for optimization [17].

Generally, fuel used for powering the fuel cell can be any chemical substance that has the ability to undergo chemical oxidation, have a negative Gibbs free energy for its underlying reaction and can be supplied continuously. Similarly, the oxidant can be any fluid that can easily undergo reduction. Hydrogen and air meet these conditions, but only in the PEMFCs design setup. The anode, negative electrode, is where the oxidation of hydrogen takes place, while the positive electrode, i.e. the cathode is where the reduction of oxygen occurs. The

electrochemical reaction i.e. the reduction and oxidation reaction at both sides of the membrane occurs simultaneously. The basics of the PEMFCs electrode reactions are itemized below [17]:

- Hydrogen, is fed to the anode where a catalyst separates hydrogen's negatively charged electrons from positively charged ions/protons,

$$H_2 \rightarrow 2H^+ + 2e^- \tag{2.1}$$

- At the cathode, oxygen combines with protons and electrons to form water,

$$^1/_2\, O_2 + 2H^+ + 2e^- \rightarrow H_2O \tag{2.2}$$

- Overall reaction at the anode and cathode,

$$H_2 + {}^1/_2\, O_2 \rightarrow H_2O_{(g)} \tag{2.3}$$

From the above equation, we realise that for every molecule of hydrogen, two electrons pass through the external circuit. Hence, for a mole of hydrogen, 2*N* electrons pass through the external circuit, where *N* is the Avogadro's number which is equal to 6.022 x 10^{23}. Therefore, taking the above into consideration, it can be inferred that for one mole of hydrogen consumed, the total charge of electrons, *q*, is given as:

$$q = -2Ne = 2F\ Coulombs \tag{2.4}$$

F = Faraday's constant = 9.6458 x 10^4 Coulombs, e^- = 1.602 x 10^{-19} Coulombs.

2.5.3 FUEL CELL ELECTROCHEMISTRY

The ideal potential (reversible potential) shows the potential difference or maximum obtainable electrical energy output across the terminal of the electrodes whenever a fuel cell is operated under reversible standard state thermodynamic conditions.

If *E*, represents the fuel cell's voltage, the work done by one mole of hydrogen in transferring charges through the cell is denoted by W_e (joules) as:

$$W_e = -2FE = -qE\ joules \tag{2.5}$$

The Gibbs free energy, ΔG of the overall reaction above is equivalent to the maximum electrical energy generated in a fuel cell, hence:

$$W_{el} = -\Delta G \tag{2.6}$$

From the above relation, the theoretical potential *E*, of the PEMFC can be calculated using,

$$E = \frac{-\Delta G}{nF} \tag{2.7}$$

n =2, the number of electrons

F = 96,485 Coulombs/electron-mole, Faraday's constant

Since ΔG, *n* and *F* are all known, the theoretical H_2/O_2 fuel cell potential is then calculated to be 1.23V at 25^{o}C and atmospheric pressure.

However, actual cell potentials of PEMFC are often lower than 1.23V, this is due to several reversible losses taking place during the operation of the PEMFC. On the average, single PEMFC operates at approximately 0.7V while at a current density of 1 A/cm^2, which is not useful for most real life applications. To increase the voltage in real-world applications, a fuel cell stack has to be built, which is a series connection of several single cells. The power in a fuel cell stack can be modified to fit any domestic/industrial use, by varying the number of single cells in it as well as the active area of the PEMFC.

Generally, an electrochemical reaction can be illustrated by the equation below:

$$uA + vB \leftrightarrow wC + xD \tag{2.8}$$

The equilibrium concentration is illustrated using the rate constant, hence the activity coefficient, *k*, for the reaction is represented by Equation (2.9) below:

$$k = \frac{[C]^w\,[D]^x}{[A]^u[B]^v} \tag{2.9}$$

Where *[A]*, *[B]*, *[C]* and *[D]* represents the concentration of *A, B, C* and *D* while *u, v, w*, and *x* are their activity coefficients respectively.

However, under non-standard conditions, there is need to apply a correction for activity, hence the Gibbs free energy of reaction for the reaction is thus:

$$\Delta G = \Delta G^o + RTInK \tag{2.10}$$

R = universal gas constant (8.314J/Kmol), and *T* = temperature (Kelvin)

From Equations (2.9) and (2.10) we obtain Equation (2.11) below which is also referred to as the Nernst Equation:

$$\Delta E = \Delta E^o - \frac{RT}{nF} In\, \frac{[C]^w\,[D]^x}{[A]^u[B]^v} \tag{2.11}$$

Butler –Volmer Equation

The Butler-Volmer Equation also known as Erdey-Grúz-Volmer Equation is used to illustrate one of the most fundamental relationships in electrochemical kinetics. It clearly shows the relationship between voltage and current in an electrochemical system such as fuel cell where there is no mass deposition at the electrode. Simply put, it provides insight into how the electrical current on an electrode depends on the electrode potential, the potential measured across the electrode junctions, and the composition adjacent to the electrode surface [18, 19], considering that both oxidation and reduction reaction occurring on the same electrode. The equation is given as:

$$i = i_o \left[exp\left(\frac{-\alpha_a F\eta_s}{RT}\right) - exp\left(\frac{-\alpha_c F\eta_s}{RT}\right)\right] \tag{2.12}$$

R is the rate constant, *T* is temperature and *F* is the Faraday's constant.

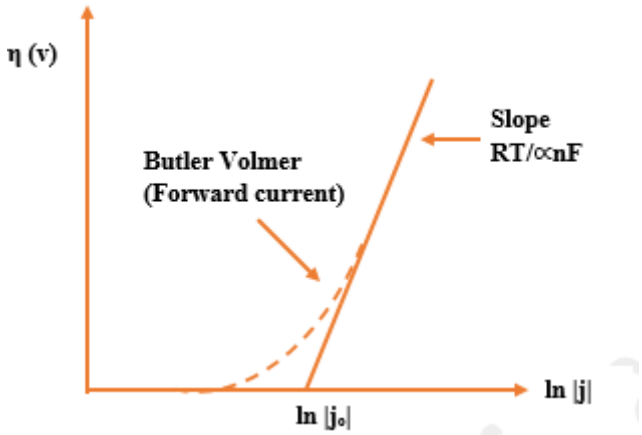

Figure 2.6: Exchange current density effect on chemical polarization.

Figure 2.6 shows an overview of the effect of the exchange current density on chemical overpolarization as predicted by the B-V Equation. The Surface overpotential η_s is the relative difference between the working electrode and a reference electrode, where E_r is the reference electrode and E_w is the working electrode

$$\eta_s = E_w - E_r \tag{2.13}$$

i_o Is the exchange current density (A/cm^2) and α_a and α_c represents the charge transfer coefficient at the anode and cathode respectively.

At low overpotential, the B-V Equation is reduced to:

$$i = i_o \left[exp\left(\frac{\alpha_a+\alpha_c)F\eta_s}{RT}\right)\right] \tag{2.14}$$

Similarly, at high overpotential values, the B-V Equations behaves like a straight lines and it is reduced to:

$$i = i_o \left[exp\left(\frac{\alpha_a F\eta_s}{RT}\right)\right] \tag{2.15}$$

This equation is known as the Tafel Equation.

2.6 FUEL CELL COMPONENTS

2.6.1 Gas Diffusion Layer (GDL):

Gas diffusion layers (GDLs) are usually made up of carbon. They may be in the form of a woven carbon fabric or a non-woven pressed carbon fibre paper configuration. GDLs serve as a distribution path for the reactant gases to the electrodes, providing the necessary electrical contact between the current collector plates and the electrodes. GDLs also play a crucial role in water management of the fuel cell, allowing the easy passage of water between the flow channels and the electrodes and allow water to also leave the surface of the electrode [20]. Typically GDLs also consist of a thinner microporous layer (MPL) which is interfaced with the adjacent catalyst layer to ensue electrical contact and adequate water transport. GDLs are treated with a hydrophobic material such as polytetrafluoroethylene (PTFE) which enables them to efficiently repel water from the membrane to avoid flooding.

2.6.2 Bipolar Plates (BP):

Bipolar plates are also referred to as flow-field plates. The common materials used for making the bipolar plates are graphite composite and metallic plates. This is because these materials meet the condition required for fuel cell applications which include corrosion resistant, electrical and heat conduction, strong enough to help in providing mechanical structure for the fuel cell and also cheap in order to cut down the cost of the fuel cell as a whole [21]. The BP connects several cells in series in the fuel cell stack to increase output voltage since a single PEMFC has between 0.6-0.9V.

2.6.3 Electrodes (Catalyst Layer)

The electrodes or the respective catalyst layers is where the electrochemical reaction occurs on the catalyst surface. The PEMFC electrode is typically a thin catalyst layer pressed between a porous electrically conductive substrate and the ionomer membrane. The electrodes are

generally described as porous structures containing a catalyst with high activity for the oxygen reduction reaction (ORR) at the cathode and hydrogen oxidation reaction (HOR) at the anode. The most common catalyst for the PEMFC's ORR and HOR is platinum [17]. Electrons, protons and gases all participate in the electrochemical reaction taking place on the electrodes, hence it is expedient that the reaction take place where all the three species have access too, which is termed the reaction zone on the catalyst layer. In order to increase the reaction zone, the catalyst particle size can be reduced or by roughening the surface of the membrane as well as by adding a catalyst support or fillers. The larger the catalyst's surface area, the faster the reaction takes place, hence it is important to ensure an increase in the catalyst surface area and not the weight of the catalyst, small platinum catalyst (< 4nm) are often finely dispersed with large surface area on the surface of a catalyst support which is typically carbon [20].

2.6.4 Membrane Layer

The membrane is the heart of the PEMFC. The PEMFC membrane must exhibit high proton conductivity, electron resistant, present a strong enough barrier to the mixture of fuel (gases) and reactant and must maintain high chemical and mechanical stability during the operation of the PEMFC [22].

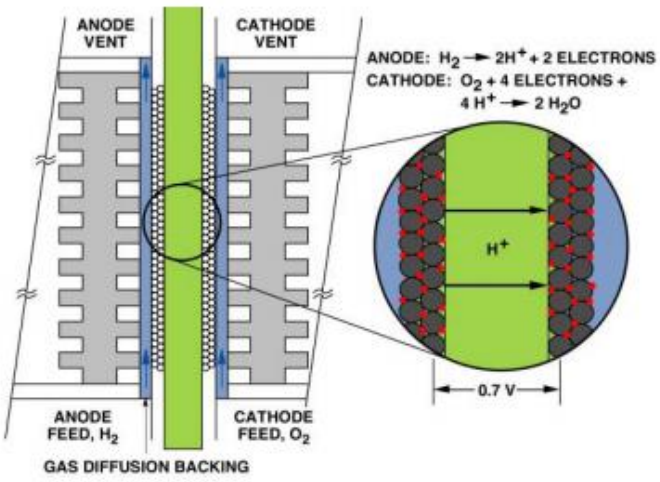

Figure 2.7 Pictorial view of the MEA in a PEMFC [22].

The membrane serves as a gate that allows protons to pass through in order to complete the overall reaction while repelling electrons, channelling these electrons to the external circuit. While PEMFC membranes are permeable to hydrogen anions, they must be impermeable to oxygen anions. [20, 23].

The PEMFC membrane layer consists of a polymer matrix. When the membrane layer is coated with the catalyst layers, it is infused between the gas diffusion layers (GDL), then it is referred to as the membrane electrode assembly (MEA). The membrane material for PEMFC are made of perfluorocarbonsulfonic acid ionomer (PFSA). A PFSA is a co-polymer of tetrafluoroethylene (TFE) and various perfluorsulforate membrane.

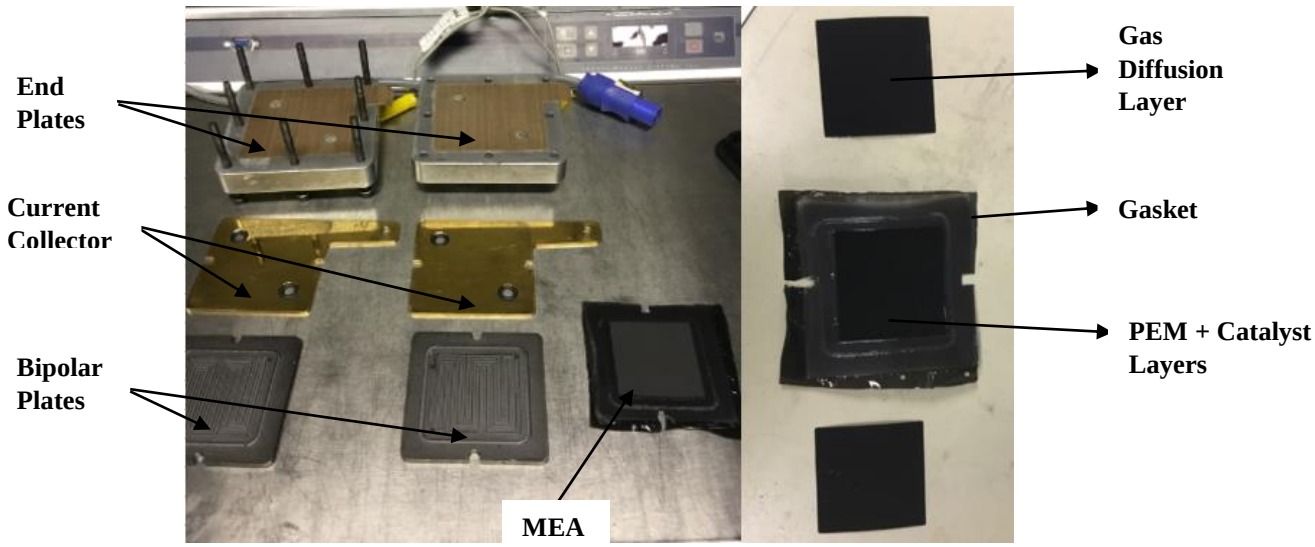

Figure 2.8: Fuel cell components.

2.6.5 Nafion® Ionomer

Dr. Walther Gustav of DuPont de Nemours discovered the sulfonated tetrafluorethylene copolymer which he called Nafion in mid-19th century. Nafion was the first of a class of perfluorinated ionomers which typically is a fully fluorinated polymer material terminated at points with ionic groups. Although, it was originally developed as a membrane material for the chloro-alkali process, it didn't take long before it was soon channelled into fuel cell application

for use as a membrane [43]. Presently, Nafion® membranes are the most commonly used membrane material having shown relatively enviable stability using a perfluorosulfonylflouride elthyl-propyl-vinyl ether (Nafion® membranes have a sulphonic group attached to a polymer backbone). Nafion® membranes must be well hydrated in order to allow proper proton conduction. The proper hydration of the membrane allows for easy movement of protons particle from one sulphonic group to the other until they eventually gets to the cathode side of the PEMFC where they complete the reaction.

The use of Nafion® also presents some challenges such as high cost, complicated chemistry and loss of conductivity at temperatures exceeding 95 ^{o}C [24]. Several advances has been made in this regard, such as the development of techniques to enable the reduction of membrane thickness, from several hundreds of microns to only few, hence giving rise to lower membrane resistance and improved hydration due to faster back-diffusion of water from the cathode to the anode. However, the thinning (size reduction) of the membrane has its own limitations which include but not limited to lower mechanical stability and high reactant cross over rate. Nafion® has an aliphatic perfluorinated backbone (which is essentially a PTFE) with ether-linked side chains ending in sulfonate cation exchange sites. It is a copolymer of tetrafluoroethylene and sulfonyl fluoride vinyl ether and has a semi-crystalline structure.

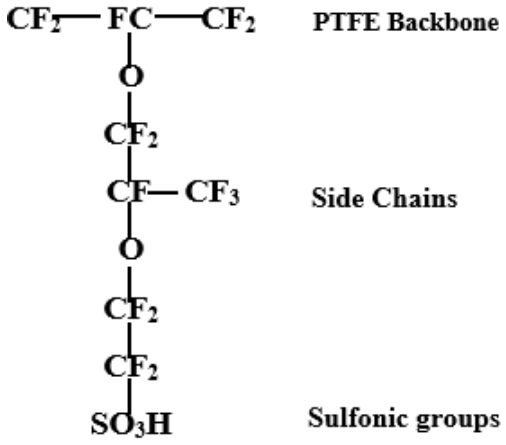

Figure 2.9: Polymer structure for long side chain (LSC) Nafion® ionomer.

This Teflon-like structure gives Nafion® its exceptional resistance to harsh chemical environments, good mechanical strength, and a fairly high maximum operating temperature, as well as its long term stability in oxidative or reductive conditions [44-45].

Nafion®, consists of three regions:

- The Teflon-like, fluorocarbon backbone, hundreds of repeating – CF_2 – CF – CF_2 – units in length,
- The side chains, –O– CF_2 – CF – O– CF_2 – CF_2 –, which connect the molecular backbone to the third region,
- The clusters of ion consisting of sulfonic acid ions, SO_3^- H^+.

The negative ions, SO_3^-, are static, being permanently attached to the side chain. However, upon absorption of water, the membrane becomes hydrated thereby causing the hydrogen ions to become mobile. The ion movement occurs as a result of the protons, bonded to water molecules, moving from one SO_3^- site to another within the membrane. Due to this mechanism, the solid hydrated polymer electrolyte is an excellent conductor of hydrogen ions [51].

Generally, the durability of the PEMFC is dependent particularly on the lifetime of the MEA. Although thinner membranes may have some good properties such as better performance efficiency and proton conductivity, there is the challenge of reduced physical strength as well as higher gas permeability, leading to a higher gas cross over rate which accelerates degradation of the membrane and ultimately the life span of the PEMFC reduces [46, 47].

The technology for solid polymer electrolyte membranes requires very thin films that is very stable electrochemically. This is a challenge with the present day Nafion® ionomer membranes, as membranes thinner than 50 microns, seldom work mechanically during fuel cell operation due to high porosity and increased fuel cross over rate. When approaching the

thin film limits, interfacial effects become significant to structure dynamics and consequently, the stability of the membranes [47].

2.6.6 Aquivion® Ionomer

Solvay Solexis designed a new kind of membrane that focuses on the incorporation of a short-side-chain ionomer in their membrane and dispersion products. This short side chain (SSC) membrane is popularly referred to Aquivion®. Aquivion® SSC ionomer membrane like its Nafion® counterpart is made through the use of a radical copolymerization of the sulfonyl fluoride vinyl ether (SFVE) monomer with the tetrafluoroethylene (TFE) in an aqueous media by using a fluorinated surfactant in emulsion conditions. By shortening the length of the polymer's side chains it was possible to design a membrane with higher mechanical stability of the polymer. Figure 2.10 shows a depiction of the Aquivion ionomer in contrast to the Nafion® ionomer.

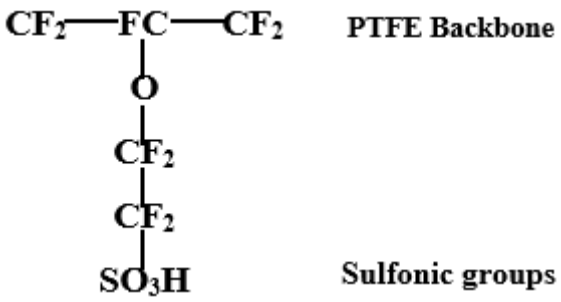

Figure 2.10 Polymer structure for short side chain Aquivion® PFSA ionomer [50].

With the aid of a Differential Scanning Calorimetry it was shown that there was an increased level of crystallinity for shorter pendant group chains when comparing equal equivalents weight (EW) or ion-exchange capacity (IEC), respectively [48, 49].

2.7 FUEL CELL STACK

Typically, the ideal voltage of a PEMFC is 1.23V, however due to losses within the cell which will be discussed in the following section, the open circuit voltage (OCV) is often between the range of 0.8 and 0.97V. This voltage is too small to power most portable and commercial

devices, hence several single cell units are connected or stacked together in series or in parallel in order to multiply its voltage. The conventional way is to connect the cells in series, in this case, the anode from one cell is connected to the cathode from another cell and the sequence is repeated throughout the cell. If peradventure the cells are needed to be connected in parallel based on application needs, then all the anodes are connected together and all the cathodes are also connected together.

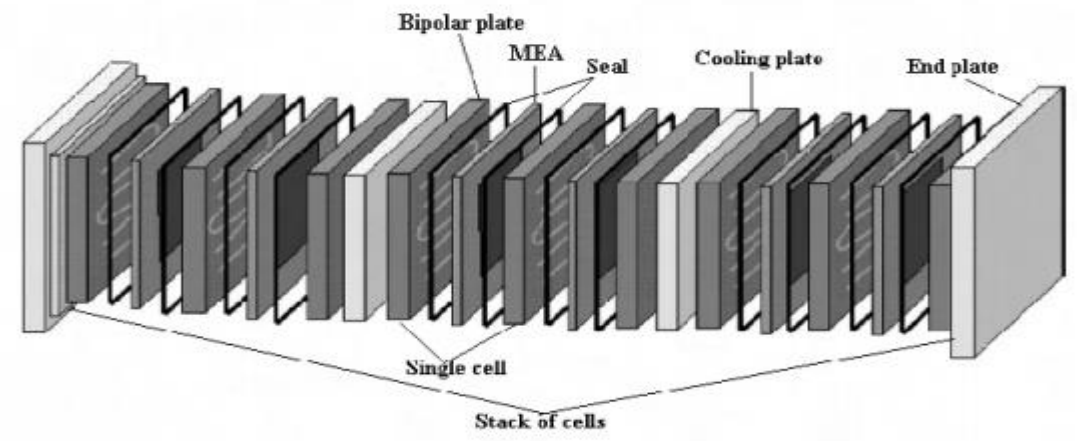

Figure 2.11: Fuel Cell Stack [53].

The goal here is also to increase the active area so as to increase the stack current, since the cell's current output is dependent on the active area. In a stack system, a single bipolar plate is used to electrically connect the different cell units, thereby the effect of electrical resistance is reduced as the distance the electrons needs to travel has been shortened.

2.8 FUEL CELL EFFICEINCY

The efficiency of any current producing device is defined as:

$$\varepsilon_f = \frac{theoretical\ amount\ of\ reactant\ required\ to\ produce\ a\ given\ current}{actual\ amount\ of\ reacant\ consumed} \tag{2.16}$$

The typical real life fuel cell is not 100% efficient as much is lost to irreversible losses experienced by the cell. The actual voltage is always less than the reversible cell potential. Voltage efficiency is given as:

$$\varepsilon_v = \frac{actual\ voltage}{reversible\ potential} = \frac{V}{E} \tag{2.17}$$

Overall energy efficiency is thus the product of the voltage and current efficiency.

$$\varepsilon = \varepsilon_v * \ \varepsilon_f \tag{2.18}$$

Typically, overall cell efficiency determined as a ratio of the output useful energy (electrical energy generated) and its input energy (enthalpy of hydrogen). If all the Gibbs free energy can be converted into electrical energy, using the hydrogen's higher heating value (ΔH_{HHV}) of 286.02 or the lower heating value (ΔH_{LHV}) of 241.98 possible efficiency of a fuel cell is given as:

$$\varepsilon = \frac{\Delta G}{\Delta H_{HHV}} = \frac{237.34}{286.02} = 83\% \quad \text{Or} \quad \varepsilon = \frac{\Delta G}{\Delta H_{LHV}} = \frac{237.34}{241.98} = 94.5\% \tag{2.19}$$

However, under working conditions, fuel cells only reach their highest output voltage under no load condition (open circuit) and with increasing current drawn, the voltage begins to drops. This is known as Polarization. The Polarization effect is due to losses, some of the losses in a working fuel cell include activation losses, ohmic losses, concentration losses, fuel crossover. These losses are further explained in subsequent sections.

2.9 PEMFC PROCESS PARAMETERS

The optimal performance of the PEMFC is dependent on the right alignment of several structural and process parameters. This section gives an overview of these parameters which will be further discussed in detail in subsequent chapters of this thesis.

Changing the PEMFC process parameters could possibly have either a beneficial or a negative effect on PEMFC performance and on the performance of other system components. Generally, to optimize the performance of the cell, there's a need for compromise in the operating parameters per application. However as an overview, the major process parameters including

temperature, pressure, humidity and stoichiometry ratio are introduced in this section. We can optimize the efficiency of the cell by defining necessary system specific requirements such as voltage, current, power requirement among others.

2.9.1 Temperature

Operating the PEMFC at a higher temperature produces an improved reaction rate due to improved mass transfer that is attainable at this higher temperature. An improved mass transfer rate means a corresponding reduction in cell resistance and an improved polarization curve, indicating better cell performance. PEMFC voltage increases with increasing operating temperature. However, caution needs to be taken when increasing the cell temperature due to system design limitations. The operating temperature should be chosen on par with the operating pressure with focus not just on optimizing cell performance but also on the cell limitations based on system requirements [25]. Cell temperature above 100^{o}C results in poor performing cell because the accumulated water at the cathode begin to evaporate, changing phase from liquid to gas. Operating beyond the boiling point of water results in steam which severely reduces the partial pressure of oxygen and also causes oxygen starvation hence resulting in a poorer performing cell. Typically the optimal cell operating temperature is often between 70^{o}C – 90^{o}C.

2.9.2 Relative Humidity

Humidification is essential to the operation of the PEMFC. Relative humidity is simply a measure of a gase ability to retain water at a certain pressure and temperature. With higher temperature comes higher water retention capabilities of a gas. A humidified hydrogen gas for instance gives rise to a humidified hydrogen ion – (humidified proton) as it passes through the membrane in its ion exchange reaction taking place within the PEMFC. Insufficient humidification causes mechanical stress to the cell as it forms cracks and holes in the membrane thereby causing an increase in the ionic resistance, formation of hot spots and chemical short

circuiting. This results ultimately in a poorer performing cell and in worst case scenario could lead to a fire outbreak as reactant gases mix together. Also, excess humidification leads to flooding of the cell and might also result in condensation of the gases, thereby reducing cell temperature and ultimately the cell performance. Too much or too little water can reduce the lifetime of the cell, hence there is a need for efficient water management to maximize cell performance.

2.9.3 Pressure

The electrochemical rate of reaction of a PEMFC is directly proportional to the partial pressure of the reactant gases – hydrogen and oxygen. The PEMFC can be operated both at ambient pressure as well as at higher pressure. Operating the cell at high pressure means a higher pressurizing force enacted on the reactant gases to bring them into contact with the electrolyte, thus there is an improved cell performance as a result of higher pressure of reactant gases. However, with higher reactant pressure comes the challenge of higher compression of the reactant gases and could possibly result in gas leakage or rapturing of the membrane. Hence, there is a need to strike an optimal balance in determining the reactant pressure to optimize the PEMFC performance.

2.9.4 Stoichiometry Ratio

The stoichiometry ratio relates the amount of available gas to the needed gas to complete the reaction.

$$Stoichiometry\ ratio = \frac{Amount\ of\ gas\ present}{Amount\ of\ gas\ needed} \qquad 2.20$$

A stoichiometry ration of 1.0 means that the exact amount of gas needed to complete the reaction is present. Below this ratio, means insufficient gas available and above this ratio means excessive gas is available than needed for the reaction. A higher stoichiometry ratio increases the performance of the cell, as it means that there is an increased chance of the reactant gases-

hydrogen and oxygen interacting with the electrolyte [26]. Optimizing the stoichiometry ratio is important, because having too much gas at the anode or the cathode might result in mass transfer effect, and not having enough might leads to fuel starvation which both result in performance loss of the PEMFC.

2.10 DEGRADATION PROCESS

PEMFC degradation is defined as an irreversible process wherein one or more characteristics of the cell diminishes with either time, continuous usage or external factors adversely affecting cell performance. During the lifetime of the PEMFC, some components of the cell gets worn, oxidised or degraded with time. With this ageing phenomenon comes a reduction in performance of the cell. An easy way to investigate this reduction in performance is by studying the power delivered to the cell at constant load, whereby it would reduce with time rather than remain constant. This thesis uses an accelerated stress test on various parts of the MEA to replicate this effect.

2.10.1 Degradation of the Bipolar Plates:

On the bipolar plate, three main types of degradation are often evident, including [27-29]:

- Corrosion of the plates leading to the production of multivalent cations that has an adverse effect on the durability of the catalyst layer as well as the membrane.
- Presence of a resistive surface layer which may eventually lead to a higher ohmic resistance.
- Deformation or fracture of the plates as a result of thermal cycles, non-uniform currents or uneven heat distribution.

2.10.2 Degradation of GDL

The GDL is a very important component of the PEMFC, hence its degradation leads to a drastic drop in the performance of the cell. Three degradation mechanism are observed in the GDL, they include:

- Loss of hydrophobicity
- Carbon corrosion and changes
- Changes in electrical and thermal resistance.

Even though each of the three forms of degradation are equally harmful to the cell, it is however the loss of hydrophobicity that causes the most performance drop in the cell. When a cell loses its hydrophobicity, it is replaced with a hydrophilicity-which is the attraction of water and hence causes flooding of the GDL [30]. Excess water in the cell further causes the GDL to lose more of its hydrophobicity and further degrades the cell. It has been shown that gas diffusion within the cell reduces with increase in the hydrophilic pores [42].

2.10.3 Electrode Degradation

Degradation of the electrodes results in a loss of electrochemical active surface area (ECSA) which leads to diminishing of the electrochemical activity of the cell. Electrode degradation is divided into two categories, which include [31]:

- **The catalyst layer degradation**
    I. The platinum (Pt) catalyst layer has small Pt particles which dissolves and diffuses with the ionomer where they are deposited on other particles forming a bigger particle, this phenomenon is known as Ostward ripening. The bigger particles formed can end up forming a barrier, blocking the hydrogen cross over from the anode to the cathode, hence causing a drastic decrease in membrane conductivity and stability.

II. Agglomeration – (coming together) of Pt particles in the cell leads to formation of dioxides and also causes the corrosion of the carbon support and hence reduction of the active area for reaction to take place, and thus reduces the cell performance

III. Contaminants can be transported into the cell by the reactants, and some of these contaminants are very harmful to the cell, for instance, the presence of CO is very detrimental to the Pt catalyst.

- **The carbon support degradation**

I. Transmitting between start–up and shut-down cycle causes an uneven distribution of fuel on the anode and also leads to oxygen cross over through the membrane. This affects the C-support as the oxygen that crossed over can react with the carbon support and form CO_2, hence reducing the carbon support.

II. Fuel starvation is as a result of blockage of fuel (H_2) from a portion of the anode under steady state operating condition. Thus, there is not enough hydrogen to maintain the demand current.

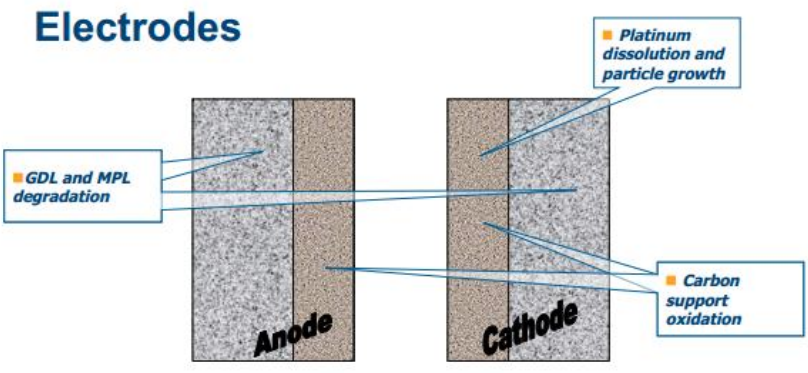

Figure 2.12: Degradation Process at the Electrodes [31].

Electrode degradation do not affect both electrodes (anode and cathode) equally. The anode for instance is almost totally unaffected by the dissolution, oxidation and agglomeration of Pt regardless of the conditions whereas the cathode is most affected as a result of these conditions. Potential cycling, the number of cell cycles, cell temperature and humidification levels are the most important factors when considering cathode degradation.

2.10.4 Membrane Degradation

The membrane is the heart of the PEMFC – therefore any hindrance to its proper functioning is definitely a point of concern. Degradation processes in the membrane can be divided into three main sections which include [32]:

- **Chemical/Electrochemical degradation**: This is often due to direct attacks of the polymer by radical species such as cationic ions, air pollutants and fuel impurities thus leading to the decomposition of the membrane. The chemical degradation is characterized by membrane thickness reduction (membrane thinning) and the emission of CO_2, HF and H_2SO_4 in the output product. Reduction of the membrane thickness result in increased gas crossover rate as well as weakness and fatigue of the membrane. The chemical degradation can be quantified by monitoring the hydrogen crossover rate and measuring the HF particles at the output product [32].

  The main causes of chemical membrane degradation are the presence of radicals and hydrogen peroxides in the cell. When the H_2O_2 is decomposed to its constituent 'OOH' and 'OH' radicals, they have a detrimental effect on the membrane.

- **Mechanical Degradation:** Cracks, pin-hole formation, thinning and membrane elongation are all products of mechanical stress or strain on the membrane due to repeated swelling and shrinking of the membrane with temperature and water absorption and adsorption. The absence of water in the membrane on the other hand makes the membrane brittle and fragile. Electrical condition such as current flow inside

the membrane can cause local hotspots to be created in the membrane and this can lead to the membrane malting. Mechanical degradation is often the early life failure of the membrane, and most times it is non-reversible.

- **Thermal Degradation:** This is obviously as a result of operating the PEMFC at higher than normal operating temperatures. Heating the membrane at temperature above 95^{o}C reduces the conductivity of the membrane and operating the cell below freezing point results in the formation of ice which is destructive to the membrane.

  Often times, when operating the cell at standard operation conditions, the effect of thermal membrane degradation can be neglected.

Other types of degradation that affects the PEMFC life time includes:

- **Membrane shortening**: This occurs as a result of ohmic shortening by electrons which passes through the membrane instead of passing through the external power device. These electrons passes directly from the anode through the membrane to the cathode, thus reducing the cell performance and also leads to the formation of local heated site within the membrane which are very difficult to detect.

Figure 2.13 shows the degree of criticality of the PEMFC components degradation from left to right, with the membrane degradation having the most critical effect on the PEMFC performance and durability and the gasket at the extreme left having the least effect.

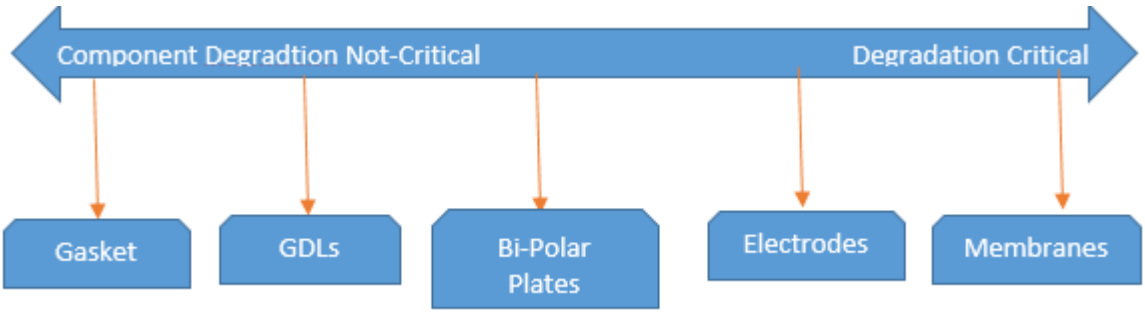

Figure 2.13: Degree of criticality of PEMFC component degradation

2.11 POLARIZATION CURVE

As earlier mentioned, the PEMFC during real life operation experiences several irreversible losses and hence the voltage does not equal its theoretical maximum value. There are numerous reasons for the performance drop of the fuel cell during active operation, they include reactant crossover through the membrane, internal electrical and ionic resistance, kinetics of the electrochemical reactions (activation polarization), and mass transport limitation due to difficulties in getting the reactants to the reaction sites [17]. The polarization curve is the most important characteristic of the fuel cell, it is a pictorial representation of the performance of the fuel cell during operation plotting the relationship between the potential and the current density of the cell. The polarization curve serves as an important analytical tool for troubleshooting issues within the fuel cell. It also has the ability to display hysteresis by increasing and decreasing the current. The polarization curve efficiently indicates a change in fuel cell conditions, such as drying or flooding of the membrane. As discussed in Section 2.5.2, inefficient water management could either lead to drying or flooding of the membrane, conditions that lead to decrease in cell performance and reduces reactant diffusion. Although, the polarization curve is a good diagnostic tool in detecting fuel cell flooding and drying, as it is sensitive to both effect, however, it can only detect these faults, it cannot distinguish between the two faults since both drying and flooding results in voltage drop. Polarization curve is also a very intrusive method, making it non suitable for on-line applications.

The polarization curve is dependent on design (hardware) conditions such as flow field design, catalyst layer structure, membrane thickness and state of hydration. Operational conditions such as temperature, flow rates, reactant gases concentration, pressure and humidity also influences the performance and therefore polarization curve. A typical polarization curve consist of three important regions, namely – activation, ohmic and concentration polarization regions. Each of these contributes to the voltage loss happening in the cell during operation.

Figure 2.12 shows a typical proportion of these losses and the resulting polarization curve [17, 33]. Under no load condition or open circuit voltage (OCV), the fuel cell is not expected to generate any current, the cell potential should therefore be at or close its theoretical cell potential at normal cell operating conditions. However, as can be seen in the Figure 2.14, the OCV is lower than the theoretical cell potential, indicating that there are some losses in the fuel cell even at no load condition. Furthermore, upon application of a load, the cell potential drops further as a result of these unavoidable losses.

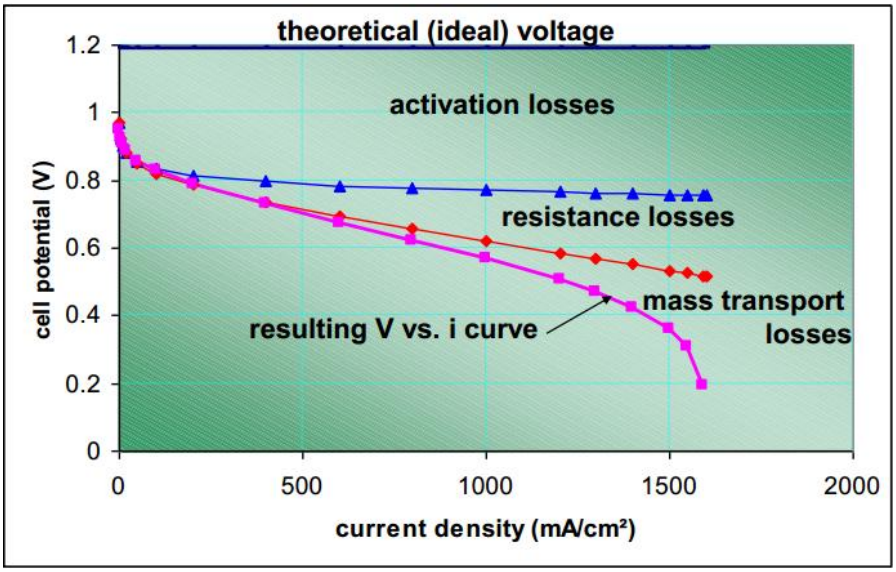

Figure 2.14: Polarization Curve [17].

Electrical energy is obtained from a fuel cell only when current is drawn, and the cell voltage drops due to several irreversible loss mechanisms. The loss is defined as the change in the cell potential (V_{irrev}) from the theoretical potential (V_{rev}) [34]:

$$V_{(i)} = V_{rev} - V_{irrev} \tag{2.21}$$

The open circuit voltage, which is the reversible voltage of the cell is quite lower than the theoretical voltage. This difference is due to internal currents and specie cross over from one electrode to the other through the membrane. The voltage of the fuel cell is the summation of the effect of these losses on the overall cell voltage, *V*, as shown in equation (2.22).

$$V = V_{ocv} - V_{activation} - V_{concentration} - V_{ohmic} \quad (2.22)$$

$$V_{(i)} = V_{rev} - v_{act_{anode}} - v_{act_{cathode}} - v_{ohmic} - v_{conc_{anode}} - v_{conc\_cathode} \quad (2.23)$$

The fuel cell polarization curve, showing the relationship between the fuel cell potential and the current density is given by the equation below:

$$E = E_r - \frac{RT}{\alpha_c F} In\left(\frac{i}{i_{0,c}}\right) - \frac{RT}{\alpha_a F} In\left(\frac{i}{i_{0,a}}\right) - \frac{RT}{nF} In\left(\frac{i_{L,c}}{i_{L,c}-i}\right) - \frac{RT}{nF} In\left(\frac{i_{L,a}}{i_{L,a}-i}\right) - iR_i \quad (2.24)$$

In simpler terms, Equation 2.22 can be written as:

$$E = E_r - \frac{RT}{\alpha F} In\left(\frac{i+ i_{loss}}{i_0}\right) - \frac{RT}{nF} In\left(\frac{i_L}{i_L-i}\right) - iR_i \quad (2.25)$$

Where V_{ocv} is the open circuit voltage of the cell, $V_{activation}$ is the voltage loss due to activation polarization, V_{ohmic} is the voltage loss due to ohmic polarization and $V_{concentration}$ is the voltage loss due to concentration polarization.

2.11.1Activation Polarization:

The main causes of drop in potential especially at the cathode for low and medium temperature fuel cells are activation losses. Activation polarization is the voltage overpotential needed to overcome the activation energy due to the electrochemical reaction on the catalytic surface. Activation losses occur as a result of increase in energy required to drive the electrochemical reaction at the anode and cathode of the PEMFC, as a result of slow reaction rates. It is dominant at lower current and gives a direct measurement of how effective the catalyst is at a given temperature. During fuel cell operation, there is a deviation of the electrode potentials from their equilibrium values as electric current passes through both anode and cathode electrodes. The voltage drop due to activation polarisation is represented by the Tafel Equation as follows:

$$\eta_{act} = \frac{2.3\ RT}{\alpha nF} \log\left(\frac{i}{i_o}\right) \quad (2.26)$$

From equation (2.26), i_o, the exchange current density and i is the current density. We can also infer that a rise in temperature might result in an increase in the η_{act}, however, during practical operation of the fuel cell, it is observed that the determining factor for η_{act} is 'i_o'. The smaller the value of i_o, the greater the voltage drop; usually the value of i_o is smaller at the cathode relative to the anode for hydrogen fed fuel cells. The total voltage drop would be given by Equation (2.67) below

$$V_{drop} = b_{anode} \log\left(\frac{i}{i_{o,a}}\right) + b_{cathode} \log\left(\frac{i}{i_{o,c}}\right) \quad (2.27)$$

i_{oa} is anode exchange current density while i_{oc} cathode exchange current density. $b_{anode}/b_{cathode}$ anode and cathode Tafel constants, respectively.

Equation (2.27) is equivalent to equation (2.26). Hence, it is possible that either one or both electrodes is/are responsible for the activation polarisation. By increasing the value i_o, the activation polarization can be effectively reduced, hence emphasis is placed on increasing the exchange current, and this can be done by using the right kind of catalysts.

Another way to minimize the effect of activation polarization is by increasing the rate of reaction. This can be achieved by operating the cell at higher temperature, making use of effective and efficient catalysts, increasing catalyst's surface area, and increasing the amount of reactant or increasing the pressure.

2.11.2 Ohmic Polarization: Voltage Loss Due To Charge Transport

As indicated in earlier sections, the fuel cell consists of electrodes and electrolytes which offers resistance to the flow of electrons and ions (protons) respectively. Ohmic losses are observed at the mid-point of the polarization curve, where the internal resistance causes a drop in cell voltage. The ohmic losses occur due to the flow of electrons at cathodes and flow of ions through the electrolyte. These losses can be expressed by Ohm's law [17, 36]:

$$\Delta V_{ohm} = iR_{\Omega} \quad (2.28)$$

i = current density, Acm^{-2}, R_{Ω} = total ohmic resistance

The total ohmic resistance can be divided into three terms, as in equation (1.9), where Re^{-} is the electronic resistance, $RH^{+}_{,mem}$ is the protonic resistance in the membrane and $RH^{+}_{eff,ca}$ is the effective protonic resistance in the cathode electrode.

$$R_{\Omega} = Re^{-} + RH^{+}_{mem} + RH^{+}_{eff,\ ca} \quad (2.29)$$

To reduce ohmic losses, thinner membranes can be used for easier ionic movement and use of electrodes with high conductivities. However, in making the membrane thinner, one must consider the possibility of fuel crossover which occurs when the membrane is too thin, and thereby reducing the ability to provide support for the electrodes or causing the electrodes to become insulated from each other and thus prevent shortening.

2.11.3Concentration Losses (Mass Transport Losses)

The concentration losses are also known as mass transport losses. Mass transport losses emanates as a result of reactant concentration at the electrode's surface while the fuel is being consumed. At maximum current, the reactant concentration at the catalyst surface is practically zero, this is because the reactants are consumed as soon as they are supplied to the surface. In a fuel cell, under high load condition which indicates excess current is being drawn from the cell than normal, this leads to a very fast electrochemical reaction rate on the electrode surface, hence the mass transfer rate of the reactants becomes slower, making it unable to provide enough reactants to the electrode surface [17]. Thus, there is a drop in cell voltage as a result of the reduction of reactant presence on the electrode surface. The mass drop can be calculated by using Equation (2.30)

$$\Delta E_{mass\ transfer} = m\ exp(ni) \quad (2.30)$$

Where *m* and *n* are the mass transfer parameters simulated from the polarization curves.

2.11.4 Fuel Crossover and Internal Current Losses

It is not impossible to see some reactant gases (fuel) and some electrons diffusing through the supposedly impermeable polymer membrane. What happens when these hydrogen gasses diffuse through the membrane is that it carries along with it, its two constituent electrons, hence indicating that the fuel cross over and the internal current are essentially equivalent. The overall effect of this is that because the hydrogen diffuses through the membrane without splitting into its constituent electrons and protons, there will be shortage of electrons travelling through the external circuits. The effects of this loss is more drastic on the potential at open circuit voltage and at lower current densities. Hydrogen crossover is dependent on the permeability of the membrane, hydrogen concentration (partial pressure) and membrane thickness [35]. A PEMFC having an OCV below 0.9V may indicate hydrogen leak or internal electrical short.

To get the total electrical current in the PEMFC, we need to consider the effect of the internal current losses on the external (useful) losses also, hence:

$$i = i_{ext} + i_{loss} \tag{2.31}$$

Where i_{ext} is the external current and i_{loss} is the internal loss.

Hence, the approximate cell potential under load is:

$$E_{cell} = E_r - \frac{RT}{\alpha F} In\left(\frac{i_{ext} + i_{loss}}{i_0}\right) \tag{2.32}$$

At OCV conditions, where $i_{ext} = 0$, the cell voltage is still significantly lower than the reversible cell potential.

$$E_{cell,OCV} = E_r - \frac{RT}{\alpha F} In\left(\frac{i_{loss}}{i_0}\right) \tag{2.33}$$

Typical values of the OCV of PEMFC is typically below 1 due to the effect of these losses.

2.12 FUEL CELL DIAGNOSTICS

During the operational cycle of the fuel cell, there often arises need to probe the effect of several processes, materials and components on the overall performance of the cell. To do this, some diagnostics tools have been created to analyse and explore the effect of these processes and operational conditions on the cell performance. Several techniques have also been developed to investigate both the online and offline operational mode of the fuel cell. However, the off-line approaches are often expensive and results in downtime, hence its use is mostly limited to fuel cell design processes to diagnose anomalies in the developed fuel cell component. Fuel cell diagnostics monitors the performance of the fuel cell in order to make informed decisions in performing high level regulation during the fuel cell operation. This also enables fuel cell prognostics scheduling to enable effective prediction and prevention of faults before they occur.

The polarization curve as discussed in section 2.11 serves as a pointer into the performance of the fuel cell. It probes the cell performance before and after the application of a current disruption or voltage spike. The polarization curve shows that increase in current leads to a reduction in the PEMFC performance as a result of losses, some of which have been highlighted in section 2.11 of this thesis. To determine the cause of the loss in performance, various diagnostics techniques have been developed with each different from the other based on the amount of perturbation of the fuel cell during diagnostics as well as ability to distinguish between faults. These techniques include but are not limited to:

- Current Interrupt
- Voltage distribution
- Electrochemical Impedance Spectroscopy (EIS)

2.12.1 Current Interrupt

The current interrupt diagnostic method overcomes the biggest problems posed by the polarization curve which is the lengthy time required to conduct the test and over-invasiveness. In this method, the fuel cell's current is interrupted within the space of a few milliseconds and the cell resistance is quickly recorded in this short time. The measured resistance is then fitted to an equivalent circuit for the purpose of analysis. An advantage of this method over the polarization curve is that it has the ability to not just detect faults like flooding and drying, it also has the ability to clearly distinguish between these faults. The limitation however is that it requires very expensive and sophisticated equipment to carry out its high precision measurement.

2.12.2 Voltage Distribution

This diagnostic technique is often applied in stack level detection. It employs a series of statistical analysis to measure the voltage within the stack. The deviation of the voltage is then calculated and compared with existing threshold, if the deviation is outside this threshold, then a fault is detected. Just like the polarization curve, it is only effective in fault localization in the stack, it cannot not distinguish between faults such as drying and flooding. It is very straight forward and easy to apply, however it is quite intrusive and not efficient for on-line diagnostics.

2.12.3 Electrochemical Impedance Spectroscopy (EIS)

The EIS is an experimental diagnostic technique that is useful in detecting and quantifying different faults within the fuel cell. It is frequency dependent AC perturbation of a steady system with a predetermined frequency and amplitude of diagnosing faults in a fuel cell. The EIS involves practically sending an electrical stimulus through the fuel cell and then the response signal is analysed. This frequency dependent analysis of the system provides a more

in-depth analysis of various electrochemical processes taking place within the fuel cell than a polarization curve.

An equivalent circuit model (ECM) is used to extract meaningful information from the fuel cell by modelling the different regions of the fuel cell as an electrical circuit having ideal resistors (R), capacitors (C), and inductors (L). Specialised circuit element such as constant phase element (CPE) and Warburg element (Z_W) are used to model the anomalous behaviour of the cell as it deviate from ideal behaviour. The Warburg element represents the diffusion or mass transport impedances of the cell [38].

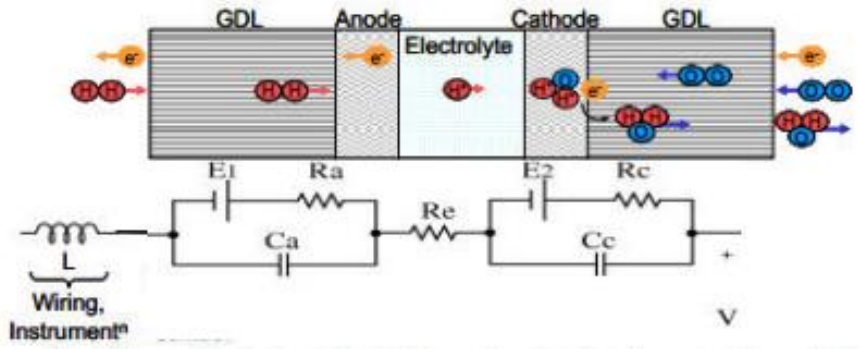

Figure 2.15: Equivalent Circuit Model of the PEMFC processes [38].

For a simplified equivalent circuit, shown in Figure 2.13, the properties of the electro de-material system are assumed to be time invariant, hence the response signal is employed to ascertain the degree of dependencies and interrelations among the system. For complex electrochemical systems such as the fuel cell, the electrochemical impedance spectroscopy is used to distinguish between different processes occurring at the same time, but on a different time-scale. The effect of faster processes, such as electronic, ionic conduction or the anode's hydrogen oxidation reaction (HOR) can be separated from slower processes like diffusion.

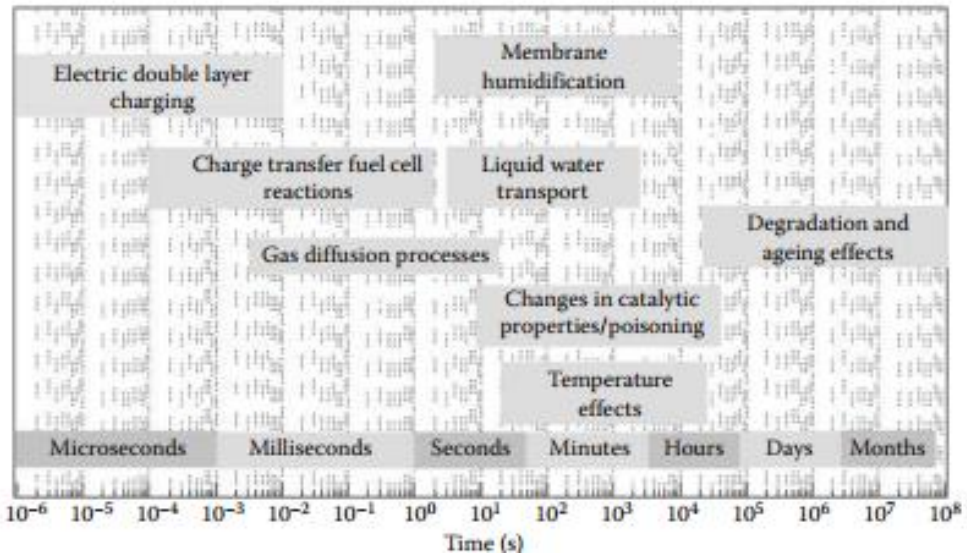

Figure 2.16: Timescale of Dynamic processes within Fuel Cells as measured with EIS [37].

From Figure 2.16, we get an overview of the diverse dynamic processes occurring during the operation of the fuel cell and its respective timescale. Typically, the range of frequency is often between 10 kHz and 0.1 Hz to put into consideration all time constant processes occurring in the fuel cell: at high frequencies within the kHz range, fast processes such as the hydrogen oxidation reaction, and ionic or electric conduction dominate the impedance data. The intermediate frequency band ranging several 100 Hz and about 1 Hz is predominantly influenced by the charge transfer of the ORR. The much slower processes occur below a frequency of 1 Hz, an example of such process is the diffusive mass transport effects [37].

EIS can be done either in the potentiostatic or galvanostatic modes. Operating the EIS in the potentiostatic mode involves the application of a sinusoidal potential and current measurement is done from which the cell impedance is computed and analysed. The reverse is done in the galvanostatic mode such that an AC current is applied to the sample across a current which is measured across the cell from which the cell impedance measurement is computed and analysed. When carrying out the EIS analysis in galvanostatic mode, an alternating current (AC) signal is sent through the cell at different frequencies ranging from a few kHz to a few

mHz and for each frequency the magnitude and phase of the resulting impedance signal measured. The activation polarization, electrolyte resistance, and mass transport polarization are determined from the interpretation of the data from response signal. The Bode plot and Nyquist plot are often used as diagrammatic representation of the data collected during EIS analysis. There are four very important regions on a Nyquist plot with each representing the different types of polarization losses that can occur in a fuel cell [39, 40].

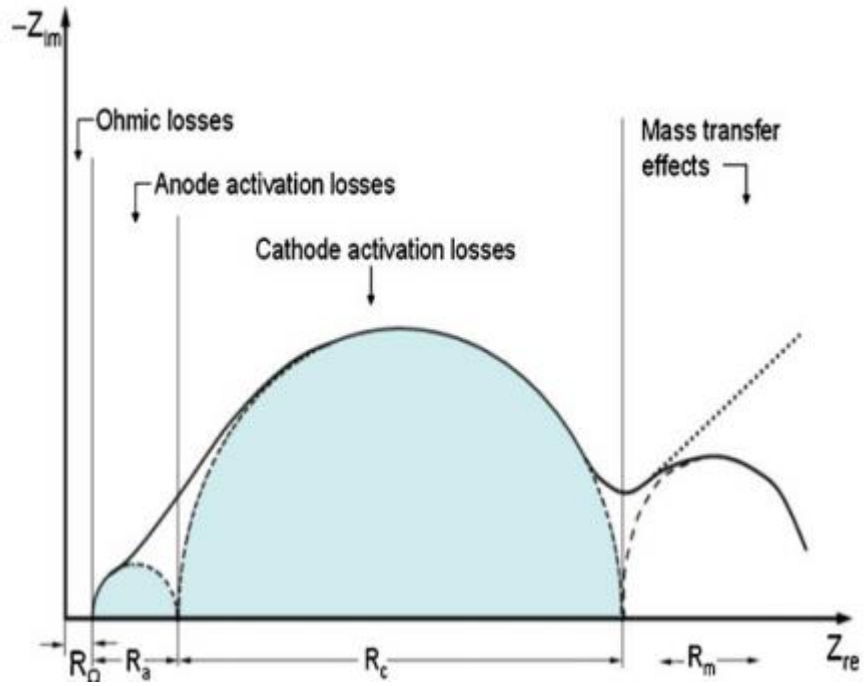

Figure 2.17: Nyquist plot of PEMFC [39].

As shown in Figure 2.17, typically a fuel cell's Nyquist plot is often consisting of two semi-circular regions which are indicative of activities at the anode and cathode, respectively. In a Nyquist plot, the frequency increases form left to right, with the semicircle on the left side corresponding to the high frequency spectra of a few hundred kHz thus correlating with activity in the anodic section of the cell and the right hand side corresponding to low frequency spectra of a few hundred mHz and correlates with activity in the cell's cathodic region [39].

EIS is a powerful diagnostic tool that is non-intrusive, hence making it suitable for on-line application. It also has the ability to differentiate between different fault conditions within the cell such as flooding and drying out of cells, hence making it more comprehensive compare to the polarization curve.

References

[1] Grove, W.R., "Voltaic Series and Combination of Gases by Platinum", London and Edinburg Philosophical Magazine and journal of Science, series 3, 14, 127-1300420, 1839.

[2] Nadal, M and F.Babir, "Development of a Hybrid Fuel Cell/Battery Powered Electric Vehicle", *Hydrogen energy Progress X, Vol.3 International Association of Hydrogen Energy, Coral Gables, FL,*, pp 1427-1440 1994.

[3] Chen, E., "Thermodynamics and Electrochemical Kinetics", Fuel Cell Tech handbook – CRC Press, Boca Raton, FL, 2003.

[4] Stone C. and A.E Morrison, From Curiosity to "Power to Change the World," Solid State Ionics, Vol 152-153, pp. 1-13, 2002.

[5] First Fuel cells http://autocar.ethiopianfestival.org/first-fuel-cell.html accessed 18/02/2018.

[6] O. Z. Sharaf and M. F. Orhan, "An overview of fuel cell technology: Fundamentals and applications," *Renewable and Sustainable Energy Reviews*, vol. 32, pp. 810–853, 2014

[7] S. Srinivasan, "Fuel cells: from fundamentals to applications". Springer Science & Business media, 2006.

[8] Fuel Cell Today: http://www.fuelcelltoday.com/about-fuel-cells/benefits accessed 18/02/2018

[9] Hammet A. "Fuel cells and their development." The Royal Society London, pages 653–699, 1996. 1.3.1.3, 1.3.1.4

[10] C. S. Spiegel, "Designing & Building Fuel Cells", Mc Graw Hill, New York (2007).

[11] Fuel Cell technology office https://energy.gov/eere/fuelcells/types-fuel-cells accessed 18/02/2018.

[12] US DOE. "Fuel cell handbook", National Energy Technology Laboratory, 2004.

[13] R. O'Hyare, S. Cha, W. Colella and F. Prinz, "Fuel Cell Fundamentals", John Wiley & Sons, New York (2006).

[14] Larminie,J.and A.Dicks, "Fuel Cell Systems Explained", 2nd ed –John Wiley 2003.

[15] FuelCell Today, "The fuel cell Industry review 2012", Available online: http://www.fuelcelltoday.com/analysis/industry-review/2012/the-industry-review-2012, accessed: 18/02/2018.

[16] Yong Hun Park, "Investigation of the performance and water transport of a polymer electrolyte membrane (PEM) fuel cell" Dissertation Texas A&M University 2007.

[17] F. Barbir, "PEM Fuel Cells Theory and Practice" Elsevier, 2005.

[18] Bard, A.J and L. R. Faulkner, "Electrochemical Methods" John Wiley & Sons, New York, 1980.

[19] John S. Newman. "Electrochemical systems" Prentice Hall International Series in the Physical and Chemical Engineering Sciences, pp. 186–188, 1991.

[20] Colleen Spiegel. "Designing and Building Fuel Cells". McGraw- Hill Professional, 2007.

[21] Borup RL, Vanderborgh NE. "Design and testing criteria for bipolar plate materials for PEM fuel cell applications". *Mat Res Soc Symp Proc* 1995; 393:151–5.

[22] Office of Fossil Energy United States Department of Energy. "Fuel cell handbook." National Energy Technology Laboratory, 2004.

[23] V. Metha and Joyce Smith Cooper. "Review and analysis of PEM fuel cell design". *Journal of Power Sources*, pp. 32–53, 2003.

[24] James Larminie and Andrew Dicks. "Fuel Cell Systems Explained" John Wiley & Sons Ltd, 2003.

[25] Jiujun Zhang "PEM Fuel Cell Electrocatalysts and Catalyst Layers Fundamentals and Applications" Springer 2008.

[26] Shikha Bhatta, Bhupendra Guptaa*, V. K. Sethib, Mukesh Pandey "Polymer Exchange Membrane (PEM) Fuel Cell: A Review" International Journal of Current Engineering and Technology 2012.

[27] J. Wind, R. Späh, W. Kaiser, G. Böhm, *J. Power Sources*, 105 (2002) 256-260.

[28] A. Pozio, R.F. Silva, M. De Francesco, L. Giorgi, Electrochim. Acta, 48 (2003)

[29] R. C. Makkus, A. H. H. Janssen, F. A. De Bruijn, R. K. A. M. Mallant, *J. Power Sources*, 86 (2000) 274-282.

[30] L. Cindrella, A.M. Kannan, J.F. Lin, K. Saminathan, Y. Ho, C.W. Lin, J. Wertz, *J. Power Sources*, 194 (2009) 146–160.

[31] W. Schmittinger and A. Vahidi, “A review of the main parameters influencing longterm performance and durability of PEM fuel cells,” Journal of power sources, vol. 180, no. 1, pp. 1–14, 2008.

[32] C. S. Gittleman, F. D. Coms, and Y.-H. Lai, “Chapter 2 - membrane durability: Physical and chemical degradation, in Polymer Electrolyte Fuel Cell Degradation (M. M. Mench, E. C. Kumbur, and T. N. Veziroglu, eds.)”, pp. 15 – 88, 2012.

[33] Zhang J, Wang H, Wilkinson DP, Song D, Shen J, Liu Z. “Model for the contamination of fuel cell anode catalyst in the presence of fuel stream impurities”. J Power Sources 2005; 147: 58–71.

[34] H. A. Gasteiger, S. S. Kocha, B. Sompalli, F.T. Wagner, Applied Catalysis B: Environmental 56 (2005) pp.9–35

[35] Kocha, S, et al. (2006). “Characterization of gas crossover and its implications in PEM fuel cells”. AIChE Journal 52:1916 – 1925

[36] Carter, R. N., et al. (2009). “Handbook of Fuel Cells - Fundamentals, Technology and Applications”, vol. 6. John Wiley & Sons, Ltd., 2 edn. Part 2, Chapter 56.

[37] Haijiang Wang, Xiao-Zi Yuan, Hui Li “PEM Fuel Cell Diagnostic Tools” CRC Press Taylor & Francis Group, 2012

[38] Scribner Associates, Inc.” Electrochemical Impedance Spectroscopy (EIS): A Powerful and Cost Effective Tool for Fuel Cell Diagnostics”, Tutorial, 2014

[39] Robert U. Paynea Wenhua H. Zhua and Bruce J. Tatarchuk. “Pem stack test and analysis in a power system at operational load via ac impedance”. Journal of Power Sources, 168:211–217, 2007.

[40] Yousfi-Steiner, Ph. Mocoteguy, D. Candusso, A. Hernandez, and A. Aslinides. “A review of pem voltage degradation associated with water management: Impacts, influent factors and characterization.” Journal of Power Sources, pp. 260 – 274, 2008.

[41] Blum, Ludger. (2016). An Analysis of Contact Problems in Solid Oxide Fuel Cell Stacks Arising from Differences in Thermal Expansion Coefficients. Electrochimica Acta. 223. 10.1016/j.electacta.2016.12.016.

[42] Yu. M. Vol’fkovichz, V. E. Sosenkin, N. F. Nikol’skaya, and T. L. Kulova “Porous Structure and Hydrophilic–Hydrophobic Properties of Gas Diffusion Layers of the Electrodes in Proton-Exchange Membrane Fuel Cells” Russian Journal of Electrochemistry, 2008, Vol. 44, No. 3, pp. 278–285.

[43] Mauritz, K. A.; Moore, R. B., “State of Understanding of Nafion.” Chemical Reviews 2004, 104, (10), 4535-4585.

[44] Panchenko A. “Polymer electrolyte membrane degradation and oxygen reduction in fuel cells: an EPR and DFT investigation.” Ph.D. thesis, Institute für Phzsikalische Chemie der Universität, Stuttgart, 2004.

[45] Paul William Majsztrik “Mechanical and transport properties of Nafion® for PEM fuel cells; temperature and hydration effects.” Ph.D. Thesis Princeton University, 2008.

[46] LaConti AB, Hamdan M, McDonald RC. “Mechanisms of chemical degradation”. In. Handbook of fuel cells: fundamentals, technology, and applications, vol. 3. John Wiley and Sons; 2003;647–62.

[47] Jiujun Zhang “PEM Fuel Cell Electrocatalysts and Catalyst Layers Fundamentals and Applications” Springer, 2008.

[48] A. Ghielmi et al., J. Power. Source., 145, 108-115, Fig. 3 (2005)

[49] M. Gebert, A. Ghielmi, L. Merlo, M. Corasaniti, and V. Arcella “AQUIVION™ -- The short-side-chain and low-EW PFSA for next-generation PEFCs expands production and utilization” Solvay Solexis S.p.A., viale Lombardia 20, I-20021 Bollate (MI), Italy ECS Transactions, 26 (1) 279-283 (2010)

[50] A. Stassi, I. Gatto, E. Passalacqua, V. Antonucci, A.S. Arico,, L. Merlo, C. Oldani ,E. Pagano “Performance comparison of long and short-side chain Perfluorosulfonic membranes for high temperature polymer electrolyte membrane fuel cell operation” Journal of Power Sources 196 (2011) 8925–8930.

[51] J. Peron, A. Mani, X. Zhao, D. Edwards, M. Adachi, T. Soboleva, Z. Shi, Z. Xie, T. Navessin, S. Holdcroft, J. Membr. Sci. 356 (2010).

[52] Seitarides, Th & Athanasiou, Costas & Zabaniotou, Anastasia. (2008). Modular biomass gasification-based solid oxide fuel cells (SOFC) for sustainable development. Renewable and Sustainable Energy Reviews. 12. 1251-1276. 10.1016/j.rser.2007.01.020.

[53] Jain, Nikhil & Roy, Anurag & Jain, Rajat & C. Karmakar, N. (2013). Polymer Electrolyte Membrane Fuel Cells : Alternative to fossil fuels for power supply to Heavy Earth Moving and Allied Machinery in Mining and Civil Engineering Industry. 10.13140/RG.2.1.3482.6086.

3. EXPERIMENTAL SETUP

This chapter presents a concise step-by-step summary of different processes carried out during the experiment. It focuses on the process of determining the most suitable combinations of design and operating conditions by considering the effect of flow channel depth, flow rates and other design parameters and how these parameters each influence the PEMFC performance.

3.1 FUEL CELL TEST

For the purpose of this work, an in-house FuelCon Elevator-C fuel cell test station at Hydrogen South Africa (HySA) lab as shown in Figure 3.1 was used for the PEMFC evaluation. This device has features for controlling and regulating temperature, supply pressure, back flow pressure, flow rate of reactant and relative humidity.

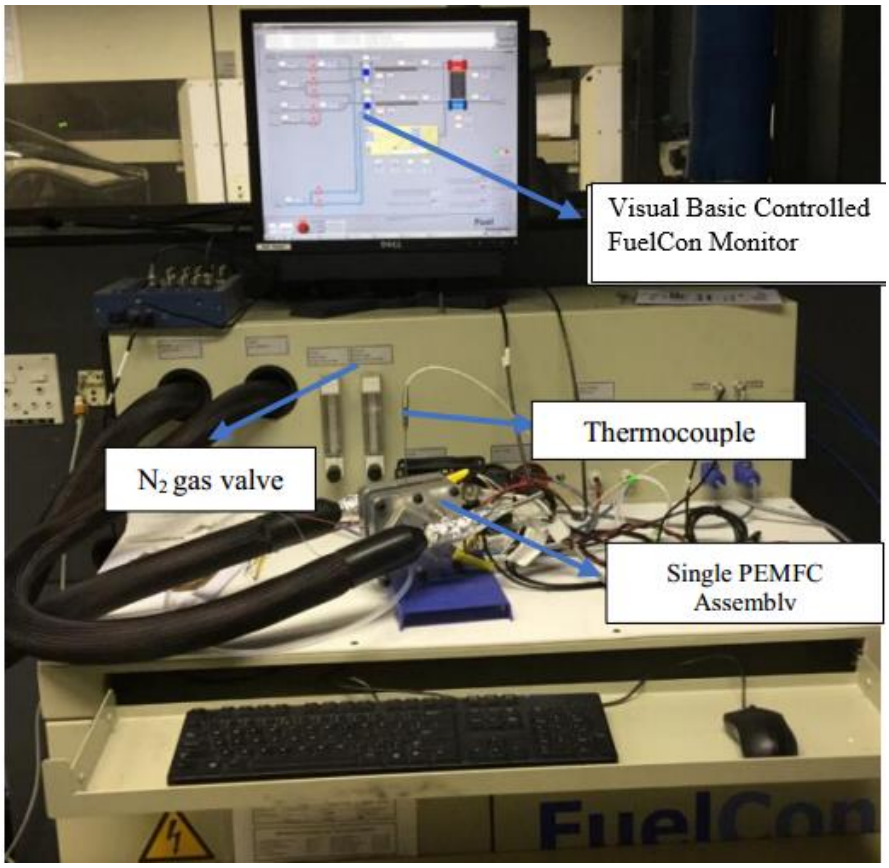

Figure 3.1: Fuel Cell test station

The cell is connected to an electronic load and the electrical responses of the cell recorded by the data acquisition system. Figure 3.2 shows a pictures of how the test item is connected to the FuelCon test stand. The test stand is linked through a computer interface that utilises Visual Basic for acquiring data, while also used to operate the fuel cell and vary the load input. An in-built electronic load is used to set defined regimens for electrical current and voltage for the test object. The electronic load bank is also controlled via the Visual Basic computer interface and is used for the characterization of the fuel cell.

The load cell-input, air flow rate, gas stoichiometry, relative humidity, temperature, and back pressure are all controlled electronically. Figure 3.3 shows the process components arranged in a closed test stand. The schematic of the PEMFC as shown in Figure 3.2 has the membrane electrode-assembly (MEA) pressed between two machined graphite plates and sealed with a Teflon gasket material that helps in providing the correct compression and also acts as a 'barrier' for potential fuel leaks and thus, maximizing efficiency. The N_2 gas is used for heating and conditioning of the cell during the break-in/activation process. The tested MEA has an active area of 25cm^2 sandwiched between two porous carbon fibre cloth material representing the gas diffusion layer (GDL).

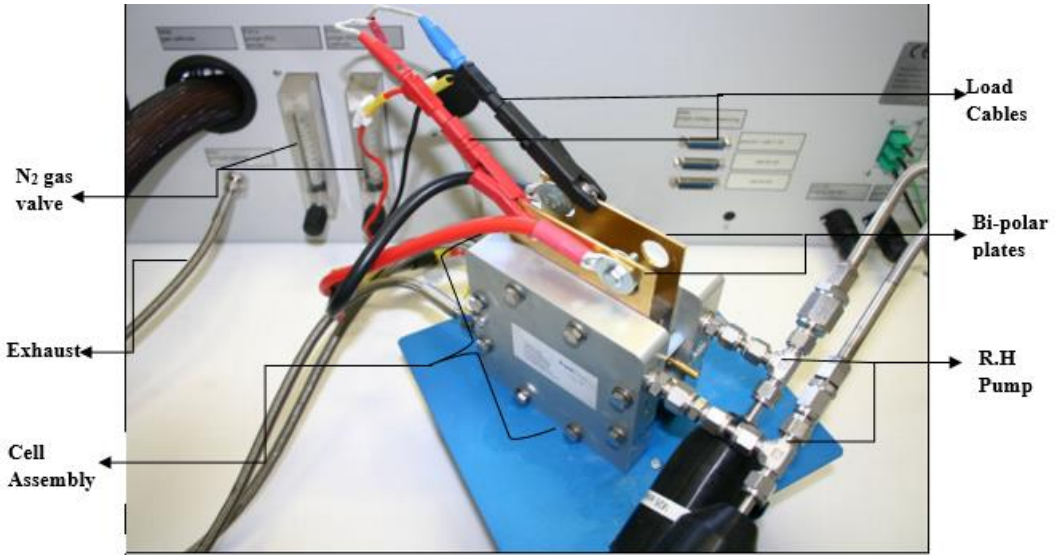

Figure 3.2: Fully connected PEMFC single cell assembly.

The GDLs consists of a fine Micro Porous Layer (MPL) and hydrophobic treatment (PTFE) binder facing either side of the catalyst coated membrane (CCM). The MEA, which is centred between two serpentine graphite plates flow fields is then compressed between two gold-plated copper plates.

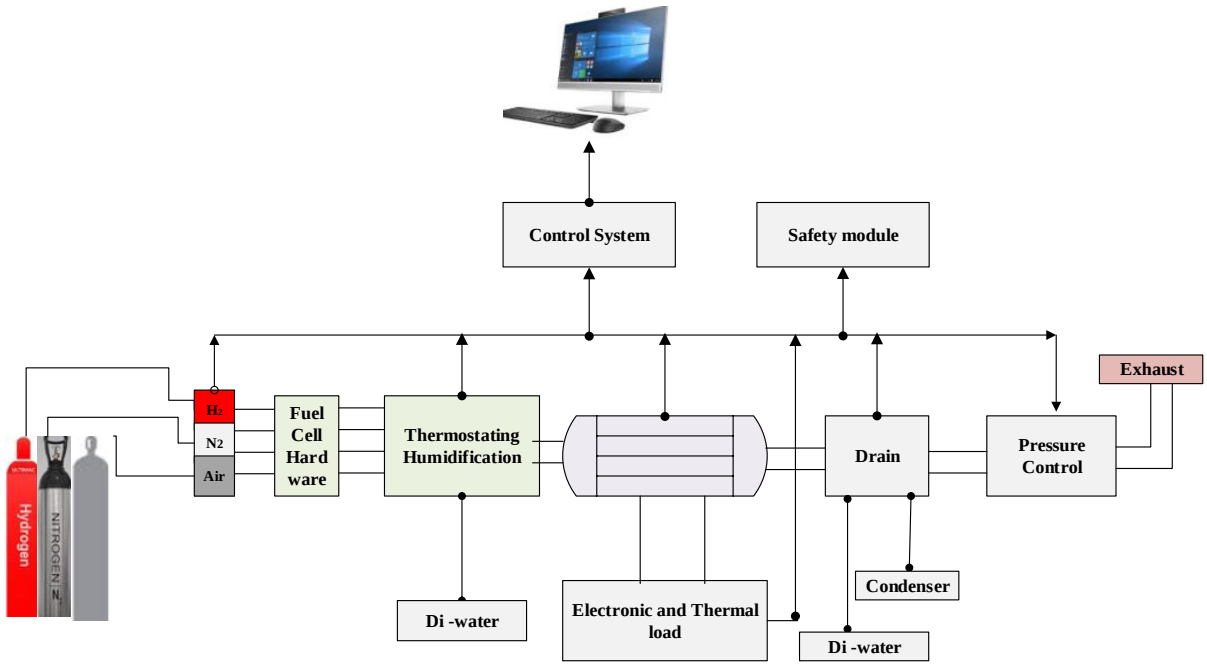

Figure 3.3: Components as arranged in a closed test stand.

For efficient performance of the cell, there is a need to ensure optimum design parameters and operating conditions for enhanced performance of the PEMFC based on standard test requirement. In this work, we studied the influence of various operating and design parameters before choosing the parameters and conditions at which the PEMFC was tested. Based on the current density, maximum power can be reached at different operating conditions, hence, it is therefore advisable to have a detailed knowledge of the complete operation map of the PEMFC to enable one make informed decision in parameters assigning [2]. Design parameters such as clamping force, torque and type of hardware used are also crucial to the efficient working of the PEMFC, if not well aligned, they could lead to failure of the cell. Different types of flow field designs and GDL types were also investigated in the quest to ascertain the optimized design and operating condition for the 25cm^2 PEMFC.

3.2 Optimization of the Design and Operating Parameters

The PEMFC used in this work is a 25cm^2 active area MEA from Baltic Inc. [20] and the membranes were made by Hydrogen South Africa (HySA) Catalysis – a centre of competence that form part of the South African Department of Science and Technology's National Hydrogen and Fuel Cells technologies flagship project. A five-channel serpentine flow fields which has a higher pressure drop compared to parallel flow field due to its long channel length and numerous turnings was used, hence helping to reduce the possibility of flooding. The monoplanar planes (MP) of the flow field was made from graphite and a cross-flow such that there are vertical channels at the cathode end and horizontal channels at the anode. Also, two different types of GDLs were tested, the AvCarb GDL and the Freudenberg GDL. Both GDLs were made from carbon fibre, the performance of the GDLs were compared under the same conditions and the better performing one was selected for our investigation.

3.2.1 Design Parameters

The 25 cm^2 Baltic PEMFC single cell test fixtures shown in Figure 3.4 is made from monopolar titanium plates. It consists of gold plated copper current collector plates at the anode and cathode side, heating cartridges with a diameter of 6.5 mm, temperature sensing knobs and 2 voltage sensors. The cell fixture offers 5 multi-channel serpentine gas flow field (1mm x 1mm) with robust aluminium end-plates and titanium monopolar plates. The single cell fixture is held tightly together by hexagonal head shaped bolts and nuts which are clamped together to a specified torque value based on the design application. The effects of this clamping torque on PEMFC performance optimization is highlighted in the following section.

Figure 3.4: Baltic Cell Fixture Set-up

3.2.1.1 Optimal Clamping Torque

The fixture for the cell assembly plays a very important role in determining the PEMFC performance. There is a need to ensure optimal choice of contact pressure to prevent reactant leakage and also attenuate contact resistance between the different combined layers. The optimal clamping torque will be one that effectively compresses the PEMFC layers and yet not impeding the flow of reactant. If less pressure is applied, problems such as fuel leakage, very high contact resistance and even internal combustion issues might be prevalent. On the other hand, applying too much pressure would lead to restriction of reactant flow through the GDL or even cause permanent damage to the cell. Applying the incorrect clamping pressure/torque results in a drop in PEMFC performance. As shown in Figure 3.5, another important factor in the cell fixture design is obtaining a uniform pressure distribution in the MEA. With non-uniformity comes poor performing cells. The set up needs to be done considering the thickness and mechanical strength of the MEA, which is weaker and thinner than the other housing components. The optimum torque is dependent on many other variables other than the ideal clamping pressure on the fuel cell layers, it is also affected for instance by the shape, length

and material of the bolt and nut, the bolt seating and threading, the stack layers, thickness, and number of layers.

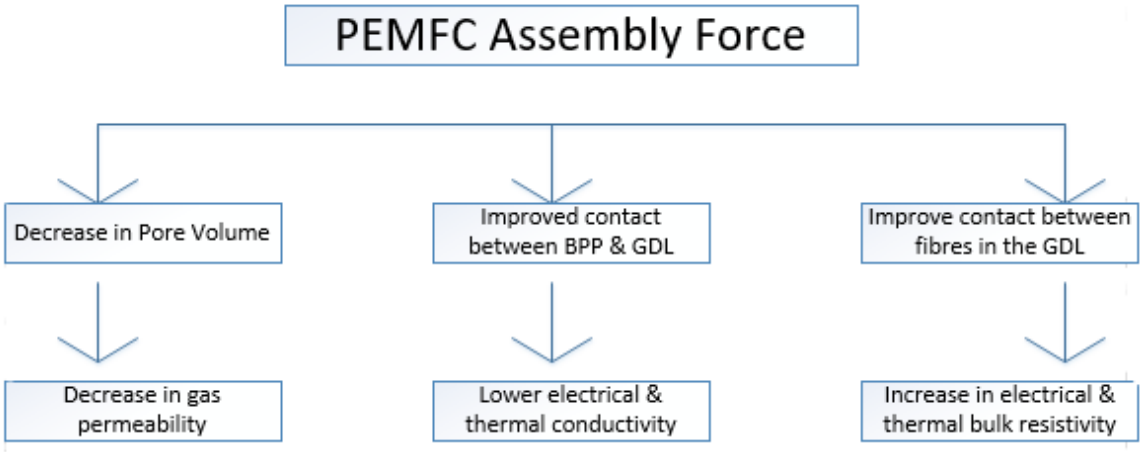

Figure 3.5: Effect of Clamping Force

To determine the optimum length of bolts and knots, we considered two types of bolts of different lengths and we did a pressure paper test to determine the uniformity of pressure distribution on the MEA embedded in the cell fixture as the cell fixture is subjected to the same compression torque. The two types of bolts has the same diameter of 1.2mm, the longer bolt is an M10 bolt with a length of 70mm while the shorter bolt is an M10 bolt 55mm long. A pressure measurement film indicating the applied pressure differences as a function of red colour density variations was used to determine this pressure uniformity. As observed in Figure 3.6(a), the shorter bolts, although having a darker imprint on the pressure paper, the distribution is not uniform across the paper, with some regions darker than others. This is an indication that with the short length knots, the cell will always be over compressed, as the GDL would possibly be damaged leading to impeding of the diffusion of gases towards the catalyst layer or it might even cause mechanical failures on the cell's membrane thereby resulting in poor performance. The longer bolts on the other hand, as observed in Figure 3.6(b) produces a not too dark and not too faint uniform impression on the pressure paper. This uniformity is key in determining

the performance of the cell. Every section of the membrane would be well accounted for during the diffusion of reactants through the membrane and this will be an indication of a well aligned and optimized cell fixture arrangement.

In this work, the 25cm^2 cell fixture is clamped using eight spherical bolts. Materials bolted together has the ability to withstand moment loads by clamping the surfaces together, where the edge of the part will then act as a fulcrum, and the bolt will act as a force to resist the moment created by an external force or moment [3].

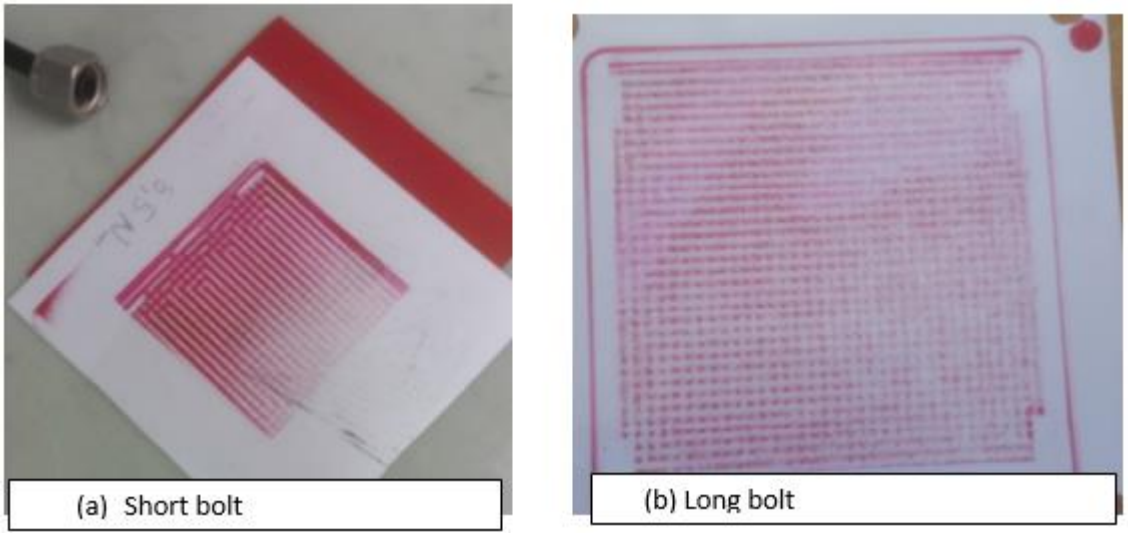

Figure 3.6: Pressure paper test of Short knot and Long knot cell fixture.

To ensure uniformity of pressure during clamping, the bolts were tightened using a special aligning format as showed in Figure 3.4. From literature, the clamping torque can be calculated using Equation (3.1) [3, 4]. However, to ensure reproducibility of results, and reduce the margin for error, in this work we decided to vary the different torque values across a range of values close to the calculated clamping torque. This thesis uses the pressure paper and polarization curve test to determine uniformity of pressure and cell performance respectively.

$$T_t = \frac{F_{clamp} K_b D_b}{N_b} \tag{3.1}$$

$$F_{clamp} = P_c A \tag{3.2}$$

T_t is the applied torque in N m, F_{clamp} is the clamping force in N, K_b is the coefficient of friction. D_b is the bolt nominal diameter in m, and N_b is the number of bolts. F_{clamp} is dependent on the clamping pressure and fixture's active area A.

The material properties of the cell components such as the bolts, geometry of holes, component stiffness, membrane thickness and contact resistance between the GDL and the bi-polar plates are also necessary to be considered in determining the optimum clamping torque of the cell.

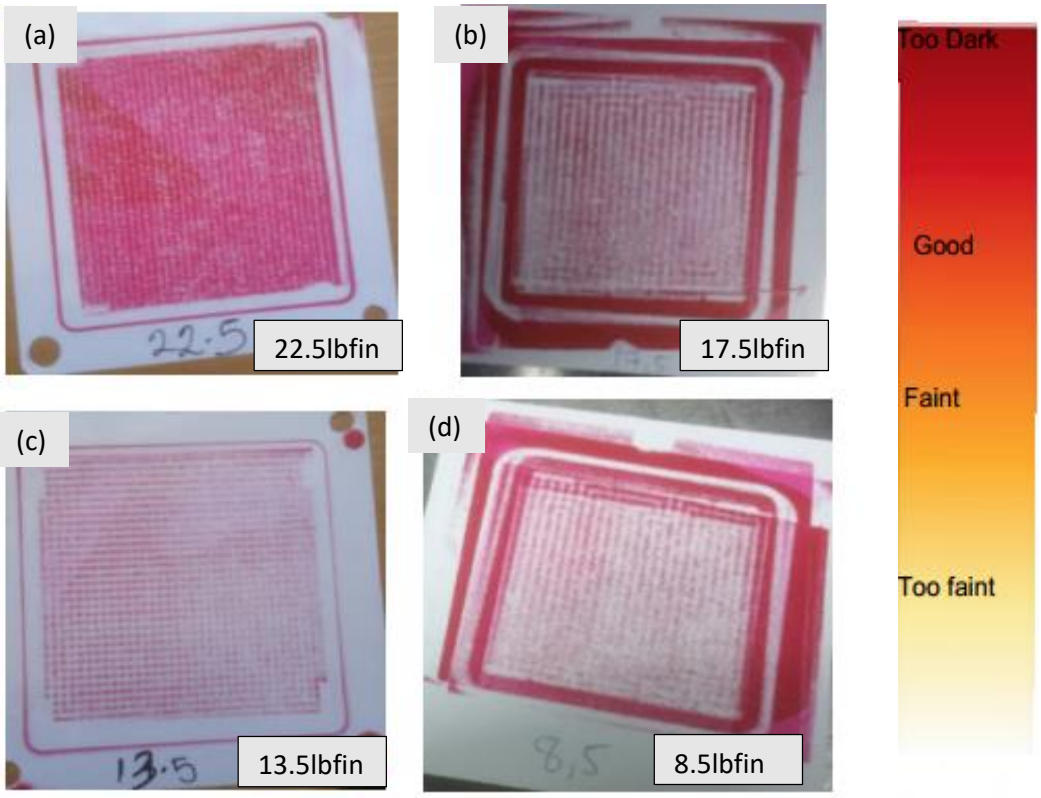

Figure 3.7: Pressure paper test on uniformity of clamping pressure.

A torque wrench was used to set the torque. The calibration on the device used was done using pound-force inch [lbfin] unit. Different torques values were applied on the bolts while tightening, ranging from 22.5 lbfin (2.54Nm) to 8.5lbfin (0.98Nm). From Figure 3.7, it is observed that the torque of 22.5 lbfin was too much, and could cause damage to the membrane considering how dark the colour on the pressure paper was. The 17.5lbfin seemed to be good enough as the colour etched on the pressure paper from the compression test wasn't too dark

nor too faint. The 13.5 lbfin was also uniformly distributed, but seemed quite faint, but it still looks fairly good, and the 8.5 lbfin was the faintest of all, an indication that there might not be enough compression at this torque. To further support these findings, polarization and power curve analysis at the different torque values were carried out under the same operating conditions of 2bar back pressure at both anode and cathode, 100% anode humidity and 81% cathode humidity. The cell temperature was set at 80^{o}C, the anode stoichiometry was set at 1.5 and cathode stoichiometry was set at 2.0. The anodic flow rate was set at 0.075 Nl/min while the cathode flow rate was at 0.3 Nl/min. The MEA made by HySA Catalysis was used for the test across all torque values. The polarization as well as the power curve analysis is presented in Figure 3.8

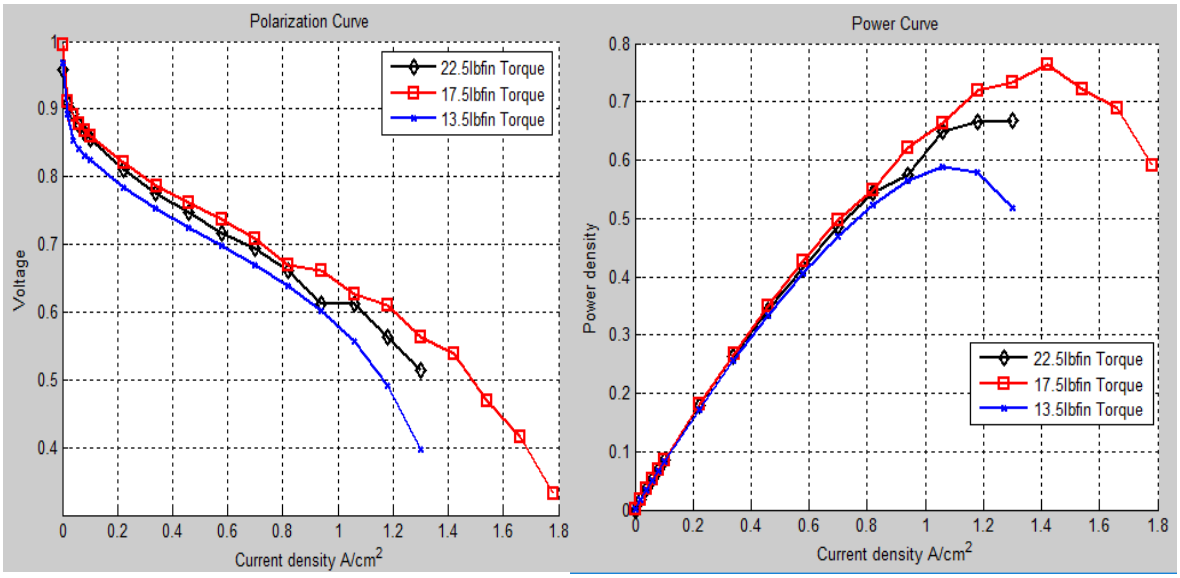

Figure 3.8: Polarization and Power Curve showing effect of varying clamp pressure.

The cell could not be operated at a torque of 8.5lbfin, as there was leakage of reactant, therefore not permitting a pressure of 2bar to be reached. From Figure 3.8, the polarization curve showed the optimal operating torque for the cell is 17.5lbfin which gave the best performance. The torque at 22.5lbfin, shown with the pressure paper test, behaved poorly, supporting our claims of possibly over compression which could cause damage to the membrane. The torque at

13.5lbfin indicated that there was insufficient compression force, resulting in increased contact resistance and thereby affecting the overall cell performance. The optimal clamping torque for the 25cm^2 PEMFC cell fixture is shown to be 17.5lbfin (1.98Nm) and all subsequent experiments were carried out using this value.

3.2.1.2 Optimizing the Gas Diffusion Layer (GDL)

The gas diffusion layer (GDL) supports the heat, water and mass transfer across the membrane electrode assembly (MEA) and is a major determinant in optimizing the performance of polymer electrolyte membrane (PEM). The gas diffusion layer (GDL) is found sandwiched between the flow field plate and the catalyst layer. For optimal performance, the GDL must have very high proton conductivity, chemically stable, and it must have ability to withstand the temperatures and compression forces of the fuel cell fixture. The GDL also helps in maintaining a stable water balance in the PEMFC as it allows only an appropriate amount of water to contact the MEA so as to keep the membrane humidified and at the same time enhances the exit of liquid water from the cathode to help eliminate flooding. As earlier stated, two types of GDL's, namely the Freudenberg H23C9 GDL and the AvCarb MB-30 GDL, were tested and their performance investigated under the same conditions.

In this thesis, a Freudenberg GDL made from carbon fibre with a thickness of 0.218mm was used. Freudenberg H23C9 GDL has high electrical and thermal conductivity, and protects the membrane from faults such as potential puncture and are tailored for optimized mass transport depending on the fuel cell operating conditions. This optimization ensures sufficient supply of the hydrogen and oxygen (air) gas reactants to the catalyst layers. Concurrently the movement of product water in gaseous and liquid states must be managed to keep catalyst sites open for reactants while preventing membrane dry-out. The Freudenberg GDL has a micro-porous layer (MPL) coating and treatment providing it with the perfect balance of electrical and thermal conductivity as well as hydrophobicity for the water management within the cell [6].

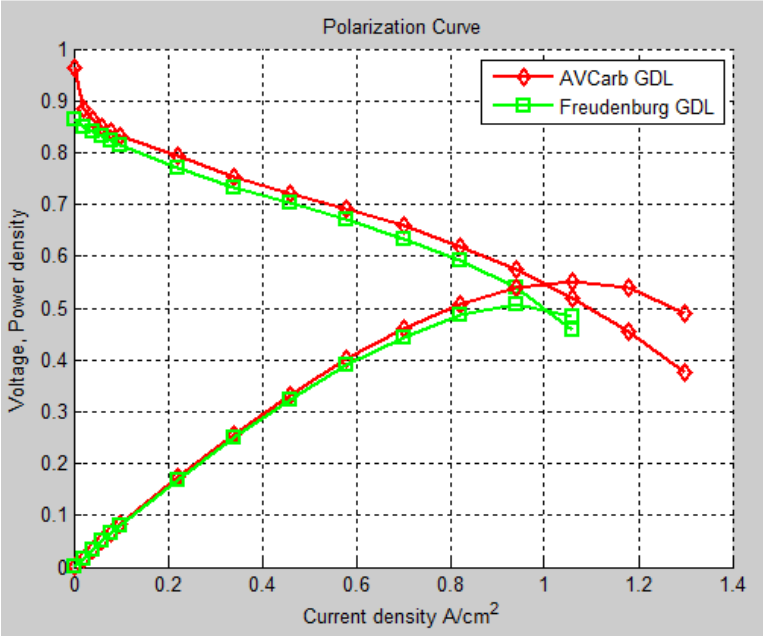

Figure 3.9: Polarization and Power Curve of GDL performance.

The AvCarb MB30 GDL like the Freudenberg H23C9 is also made from carbon fibre paper but with a thickness of 0.175mm, a PTFE treatment, and micro-porous layer coating [5]. By analysing the power curve and polarization curve of both GDL's under the same operating and design conditions as shown in Figure 3.9, the AvCarb GDL performed much better than the Freudenberg GDL under the same conditions. The AvCarb was seen to have higher proton conductivity and has higher porosity compared to the Freudenberg GDL making it possible for reactants to easily transit to the catalyst layer. Also being thinner than the Freudenberg GDL, the AvCarb GDL compressive force in the cell also appeared to have aided its performance by causing the least form of impedance to the gas flow through the porous GDL. These results suggest that the AvCarb GDL outperformed the Freudenberg GDL for this PEMFC under the specified conditions.

3.2.2 Operating Parameters

PEMFC being an electrochemical energy conversion device that converts chemical energy (fuel) into electrical energy. It has dynamic behaviour which can be explained via a series of

thermodynamic and chemical processes such as fuel purity, oxidant type, temperature, pressure, relative humidity (RH), stoichiometry ratio and gas flow rate [7]. High operating temperatures of the PEMFC increases the reaction kinetics which gives rise to certain corrosion and degradation mechanisms. The relative humidity is a function of water content in the cell and is particularly important because the membrane must be kept continually humid to enable proton conduction and not too humid to avoid flooding. The stoichiometry ratio shows the relationship between the amount of available gas and the amount needed to complete the reaction while the back pressure on the other hand speaks to the force with which the gases are being injected into the cell, with higher back pressure indicating faster reaction rate.

3.2.2.1 Relative Humidity (R.H) Optimization

Efficient water management is essential for proper optimization of the PEMFC performance. Water transport takes place when the migrating protons drag water from the anode to the cathode through an electro-osmotic drag transport, this together with electrochemical water production results in water accumulation on the cathode side.

Conversely, water concentration gradient between the anode and cathode causes back diffusion which helps to keep the anode side also well hydrated. Elif et al. [8] and Cheng et al. [9] showed in their works that increasing the anode's R.H leads to improved performance of the PEMFC, and at higher current density, reduction in cathode's R.H lead to an enhancement in PEMFC performance. The humidity is controlled via the inlet temperature. For the purpose of this study, the optimized R.H for both anode and cathode was set at 80^{o}C and 75^{o}C respectively corresponding to 100% humidity level at the anode and 81% humidity level at the cathode.

From Figure. 3.10(a & b), it is however observed that R.H gradient between the anode and cathode has significant impact on the fuel cell performance especially at high current densities. The smaller the R.H gradient, the better the PEMFC performance. This is because the water

concentration gradient between the anode and cathode side is what causes back diffusion, which is needed to keep the cell's anode side from drying out.

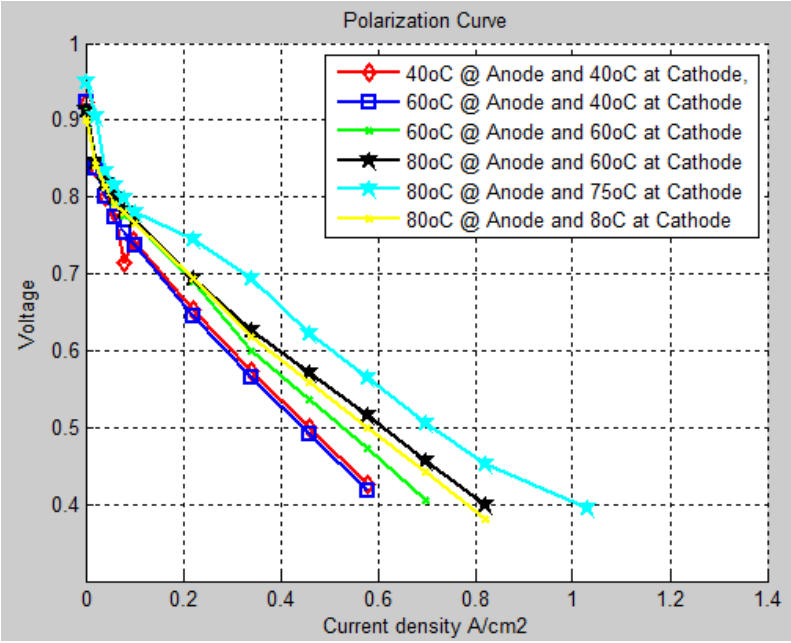

Figure 3.10(a): Polarization Curve Showing the Effect of R.H (Cell operated at 80^{o}C).

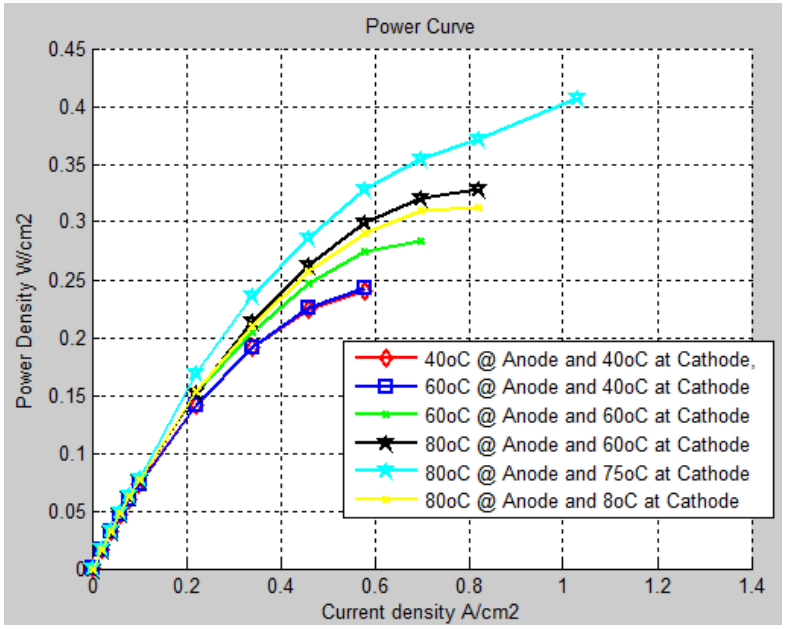

Figure 3.10(b): Power Curve showing the Effect of R.H (Cell operated at 80^{o}C).

At low current densities, electroosmotic drag prevails over back diffusion and thus the anode will tend to dry out, irrespective of whether the cathode is hydrated or not. High R.H values at

the anode gives rise to an enhanced chemical reaction and proton conduction since there is more water in the membrane thus leading to improved PEMFC performance. However, when operating the PEMFC at high cathode R.H values, the cell performance increases at low current densities because the water vapour concentration is enhanced to reach saturation level causing reduction in ohmic polarization. At higher current densities, a higher R.H value at the cathode causes it to accumulate excess water which blocks the pores of the membrane, hence inhibiting gas transport and ultimately cell performance. When the cell was operated at 100% humidity level (80^{o}C) at the cathode, the performance of the cell dropped. This drop in performance is most likely due to accumulation of excess water at the cathode due to injecting too much water in the cathode gas inlet.

3.2.2.2 Pressure Gradient Optimization

Figure 3.11(a) and 3.11(b) shows the result of operating the cell, at both low (dry) and high (wet) R.H values at the anode and cathodes respectively, for varying pressure conditions. In Figure 3.11(a), the cell was operated at 15% R.H at the anode and cathode, In Figure 3.11(b), the cell was operated at 100% R.H at both the anode and cathode side to emulate both the dry and wet condition, for varying pressure gradients.

1A = 1bar, 2A = 2bar, 3A = 3bar at Anode. *And 1C = 1bar, 2C =2bar, 3C= 3bar* at Cathode.

It is observed that increasing the pressure at both the anode and cathode would lead to an increase in cell performance due to an increase in concentration of reactant. However, creating a pressure gradient between both electrodes leads to anomalous behaviour, the balance between the supplied gas is compromised. A higher anode back pressure means there is a higher supply of H_2 gas than there is air, and similarly, higher cathode pressure means more air is supplied than H_2 gas, thus increasing the possibilities of fuel crossover, mass action and other performance inhibiting defects.

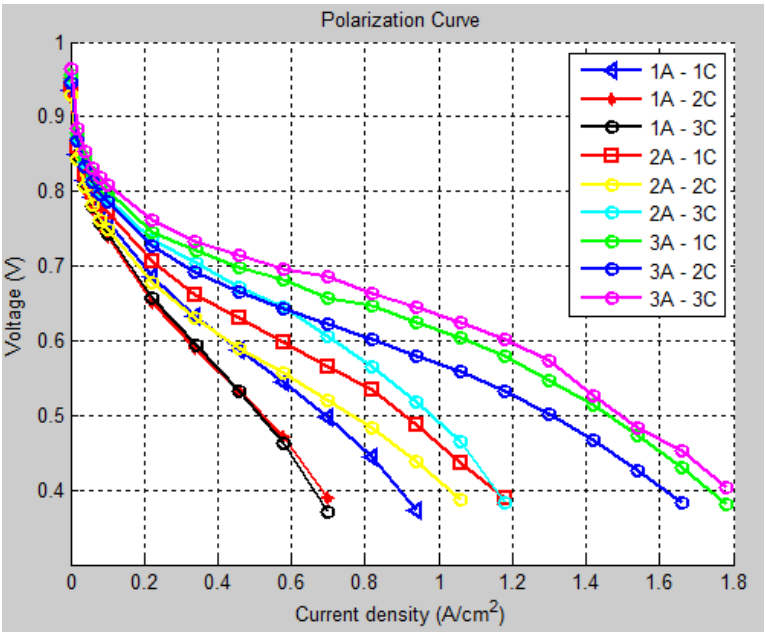

Figure 3.11(a): Effect of pressure (Cell operated at 80ºC) 15% R.H at both electrodes.

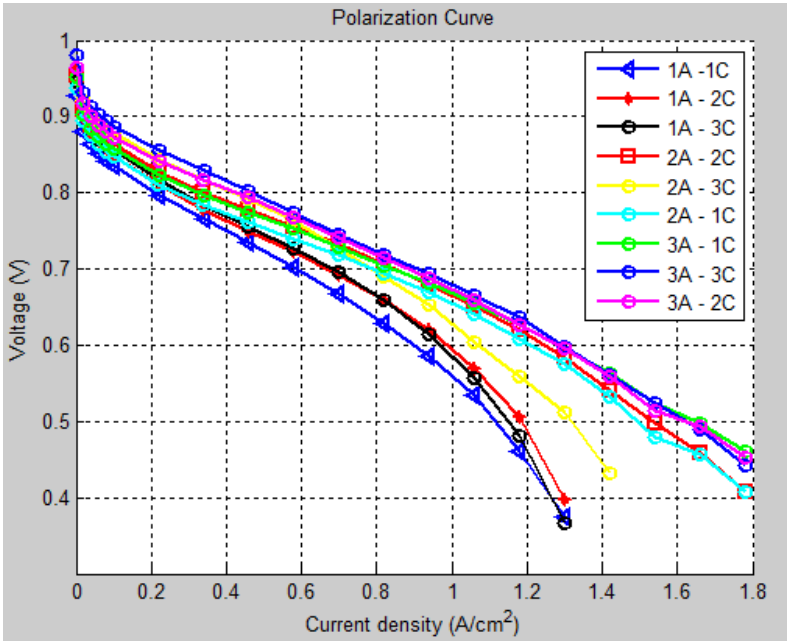

Figure 3.11(b): Effect of R.H (Cell operated at 80oC) 100% R.H at both Anode and Cathode.

The pressure gradient in the cathode to anode direction shows that at lower current density the cell performance drops at low RH with increasing pressure, but at higher current density, the cell performance increases with increasing cell pressure as a result of convective water flux which increases hydration of the membrane at the anode.

From the Polarization-Curve analysis, it is observed that the pressure gradient in the cathode to anode direction (low cathode, high anode) negatively affects the performance of the PEMFC under both the wet and dry condition. Conversely, pressure gradient in the anode to cathode direction (low anode, high cathode) shows an improved performance to the latter and even outperforming the equal (3A- 3C) pressure condition at low RH (dry) condition, thus indicating that the performance of the PEMFC is more dependent on the cathodic reactant than on the anodic reactant concentration. In the dry condition, the higher the gradient in the anode to cathode direction the better the performance and reverse is the case for the cathode to anode pressure gradient for both wet and dry conditions.

The presence of a gradient in back pressure at both anode and cathode have the potential to adversely affect the performance of the cell. It is therefore better to operate the cell at equal anode and cathode back pressure.

3.2.2.3 Optimizing Fuel Cell Operating Temperature

Based on several literatures and the Department of Energy (DOE) reports, the PEMFC has been said to have a working temperature ranging from 60^{o}C to 100°C while operating with an efficiency of about 50% with the remainder discharged as heat. This discharged heat needs to be well channelled and discharged from the cell in order to prevent it from causing damage to the membrane [10].

It is well known that the operating temperature has a significant influence on PEMFC performance. With the cell operated at high temperature, we can effectively improve the PEMFC performance by enhancing reaction kinetics, improving heat rejection, increased mass transfer rate, and improved catalyst tolerance while lowering the cell ohmic resistance that arises as a result of the higher ionic conductivity of the electrolyte membrane [11]. However, the concern with PEMFC is that increasing the cell temperature higher than the optimal

operating temperature will result in membrane dry out and reduced proton conductivity which decreases cell performance. It is expedient however, to know the optimal temperature that provides the maximum possible power based on pre-set working points of the current density. Depending on the current intensity, the operating conditions to attain the maximum power vary. It is therefore important to have a full grasp of the complete operation map of the cell taking into account the cell size, system requirement and the parasitic power requirement of the heat management subsystem [12-13].

The optimal operating temperature of the 25cm^2 PEMFC assembly was investigated by varying the operating temperature between 40^{o}C and 100^{o}C at an atmospheric pressure of 1bar and at a cathode and anode stoichiometry value of 2.0 and 1.5 respectively while operating at constant flow rate of 0.075Nl/min at the anode and 0.3Nl/min at the cathode. The bubbler R.H temperature was set at 100% at the anode and 81% at the cathode. Figure 3.12 shows an overview of the polarization curve and power curve of this analysis. It is evident from Figure 3.12 that the optimal operating temperature for the 25cm^2 cell configuration is at 80^{o}C. The increase in the PEMFC performance between 40 - 60^{o}C, in terms of the measured voltage response, is most likely due to the gas diffusivity and membrane conductivity at higher temperatures. This can also be linked to the reduction of activation losses due to improved exchange current at higher operational temperature. The diffusion of gases as well as reaction kinetics also improve with the increase in operating temperature resulting in higher voltage response.

The cell performance was observed to be increasing with increase in operating temperature until it gets to 80^{o}C. Above this temperature the PEMFC performance was seen to begin to drop drastically. The membrane conductivity decreases due to the excessively high operating temperature which results in higher rate of water evaporation resulting in a reduction in the water content of the membrane.

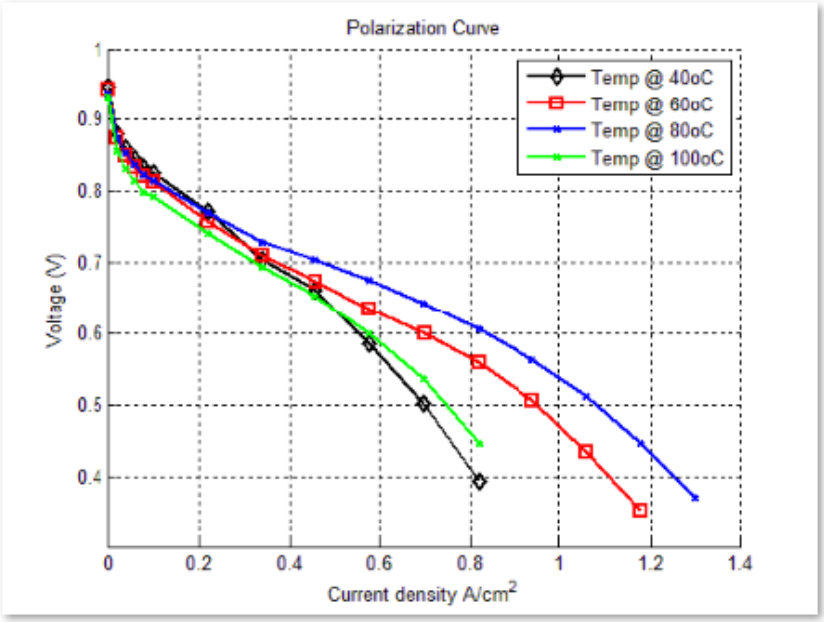

Figure 3.12(a): Polarization curve at varying operating temperatures.

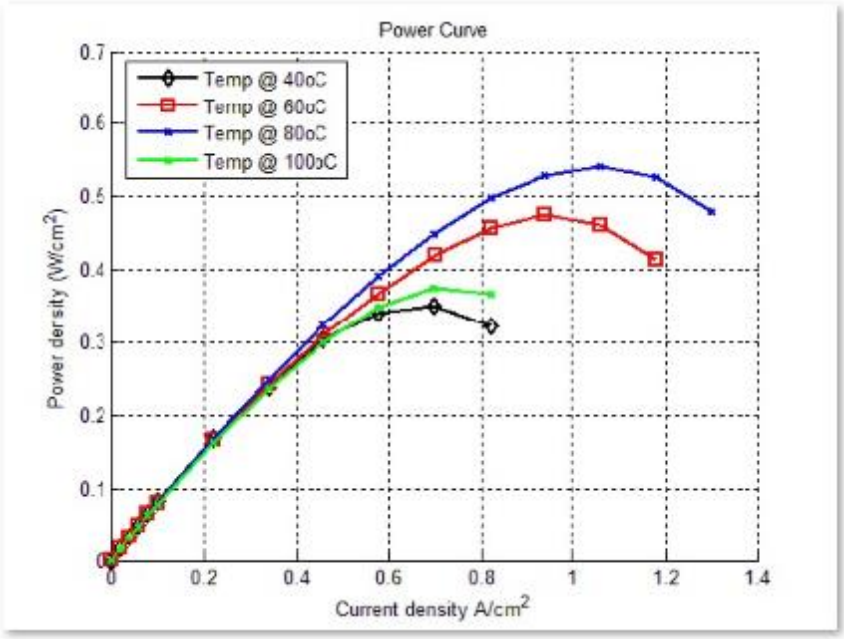

Figure 3.12(b): Power Curve at varying operating temperatures.

Operating the cell at a temperature beyond 80^{o}C exceeds the optimal temperature and we move towards a critical temperature where the amount of evaporated water exceeds the amount of produced water, causing membrane dry out [14-16].

3.3 EIS Analysis of Nafion® and Aquivion® Ionomer MEAs

An overview of EIS has been discussed in Section 2.12.3. As earlier stated, the EIS is used to calculate transfer functions such as impedance or admittance of electrode reaction through the comparison of both output with input signals in the frequency domain. An analysis of the impedance spectrum is a useful technique since it can provide vast amount of data from which many characteristic parameters of a fuel cell could be extracted. The transfer function is decided by various factors such as electrode structure, diffusion, charge transfer, reaction mechanism, thus it can be employed in analysing reactions and the condition of electrode.

For this set-up, EIS test was done using a TrueData-EIS which is a high current AC impedance meter with a maximum DC current of 1000A. The TrueData-EIS effectively measures the impedance in the frequency range between 200 µHz and 100 kHz.

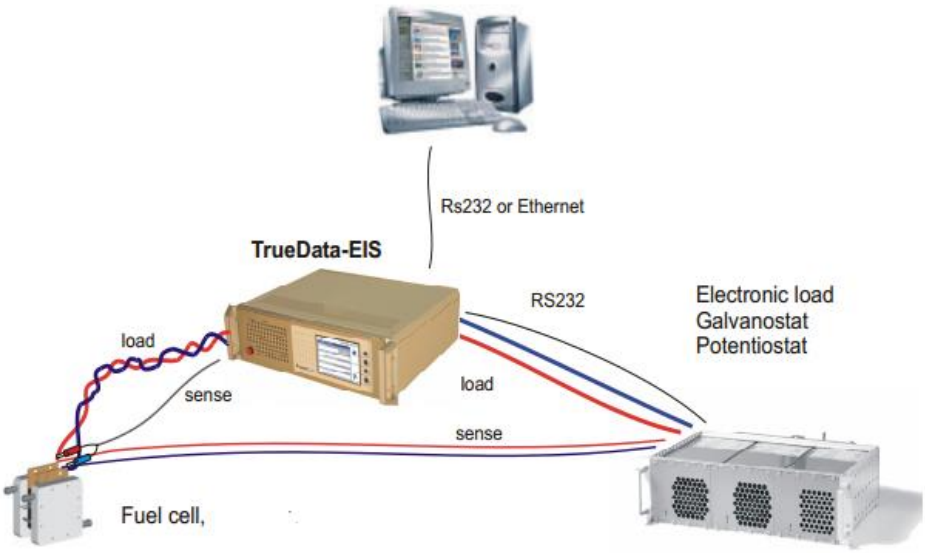

Figure 3.13: Experimental setup of the EIS interface attached to the PEMFC [17].

The TrueData-EIS device uses the single-sine technique. The TrueData-EIS directly controls an external electronic load via the RS232 interface and allows for highly accurate value measurement [17].

For the purpose of our investigation, we used the built-in FuelWork software on the Evaluator test station. With the help of the FuelWork software on the evaluator test station which has the TrueData-EIS already integrated into it, we were able to apply an automated control of the fuel cell's operating conditions. FuelWork software controlled the cell temperature, H_2 and air flow rate, gas pressure, relative humidity and even stoichiometry factor of the H_2 and air, and ultimately achieved fully automated measurement of the fuel cell's impedance spectrum under a variety of these highly controlled conditions. The current and the voltage range depends on the impedance of the test item. To an impedance of 800mΩ, the maximum modulation voltage of the test item is 20 mV (2% of the off load voltage of a single cell).

The EIS equipment was connected to the fuel cell and electronic load as shown in the Figure 3.13. The impedance analyzer TrueData-EIS in this work uses an external electronic load, allowing galvanostatic or potentiostatic modes while easily adapted for different load conditions. The interconnection between the TrueData-EIS and the electronic load is achieved through a digital RS232 interface enabling a high accuracy measurement of the impedance values.

The underlying principle behind its operation is such that the TrueData-EIS superposes an AC-current to the high DC-current of the electronic load. From the electrical side, the configuration works as a parallel wiring. The system's frequency response is independent of the electronic load's frequency response making it possible to measure impedance with high frequencies at high DC currents. Whenever the TrueData-EIS superimposes an AC current, the device also responds by superimposing a small DC current and hence reduces the DC current of the electronic load with this value. The final output of the TrueData-EIS presents the actual DC current of the test item on its display screen.

3.3.1 Electrical Circuit Model (ECM)

An equivalent circuit can be used to represent an electrode/electrolyte interface when it is analysed by EIS. For PEMFC analysis, the Randles Cell (Figure. 3.14) is the most common type of electric circuit used for EIS analysis. It includes a solution resistance, electric double layer capacitance C_{dl} and a charge transfer (or polarization resistance). The electric double-layer capacitance is in parallel with the charge-transfer resistance R_{ct}, which is assumed for the electrode with Faradaic process. In addition to being a useful model in its own right, the Simplified Randles Cell is the starting point for other more complex models. Fig. 3.15 shows the Randle's circuit model for a cell where polarization is due to a combination of kinetic and diffusion processes. In analysing the data of electrochemical impedance study, all elements are calculated by curve-fitting of experimental results on the basis of the equivalent circuit. One therefore needs to have detailed understanding of the relationship between the equivalent circuit and the impedance locus [18].

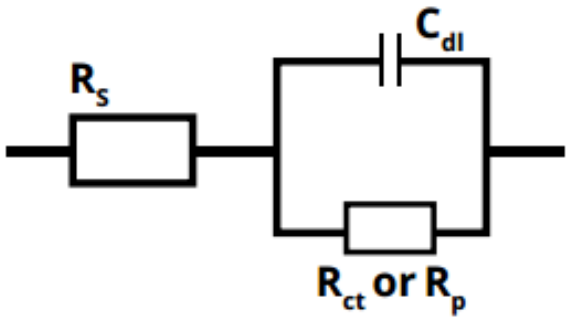

Figure 3.14: Simplified Randles Cell Schematic Diagram used for PEMFC EIS data fitting.

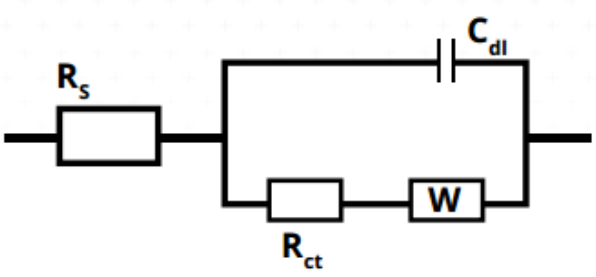

Figure 3.15: Randles Cell ECM with Mixed Kinetic and Charge-Transfer Control.

In this study, the adopted electrical circuit model (ECM) is based on the simplified model shown in Figure 3.16 [19]. It is an extension of the Randles cell for a circuit with mixed kinetic and charge transfer control. R_{Ω} corresponds to the cell's ohmic resistance, $CPE_{dl,A}$ and $CPE_{dl,C}$ are the constant phase element of the anode and cathode double layer respectively. $R_{ct,A}$ and $R_{ct,C,}$ are the anode and cathode's charge transfer resistance respectively. Like the Randles circuit, R_{Ω} is connected in series with two parallel combinations of $CPE_{dl,A,}$ - $R_{ct,A}$, and $CPE_{dl,C}$ - $R_{ct,C,}$ representing the distributed double-layer capacitive effects and the charge transfer resistances at the anode and cathode respectively. An inductive element L, was connected in parallel with the Warburg element (W) to model the low frequency inductive effect and mass action respectively.

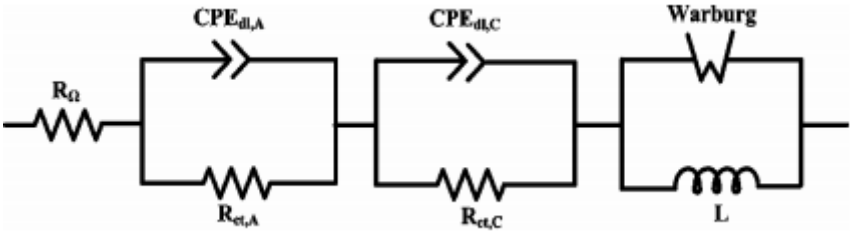

Figure 3.16: Electrical Circuit model used in the work for EIS data fitting [19].

References:

[1] FuelCon Operating manual hardware Version: BZH006_01_47 11/2008.

[2] J. A Salva, A.Iranzo, F.Rosa, E. Tapia ,E. Lopez, F. Isorna "Optimization of a PEM fuel cell operating conditions: Obtaining the maximum performance polarization curve" *International Journal of hydrogen*, 2015.

[3] C. Spiegel, "PEM Fuel Cells: Modeling and Simulation Using MATLAB", Elsevier/Academic Press, Burlington, MA, USA, 2008.

[4] N.Hassan, M. Kilic, E. Okumus, B. Tunaboylu A.M. Soydan "Exp. determination of optimal clamping torque for AB-PEM fuel cell*" J. Electrochem*. Aug, 2016.

[5] http://www.fuelcellstore.com/avcarb-mb30 accessed 03/03/2018.

[6] https://fuelcellcomponents.freudenberg-pm.com/Products/gas-diffusion-layers accessed 03/03/2018.

[7] Larminie J., Dicks A. “Fuel cell system explained”, 2nd ed., Wiley, 2003.

[8] Elif Ekee et-al, “Effect of Humidification of the Reactant Gases in the Proton Exchange Membrane Fuel Cell”, *Journal of Clean Energy Tech.* Vol. 3, No. 5, September 2015.

[9] Anh Dinh Le, Biao Zhou, “A general model of proton exchange membrane fuel cell” *Journal of Power Sources* 182 (2008) 197–222.

[10] C.Y. Wen and G.W. Huang, “Application of a Thermally Conductive Pyrolytic Graphite Sheet to Thermal Management of a PEM Fuel Cell”, *Journal of Power Sources*, Vol. 178, N°1, pp. 132 – 140, 2008.

[11] J. Peng and S.J. Lee, “Numerical Simulation of PEMFC at High Operating Temperature”, *Journal of Power Sources*, Vol., pp. 1182 – 1191, 2006.

[12] F. Barbir, “PEM Fuel Cells Theory and Practice”, *Elsevier*, 2005.

[13] Mench Matthew M. “Fuel cell engines”. 1st ed. John Wiley & Sons, Inc; 2008.

[14] Q. Yan, H. Toghiani, J. Wu. *J. Power Sources*, 158 (2006) 316.

[15] M.M. Saleh, T. Okajima, M. Hayase, F. Kitamura, T. Ohsaka. *J.Power Sources*, 164 (2007) 503.

[16] Q.Yan, H. Toghiani, H. Causey. *J. Power sources*, 161 (2006) 492.

[17] Danger.M.A., H. “Analysis of the Electrochemical Behaviour of PEMFC using simple impedance models”. Journal of Power Sources. 2008.

[18] Gamry Instruments “Common Equivalent Circuit Models”,2015.

[19] Aparna M. Dhirde, Nilesh V. Dale, Hossein Salehfar, Michael D. Mann, Tae-Hee Han “Equivalent Electric Circuit Modeling and Performance Analysis of a PEM Fuel Cell Stack Using Impedance Spectroscopy” IEEE transactions on energy conversion, vol. 25, no. 3, September 2010.

[20] http://www.balticfuelcells.de/meaE.html

4. Comparative analysis & characterization of the LSC Nafion® and SSC Aquivion® ionomers using EIS.

The polymer electrolyte membrane fuel cell (PEMFC) operates by using a water-dependent, acidic proton conducting polymer membrane as its electrolyte, coupled with platinum-catalysed electrodes. PEMFC cells operate at relatively low temperatures (below 100^{o}C) and can easily nurture its electrical output to satisfy the system's dynamic power requirements. As a result of its relatively low temperatures and the presence of precious metal-based electrodes, PEMFC need to operate on pure hydrogen [1].

The PFSA ionomer is essentially a copolymer of tetrafluoroethylene (TFE) and various perfluorosulfonate monomers. Perfluorosulfonate acid Polymer Electrolyte Membranes (PEM) have the unique ability to provide high power density at relatively low operating temperatures, hence making them very desirable in several fuel cell technology. The most widely used PFSA material has been DuPont's LSC Nafion® ionomer MEA which is based on a perfluoro-sulfonylfluoride ethylpropyl-vinyl ether (PSEPVE) [4-7]. However, this thesis considers another type of PFSA ionomer, which is the short side chain PFSA also known as Aquivion® ionomer. The properties of these two PFSA ionomers were characterised and analysed using the polarization curve, power analysis and Electrochemical Impedance Spectroscopy (EIS) under the same operating and design conditions.

4.1 Experimental Analysis

The Aquivion® and Nafion® MEAs were both prepared under the same conditions using equal %wt, and their performance was contrasted through detailed analysis of their respective

polarization curves, power curves and finally through an electrochemical impedance spectroscopy (EIS) analysis of their respective performance.

4.1.1 Comparative Analysis of the Single Cell Aquivion® and Nafion® Ionomer MEAs.

Nafion® MEA was prepared by HySA Catalysis and was used in the single cell experiment. The operating conditions were the optimized conditions for a 25cm^2 PEMFC hardware fixture, as discussed earlier. The cell was operated at 80^{o}C and the bubbler humidifier temperature was set at 80^{o}C and 75^{o}C at the anode and cathode respectively. The cell was operated at an atmospheric pressure of 1bar for the purpose of stability. The cathode and anode stoichiometry value was set at 2.0 and 1.5 respectively. The Teflon gasketed Nafion® ionomer membrane electrode assembly (MEA) was sandwiched between two AvCarb MB30 GDLs made from carbon fibre paper with a thickness of 0.175mm, a PTFE treatment and micro-porous layer coating.

The resulting geometric electrode area was 25 cm^2. The Nafion® MEA and GDLs were mounted on a 25 cm^2 Baltic PEMFC single cell test fixtures. The test fixture consists of gold plated copper current collector plates at the anode and cathode side, heating cartridges of diameter 6.5 mm, temperature sensing knobs and 2 voltage sensors. The cell fixture offers 5 multi-channel serpentine gas flow field (1mm x 1mm) with robust aluminium end-plates and titanium monopolar plates.

The cathode was supplied with air while the anode was supplied with hydrogen (99.999% purity). The FuelCon Elevator–C test station was used for setting operating conditions through its Visual Basic script which has features for controlling and regulating temperature, supply pressure, back flow pressure, flow rate of reactant and relative humidity. A constant flow rate

of 0.075Nl/min was used at the anode and 0.3Nl/min at the cathode based on the optimized experimental conditions.

The anode and cathode gases were humidified in separate bubbler tubes within the FuelCon test station which ensures an equal and even temperature. The cell fixture was heated using in-built 24Volts DC heating cartridges and the cell temperature was monitored through the use of a thermocouple. A cooling fan was connected to the device to keep the cell temperature at the desired value and avoid over heating of the cell due to overshooting during cell operation.

Similarly, the Aquivion® MEA was set up in the exact same way as the Nafion® MEA as describe above. The two MEAs therefore only differed in the ionomer type used, providing reasonable grounds for comparison.

4.1.2 Initial Conditioning

There is a need to activate the Polymer Electrolyte Membrane Fuel Cells (PEMFC) when it is being used for the first time. This process of activation is referred to as initial conditioning, activation or break-in procedure. One of the main reasons for performing this activation or break-in procedure is to effectively humidify the membrane portion of the MEA that was dried out during the hot press stage of the membrane electrode assembly (MEA) production. MEAs will not work to their full capacity until they are adequately humidified. This initial conditioning period results in an increase in performance of the PEMFC until it reaches its nominal performance. The exact mechanism of this initial conditioning is not completely understood, but it is assumed that during the conditioning process the polymer membrane, as well as the polymer in the catalyst layer, gets humidified, and the number of active catalyst sites increases [11]. How the MEA is initially broken-in can have long lasting effects on the overall performance of the MEA. In this study, we employed a potential cycling activation procedure which entails cycling the potential through 12 cycles between 0.3V and 0.8V, and

the current response was recorded after each cycle. For our single cell testing we set the cell parameters as follows:

- Fuel: Hydrogen, 1.5 Stoichiometry, 100% RH
- Oxidant: Air, 2.0 Stoichiometry, 81% RH
- Temperature (^oC): 80 ^oC
- Pressures (bar): 1bar

This break-in/activation procedure was carried out on three different Nafion® ionomer MEAs and three Aquivion® ionomer MEAs with the same parameters and conditions in order to verify the accuracy of our results. As seen from Table 4.1 and Figure 4.1, the break-in procedure for the Aquivion MEA performed better than the Nafion® MEA with its response current across its three different MEAs between 33-35A while that of the Nafion® was between 30-31A. However, when considering the ease of the breaking in procedure, the number of cycles it took to stabilize, as shown from the distribution in Figure 4.1, the activation process occurred sooner for the Nafion® ionomer compared to Aquivion® ionomer.

Table 4.1: Cyclic Conditioning of Nafion® and Aquivion® Membrane.

	Nafion®						**Aquivion®**					
No of Cycles	**MEA 1**		**MEA 2**		**MEA 3**		**MEA 1**		**MEA 2**		**MEA 3**	
	Voltage	Current	Voltage	Current	Voltage	Current	Voltage	Current	Voltage	Current	Voltage	Current
1	0.297	31.148	0.297	30.852	0.301	30.424	0.3	33.434	0.302	34.974	0.301	35.118
2	0.297	31.888	0.298	31.5	0.297	31.125	0.296	34.129	0.298	33.506	0.297	35.422
3	0.303	31.817	0.299	31.563	0.302	30.536	0.3	34.673	0.305	34.925	0.295	35.239
4	0.3	31.704	0.301	31.28	0.307	30796	0.292	34.891	0.3	34.984	0.294	35.378
5	0.3	31.363	0.3	31.325	0.297	30.583	0.289	34.98	0.297	34.164	0.299	34.541
6	0.301	31.593	0.301	30.824	0.293	30.681	0.299	35.248	0.304	33.953	0.287	34.827
7	0.302	31.467	0.304	31.208	0.3	30.776	0.299	35.495	0.305	33.909	0.298	35.002
8	0.299	31.363	0.297	30.658	0.301	30.057	0.291	34.635	0.298	33.948	0.302	34.719
9	0.296	31.378	0.3	30.793	0.3	30.063	0.297	34.653	0.299	34.524	0.3	34.68
10	0.3	31.098	0.3	31.059	0.301	30.934	0.297	34.472	0.303	34.686	0.299	34.776
11	0.293	31.225	0.302	31.323	0.299	30.912	0.312	34.222	0.298	34.706	0.302	34.587
12	0.299	31.36	0.299	31.333	0.299	30.688	0.302	34.659	0.302	34.839	0.301	34.833

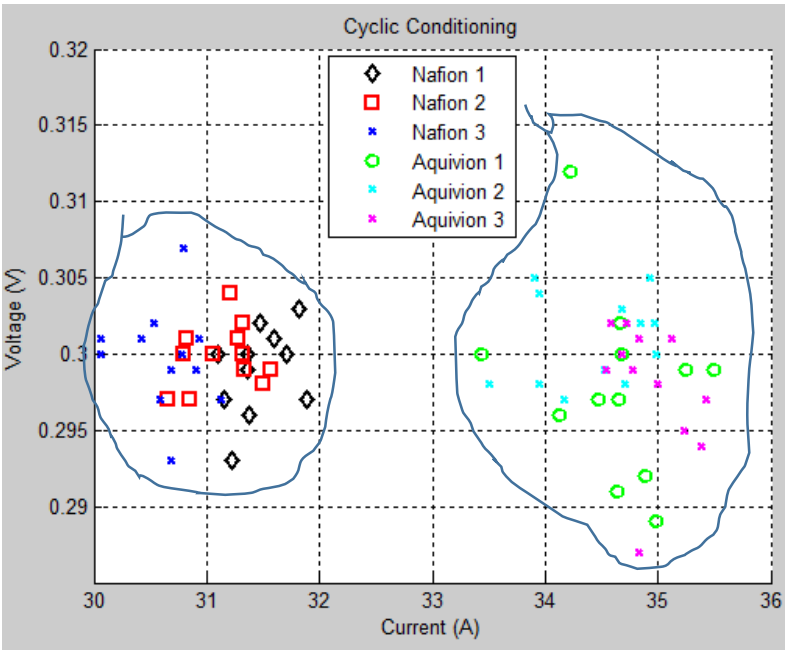

Figure 4.1: Cyclic conditioning plot of Aquivion and Nafion® MEA.

As discussed earlier, both Nafion® and Aquivion® MEAs require adequate humidification to maintain proton conductivity through the MEA's operation life-cycle [12, 13]. Both Nafion® and Aquivion® ionomers were prepared such that they have the same weight percentage (28%) in the MEA, forming the basis for justifying the comparison.

However, the Aquivion® short-side chain MEAs has better ionic conductivity at the point of cyclic conditioning break-in voltage of 0.3V compared to the Nafion® long-side chain MEAs. The possible explanation for this is that there is an easy ionic flow of the hydrated ions through the sulphonated groups in the Aquivion® MEA due to its short side chain when compared to the long side chain of the Nafion® MEA, hence this more rapid movement explains the higher conductivity experienced by the Aquivion® membrane during break-in process.

4.2 Polarization Curve Analysis

The polarization curve, as discussed in Section 2.11.1, displays the voltage output of the fuel cell for a particular current density loading. The polarization curve analysis was carried out on

the FuelCon test station by programming the load to increase by a certain step-size and the voltage response recorded over the cell's active area of 25cm^2. To further analyse the performance of the Aquivion® MEA in contrast to the Nafion® MEA, an analysis of the polarization curve for both MEAs was performed under the same operating and design conditions in this section. Figure 4.2 shows a pictorial representation of the polarization curves for the two MEAs.

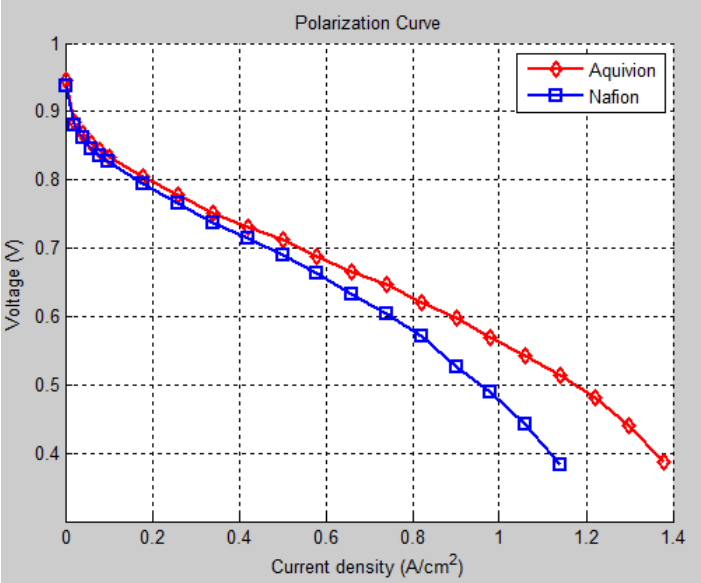

Figure 4.2: Polarization Curve Analysis of Nafion® and Aquivion® MEAs.

The fuel cell characteristic is typically depicted by the relationship between its output voltage and current. The polarization curve in Figure 4.2 is a widely used electrochemical analytical index of the performance of tested Aquivion® and Nafion® single cell MEAs. Typically, the operating voltage is determined by the standard-reversible voltage while accounting for the three types of losses, as discussed in section 2.11. These losses are worth studying to better understand their resultant effect on the reduction factor of PEMFC output. Several models and methods have been proposed in literature to elucidate the electrochemical behaviour of a PEMFC, analyse and quantify these losses holistically and individually [1 - 11]. Amphlett et al. developed a mechanical model to analyse the PEMFC and were able to separate the

activation and ohmic loss [4]. Springer et al. developed a limited model of Nafion® membrane [3]. Kim et al. using a simple empirical equation was able to isolate the different losses [13]. Squadrito et al. proposed an advanced model for analysing the concentration loss of Kim et al.'s Equation [5, 1]. Kocha and Gasteiger independently used a different approach to separate the activation and concentration loss by basing their work on analysing the IR-free voltage versus log-scaled current density plot [9, 10]. However in this work, we have employed a simple semi-empirical model that is proven to be representative of the PEMFC [1, 5] to analyse and determine the quantity of these losses within the different types of membranes.

4.3 Empirical Modelling of PEMFC

Empirical fuel cell models, are essentially used to reproduce experimentally-derived fuel cell performance data. Hence, empirical models are usually quite limited in their performance prediction capability. However, these models have been applied in many application-oriented analysis in scientific and industrial research simply because they are easy to calibrate, robust and fast. Primarily, empirical fuel cell models do not require any material or design properties of the modelled fuel cell hardware, rather, they are calibrated with a limited number of individual current/voltage measurement [20].

In this study, we used a single analytical equation to model/ represent the measured polarization curve consisting of a number of individual current/voltage measurement. Through a mechanistic similarity, the basic electrochemical theory as introduced in Section 2.5.2 was used to introduce a simple equation that fits the experimental data over the entire range of current density with optimum accuracy. The resulting equation was tested and appeared to be accurate under several experimental conditions. Using experimental data derived with a 25cm^2 H_2/air single cell using both Aquivion® and Nafion® MEAs, we were able to analyse, quantify and

contrast the degree of activation polarization, ohmic losses, and mass transfer losses in both membranes.

The output cell voltage as discussed earlier in Section 2.5.2, E_{cell}, is expressed as follows:

$$E_{cell} = E^o - \eta_{act} - \eta_{ohmic} - \eta_{con} \quad (4.1)$$

Where E^o is the initial voltage,η_{act}, η_{ohmic}, and η_{con} are the activation loss, ohmic loss, and concentration loss due to mass transport, respectively.

The work presented here extensively follows the review of the various empirical models done by Dong et al. [16] and Yutaro et al. [20]. Diverse empirical fitting equations were extracted from various works in literature and tested for conformity. Starting with the empirical equation of Kim et al. [13, 16]

$$E_{cell} = E^o - blog(i) - Ri - mexp(ni) \quad (4.2)$$

Where *m* and *n* concentration loss fitting parameters and *b* is the Ohmic loss fitting parameter. Following up on Kim's work, several improved models were formulated with the aim of modifying the mass transfer loss term. Lee et al. [14] proposed the model below, where P_o is the total pressure (Pa) and P_{O2} is the Partial pressure of Oxygen (Pa)

$$E_{cell} = E^o - blog(i) - Ri - mexp(ni) - blog\left[\frac{P}{P_{o2}}\right] \quad (4.3)$$

Developing on the earlier models, Squadrito et al. [25] proposed the modified model below where $\propto_s, k \; and \; \beta_s$ are all concentration loss fitting parameters.

$$E_{cell} = E^o - blog(i) - Ri - \propto_s i^k ln(1 - \beta_s i) \quad (4.4)$$

The model of Chu et al. [16] can be described as

$$E_{cell} = E^o - blog(i) - Ri - mexp(ni) - blog\left[\frac{P}{P_{o2}}\right] \quad (4.5)$$

Following the previous work, Xia and Chan [17] proposed an improvement of the above models and their work produced the model below:

$$E_{cell} = E^o - blog(i) - Ri - i_m exp(ni_m) \quad (4.6)$$

Pisani et al. [19] still working on the improving the mass transfer loss term proposed that:

$$E_{cell} = E^o - blog(i) - Ri - a_p \ln(1 - \frac{i}{i_l} S^{-\mu(1-i/i_l)}) \quad (4.7)$$

S and a_p are the mass transport overvoltage fitting parameter, μ is viscosity (kg m^{-1} s^{-1}) As can be clearly observed from the different models above, each is a derivative of Kim's work with only the mass action loss being the distinguishing factor in all of them. Each of these models consists of a constant voltage fitting parameter, a logarithmic term for the purpose of approximating the activation loss, a linear term depicting the ohmic loss, and one or two terms representing the mass transfer loss. The *log(i)* term in this model makes it very difficult to accurately predict the OCV and cell performance under lightly loaded conditions, because this term tends to infinity as the current density decreases to zero.

Fraser and Hacker [18] executed some modifications to Kim's model and presented a model as follows:

$$E_{cell} = E^o - blog\left(\frac{i + i_{loss}}{i_o}\right) - Ri - mexp(ni) \quad (4.8)$$

For a PEMFC, the initial voltage E^o, is equal to the thermodynamic potential, also known as reversible potential. It is calculated from the modified Nernst Equation (2.11):

$$E^o = E + \frac{\Delta\hat{s}}{nF}(T - T_0) - \frac{RT}{nF} ln\left(\frac{a_{H2O}}{a_a * a_c^{1/2}}\right) \quad (4.9)$$

where *E* denotes the standard-reversible voltage; $\Delta\hat{s}$ denotes the entropy of reaction; n is the number of electrons transferred in the reaction; *F* is Faraday's constant; *T* is the fuel cell

temperature; T_o is the reference temperature; a_{H2O}, a_a, and a_c denote the activities of water, anode gas, and cathode gas, respectively; R is the universal gas constant. From the works of Haji, using basic thermodynamics theory, the values of the above parameters were obtained to be: E = 1.229V, $\Delta\hat{s}$ = −163.23 J/mol K, n = 2, F = 96485.35 C/mol, T_0 = 298.15 K, R = 8.314 J/mol K, a_{H2O} = 1, a_a = 0.1, a_c = 0.21 (Air) or 1 (O_2). ΔG, is assumed to be 237.2 kJ/mol [28].

After reviewing existing models of polarization curves, Yutaro and Keiichi [20] developed a semi-empirical model that takes into consideration the fuel cell's operating temperature.

$$V = E_{thermo(T)} - T[b + aln(i)] - b\frac{\Delta G}{R} - R_{ohmic(T)} * i - m_{(T)}\exp(n * i) \qquad (4.10)$$

Yutaro's model [20] and Kim's model [13] gave the best representation of the fuel cell's polarization curve. Hence, we used these models to analyse differences between the Nafion® and Aquivion® MEA polarization curves. For fitting the measured data and the equations, we used the Matlab Curve Fitting tool to perform regression analysis by using the non-linear least squares method and Levenberg-Marquardt algorithm with a bisquare robust method to fit a line through the set of data.

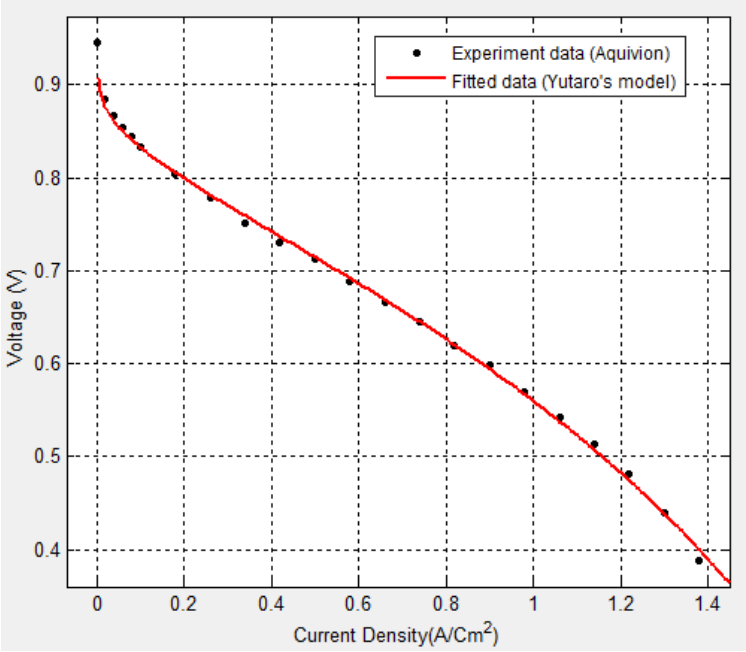

Figure 4.3(a): Yutaro's polarization curve model of the Aquivion® MEA.

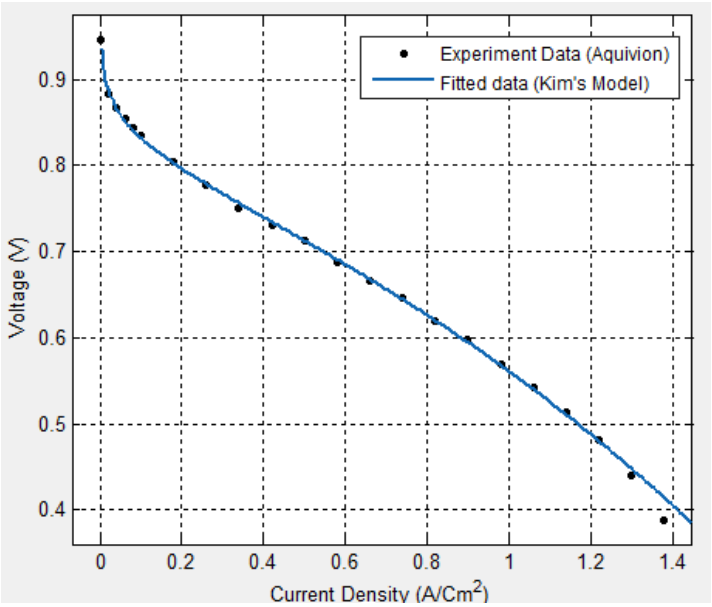

Figure 4.3(b): Kim's polarization curve model of the Aquivion® MEA.

Figures. 4.3(a) and 4.3(b) showed the Aquivion® MEA polarization curve fitted to Yutaro's model and Kim's model respectively and Figures 4.4(a) and 4.4(b) showed the Nafion® MEA polarization curve fitted to Yutaro's and Kim's model respectively for a cell operated at 80°C.

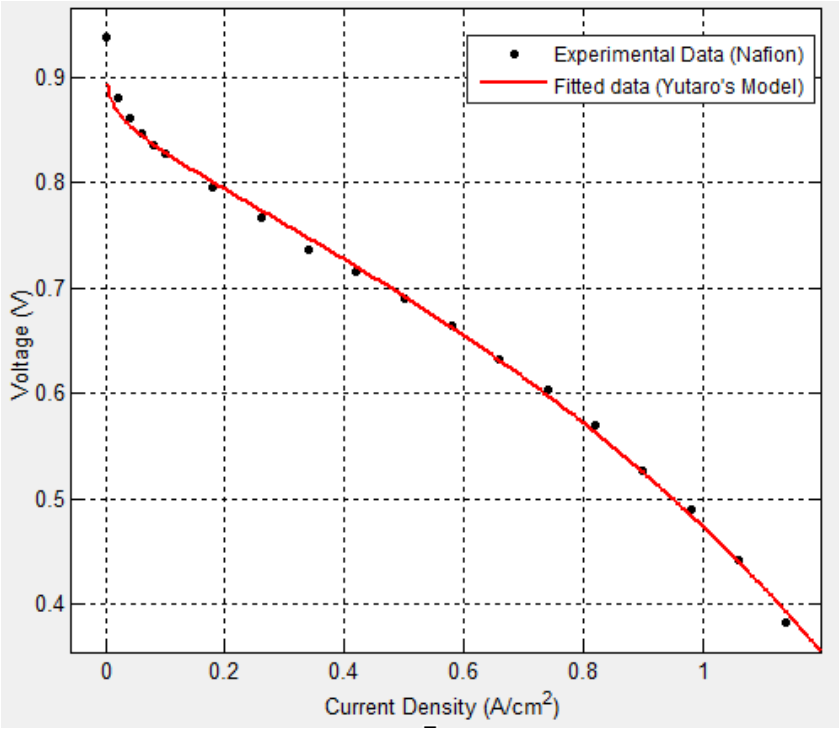

Figure 4.4(a): Yutaro's polarization curve model of the Nafion® MEA.

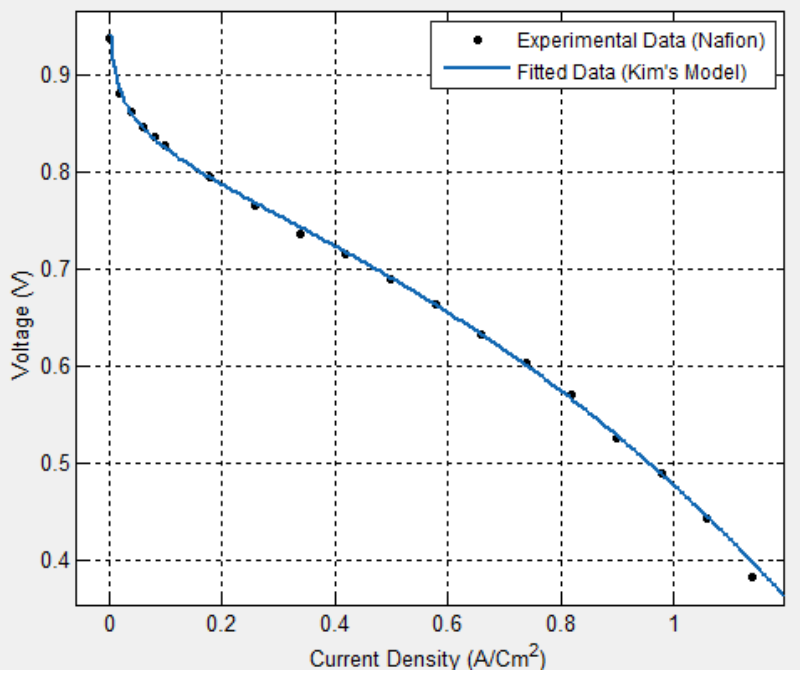

Figure 4.4(b): Kim's polarization curve model of the Aquivion® MEA.

From Tables 4.2 and 4.3, it is established that there is a good fit for both Equations, with the models fitting the data quite well and the correlation coefficients R_{corr} were greater than 0.99. The internal resistance R_{ohmic} is the core basis for our comparison since it is an indication of the cell performance. From both Yutaro's and Kim's model, it is clearly observed that the ohmic resistance for the Nafion® MEA was greater than the Aquivion® MEA's ohmic resistance. In Kim's model, the ohmic resistance of the Nafion® membrane is almost double of the Aquivion® membrane. This result is in alignment with what is obtainable in literature, Stassi et al. [8]. In their work, it was found that the ohmic resistance is only $0.11\Omega cm^2$ for the Aquivion® and in the case of Nafion® it is about twice, i.e. $0.23\Omega cm^2$. This disparity in ohmic resistance can be explained from analysis of the differences in ionomer in both MEAs. The presence of the Aquivion® ionomer in the MEA offers enhanced proton conductivity due to its shorter chain length, thus creating more space for electrons to effectively participate in the electronic conduction process, thus resulting in lower ionic and membrane resistance compared to the LSC Nafion® ionomer MEA [7].

The fitting parameter of the activation loss, *A*, was in alignment with previous studies since it falls within the range of 0.020–0.028V [24 -27]. The activation loss value *A* for Nafion® was higher compared to the Aquivion® MEA, indication that the activation overpotential loss would be higher for the Nafion® MEAs compares to the Aquivion® MEAs.

Table 4.2: Yutaro's model fitting for the MEAs

	R_{corr}	R_{ohmic} [Ωcm^2]	a [V]	b [V]	m [V]	n [cm^2/A]
Aquivion®	0.9986	0.1792	4.816e-05	0.001021	0.01566	1.76
Nafion®	0.9988	0.2258	3.213e-05	0.0008955	0.0169	2.153

Table 4.3: Kim's model fitting for the MEAs

	R	R_{ohmic}	A [V]	m [V]	n [cm^2/A]
Aquivion®	0.9986	0.1015	0.02802	0.4471	0.5429
Nafion®	0.9989	0.2123	0.02971	0.4592	0.7411

The concentration loss parameters *m* and *n* from the proposed equations for both models shows the Nafion® MEA having higher values compared to the Aquivion® MEA which indicates that the mass transfer losses for the Nafion® MEA is higher than that of the Aquivion® MEA. The fitting parameter of the concentration loss *n* is higher for the Nafion® MEA than the Aquivion® MEA likely due to the flooding on the surface due to water percolation on the surface as a result of slower reaction

4.4 EIS Analysis and Results

EIS was used to study the several electrochemical processes which takes place within the PEMFC when it is electrically stimulated. By analysing the electrical response, we endeavour to determine the Aquivion® and Nafion® MEA electrolyte resistance, kinetic and mass transport polarization losses. The EIS characterization used in this work cannot reproduce all

microscopic effects, but rather, we were only able to use it to determine the fundamental properties and dominant loss factors in the PEMFC, and how they relate with and depend on controlled variables provided by pre-set experimental conditions such as current density, temperature, fuel composition, and humidification [28].

The impedance data was taken using TrueData-EIS software which preformed galvanostatic impedance measurements over a frequency range of 0.1 Hz to 30 kHz. During the process of obtaining the impedance measurements, the system draws a small direct current (DC) while superimposing a small magnitude of alternating current (AC) – about 10% of the DC value. The EIS measurement was repeated for current density values of 100m A/cm^2, 300m A/cm^2, 800m A/cm^2 and 1000m A/cm^2 for both Aquivion® and Nafion® ionomer MEAs. These points were chosen to represent different sections of the polarization curves. The acquired data were then fitted to the equivalent circuit model (ECM), described earlier in Figure 3.16 using the EC-Lab software. The EC-lab software uses a combination of Randomize and Simplex least-square nonlinear fitting algorithm to determine the path of best fits for different data points.

The experimental data and their resulting fits are shown in Figures 4.5 - 4.9 for both Aquivion® and Nafion® MEAs respectively. These values were used to derive fitting functions that describe the circuit parameters as nonlinear functions of the current operating point and are fitted using a complex nonlinear statistical least-square fitting technique to attain representative values for the equivalent circuit components.

Table 4.4: Fitted values for the 100m A/cm^2 EIS – ECM data

Parameter	R_m	$R_{ct,\,A}$	$R_{ct,\,C}$	$C_{dl,\,A}$ (mF)	$C_{dl,\,C}$ (mF)	L(H)	Z_w
Aquivion	2.619	2.298	16.470	0.161	1.213	0.081	1.340
Nafion	2.645	12.000	18.410	1.148	3.599	0.059	5.162

Note: $R_m = R_\Omega$ = Membrane Resistance

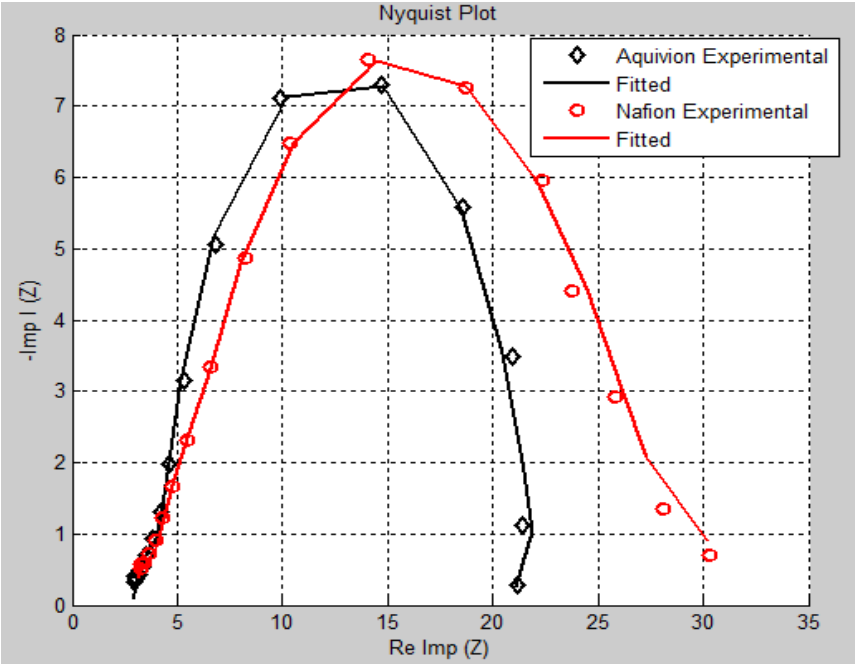

Figure 4.5: Nyquist plot of EIS measurement at 100m A/cm^2

Table 4.5: Fitted values for the 300m A/cm^2 EIS – ECM data

Parameter	R_m	$R_{ct,A}$	$R_{ct,C}$	$C_{dl,A}$ (mF)	$C_{dl,C}$ (mF)	L(H)	Z_w
Aquivion	0.231	3.058	10.320	3.003e-3	0.943	0.157e-3	8.072
Nafion	0.238	3.389	11.77	0.831e-3	3.599	0.277e-3	8.763

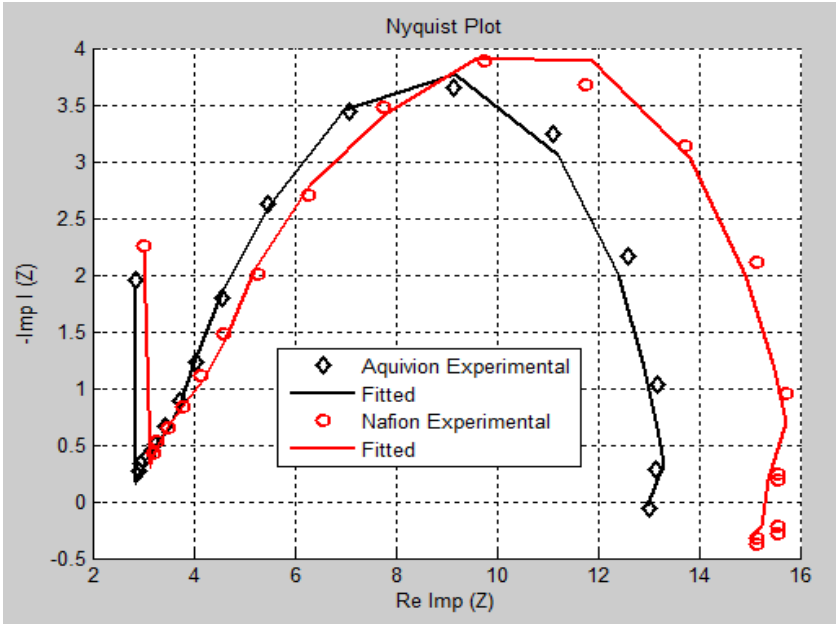

Figure 4.6: Nyquist plot of EIS measurement at 300m A/cm^2

Table 4.6: Fitted values for the 800m A/cm^2 EIS – ECM data

Parameter	R_m	$R_{ct,A}$	$R_{ct,C}$	$C_{dl,A}$ (mF)	$C_{dl,C}$ (mF)	L(H)	Z_w
Aquivion	0.079	3.449	19.540	2.289e-3	1.479	0.218	4.322
Nafion	0.089	4.763	23.060	3.651e-3	1.033	0.443	7.199

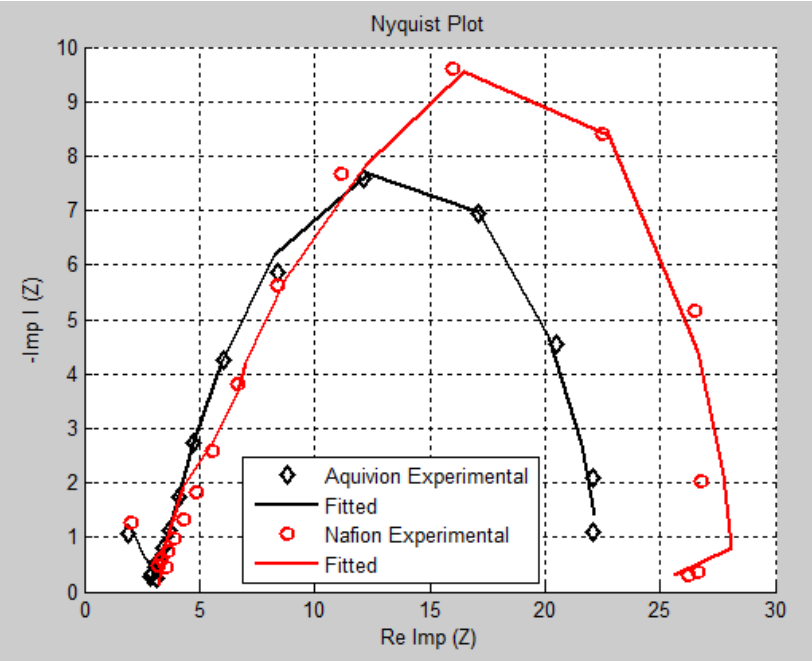

Figure 4.7: Nyquist plot of EIS measurement at 800m A/cm^2

Table 4.7: Fitted values for the 1000m A/cm^2 EIS – ECM data

Parameter	R_m	$R_{ct,A}$	$R_{ct,C}$	$C_{dl,A}$ (mF)	$C_{dl,C}$ (mF)	L(H)	Z_w
Aquivion	0.060	3.297	34.21	0.718	1.625	0.238	7.337
Nafion	0.061	3.601	47.49	1.063	1.045	0.388	9.420

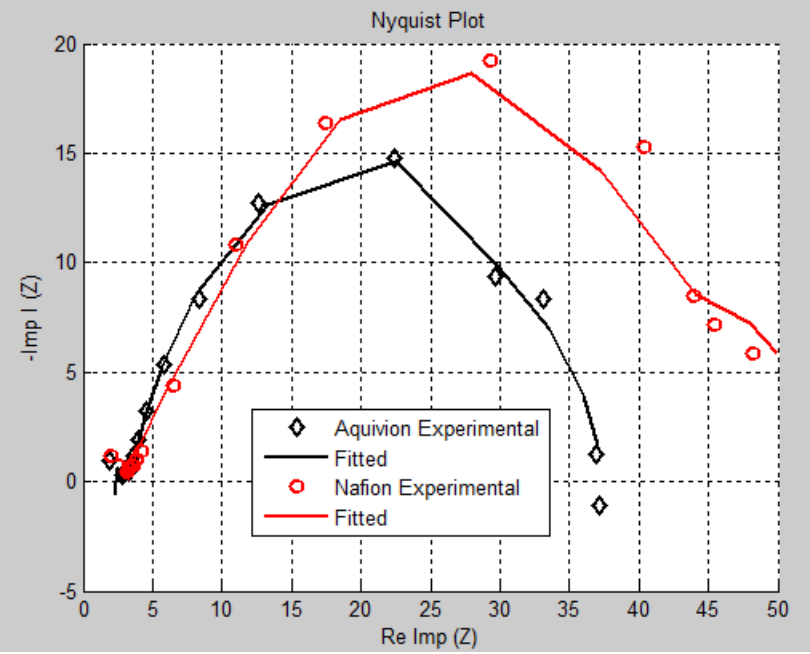

Figure 4.8: Nyquist plot of EIS measurement at 1000m A/cm^2

From Tables 4.3 - 4.7 it is observed that the membrane resistance (R_m) decreases with increasing load from 4A (100m A/cm^2 Current density) to 40A (1000m A/cm^2 Current density) across both MEAs. Such behaviour can be as a result of an increase in charge transport due to an increase in the reaction kinetics and temperature at higher current density values. The back diffusion of water taking place at high current density will also increase the water content in the membrane hence leading to an increase in membrane humidity. Since the membrane resistance is the main contributor to the ohmic resistance, a well-hydrated membrane will result in an overall reduction in electronic and protonic resistances in the fuel cell.

The Aquivion® MEA has a lower ohmic resistance compared to the Nafion® MEA, hence indicating that the Aquivion® MEA has an overall higher conductivity compared to Nafion® MEA. Another attributing factor could be the thickness of both MEAs. The Aquivion® MEA has a thickness of 30µm compared to the Nafion® membrane with 50µm, hence the ohmic resistance per cell area is minimized for the Aquivion® membrane due to its thinness compared to the Nafion® membrane.

The anodic $CPE_{dl,A}$ and $R_{ct,A}$ are observed at higher frequencies compared to their cathodic counterpart. This is because the electrochemical rate at the cathode is slow compared to that of the anode, as a result, the RC time constant of the oxygen reduction reaction at cathode has a higher $R_{ct,C}$. The reaction kinetics of the charge transfer at the anode and cathode cannot be differentiated visually, as the cathode and anode arcs overlaps with the cathode arc dominating the whole process [30]. From the extracted parameter values summarized in Tables 4.2 – 4.6, it was observed that $R_{ct,A}$ is small compared to $R_{ct,C}$ for the entire load current range. From the merged cathode and anode impedance arcs, the effective fuel cell charge transfer resistance (R_{ct}) is the sum of both, i.e.

$$R_{ct} = R_{ct,A} + R_{ct,C} \tag{4.11}$$

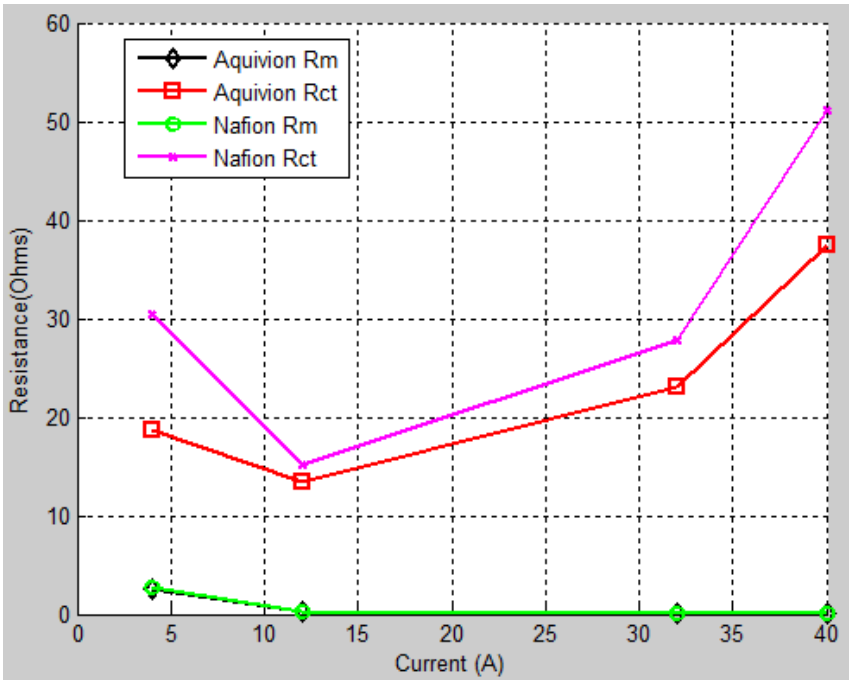

Figure 4.9: Variation of ohmic (R_{Ω}) and charge transfer (R_{ct}) with current.

The charge transfer resistance is very high compared to the ohmic resistance as shown in Figure 4.9. The Nafion® MEA has a larger charge transfer resistance compared to the Aquivion®,

thus indicating that the Aquivion® MEA boasts of a faster reaction kinetics compared with the Nafion®.

The low frequency mass transport impedance as seen from Tables 4.3 – 4.7 is higher in the Nafion® MEA compared to the Aquivion® MEA. High mass transport impedance, indicating that it takes more time for the reactants to move and penetrate further into the GDLs and electrocatalyst at both electrodes for the Nafion® compared to the Aquivion® MEA [30].

Overall, from the EIS analysis, shows that the Aquivion® MEA performs better than the Nafion® MEA as it has lower values for the ohmic losses, charge transfers losses and mass transfer losses. Polarization curves of both membranes also shows that the Aquivion® membrane is the better performing of the two.

References

[1] F. Barbir, "PEM Fuel Cells Theory and Practice", *Elsevier,* 2005.

[2] V. N. Postnov, N. A. Mel'nikova*, G. A. Shul'meister, A. G. Novikov, I. V. Murin, and A. N. Zhukov "Nafion- and Aquivion-Based Nanocomposites Containing Detonation Nanodiamonds" Russian Journal of General Chemistry, 2017, Vol. 87, No. 11, pp. 2754–2755.

[3] B Luo, Z Chen "Comparative Experimental Study on Ionic Polymer Mental Composite based on Nafion and Aquivion Membrane as Actuators" IOP Conf. Series: Materials Science and Engineering 269 (2017).Panchenko A. "Polymer electrolyte membrane degradation and oxygen reduction in fuel cells: an EPR and DFT investigation." Ph.D. thesis, Institute für Phzsikalische Chemie der Universität, Stuttgart, 2004.

[4] LaConti AB, Hamdan M, McDonald RC. "Mechanisms of chemical degradation". In. Handbook of fuel cells: fundamentals, technology, and applications, vol. 3. John Wiley and Sons; 2003;647–62.

[5] Jiujun Zhang "PEM Fuel Cell Electrocatalysts and Catalyst Layers Fundamentals and Applications" Springer, 2008.

[6] A. Ghielmi et al., J. Power. Source., 145, 108-115, Fig. 3 (2005).

[7] M. Gebert, A. Ghielmi, L. Merlo, M. Corasaniti, and V. Arcella "AQUIVION™ -- The short-side-chain and low-EW PFSA for next-generation PEFCs expands production and utilization" Solvay Solexis S.p.A., viale Lombardia 20, I-20021 Bollate (MI), Italy ECS Transactions, 26 (1) 279-283 (2010).

[8] A. Stassi, I. Gatto, E. Passalacqua, V. Antonucci, A.S. Arico,, L. Merlo, C. Oldani ,E. Pagano "Performance comparison of long and short-side chain Perfluorosulfonic membranes for high temperature polymer electrolyte membrane fuel cell operation" Journal of Power Sources 196 (2011) 8925–8930.

[9] A. S. Aricò*, A. Di Blasi, G. Brunaccini, F. Sergi, G. Dispenza, L. Andaloro, M. Ferraro, V. Antonucci, P. Asher, S. Buche, D. Fongalland, G. A. Hards, J. D. B. Sharman, A. Bayer, G. Heinz, N. Zandonà, R. Zuber, M. Gebert, M. Corasaniti, A. Ghielmi, D. J. Jones "High Temperature Operation of a Solid Polymer Electrolyte Fuel Cell Stack Based on a New Ionomer Membrane" WILEY-VCH Verlag GmbH & Co. KGaA, Weinheim 2010.

[10] Bezmalinović D, Radošević J, Barbir F "Initial conditioning of polymer eelectrolyte membrane fuel cell by temperature and potential cycling" Acta Chim Slov. 2015;62(1):83-7. PubMed PMID: 25830963.

[11] J. Peron, A. Mani, X. Zhao, D. Edwards, M. Adachi, T. Soboleva, Z. Shi, Z. Xie, T. Navessin, S. Holdcroft, J. Membr. Sci. 356 (2010).

[12] P. Majsztrik, A. Bocarsly, J. Benziger, "Water permeation through Nafion membranes: the role of water activity" J. Phys. Chem. B 112 (2008) 16280.

[13] J. Kim, S.-M. Lee, S. Srinivasan, and C. E. Chamberlin, "Modeling of proton exchange membrane fuel cell performance with an empirical Equation," Journal of the Electrochemical Society, vol. 142, no. 8, pp. 2670–2674, 1995 V.

[14] J. H. Lee, T. R. Lalk, and A. J. Appleby, "Modeling electrochemical performance in large scale proton exchange membrane fuel cell stacks," Journal of Power Sources, vol. 70, no. 2, pp. 258–268,199.

[15] D. Chu, R. Jiang ,and C. Walker, "Analysis of PEM fuel cell stacks using an empirical current-voltage Equation," Journal of Applied Electrochemistry, vol. 30, no. 3, pp. 365–370, 2000.

[16] Dong Hao, Jianping Shen, Yongping Hou, Yi Zhou, and Hong Wang "An Improved Empirical Fuel Cell Polarization Curve Model Based on Review Analysis" International Journal of Chemical Engineering Volume 2016, Article ID 4109204.

[17] Z. T. Xia and S. H. Chan, “Analysis of carbon-filled gas diffusion layer for H2/air polymer electrolyte fuel cells with an improved empirical voltage-current model,” International Journal of Hydrogen Energy, vol. 32, no. 7, pp. 878–885, 2007.

[18] S. D. Fraser Æ V. Hacker. “An empirical fuel cell polarization curve fitting Equation for small current densities and no-load operation” J Appl Electrochem (2008) 38:451–456.

[19] L. Pisani, G. Murgia, M. Valentini, and B. D. Aguanno, “A new semi-empirical approach to performance curves of polymer electrolyte fuel cells,” Journal of Power Sources, vol. 108, no. 1, pp. 192–203, 2002E.

[20] Yutaro Akimoto & Keiichi Okajima “Semi-Empirical Equation of PEMFC Considering Operation Temperature” Energy Technology & Policy (2014) 1, 91–96.

[21] A. Ghielmi, P. Vaccarono, C. Troglia, V. Arcella, J. Power Sources 145 (2005) 108–115.

[22] Pisani, L.; Murgia, G.; Valentini, M.; D’Aguanno, B. A New Semi Empirical Approach to Performance Curves of Polymer Electrolyte Fuel Cells. J. Power Sources 2002, 108, 192–203.

[23] Chaddie, D.; Munroe, N. Review of Comparison of Approaches to Proton Exchange Membrane Fuel Cell Modeling. J. Power Sources 2005, 147, 72–84.

[24] Laurencelle, F.; Chahine, R.; Hamelin, J.; Agbossou, K.; Fournier, M.; Bose, T. K.; Laperriere, A. “Characterization of a Ballard MK5- E Proton Exchange Membrane Fuel Cell Stack”. Fuel Cells 2001, 1, 66–71.

[25] Squadrito, G.; Maggio, G.; Passalacqua, E.; Lufrano, F.; Patti, A. “An Empirical Equation for Polymer Electrolyte Fuel Cell (PEFC) Behavior.” J. Appl. Electrochem. 1999, 29, 1449–1455.

[26] Haji, S. “Analytical Modeling of PEM Fuel Cell i-V Curve”. Renew. Energ. 2011, 36, 451–458.

[27] Larmine, J.; Dicks, A. “Fuel Cell Systems Explained”. Wiley: West Sussex, 2003.

[28] Danger.M.A., H. “Analysis of the Electrochemical Behaviour of PEMFC using simple impedance models”. Journal of Power Sources. 2008.

[29] X. Yuan, J. C. Sun, M. Blanco, H. Wang, J. Zhang, and D. Wilkinson, “AC impedance diagnosis of a 500 W PEM fuel cell stack, Part I: Stack impedance,” J. Power Sources, vol. 161, pp. 920–928, Jun. 2006.

[30] R. O’Hayre, S. Cha, W. Colella, and F. B. Prinz, “Fuel Cell Fundamentals”. New York: Wiley, 2006.

5. MEA degradation –life cycle test of the Nafion® and Aquivion® ionomer using Accelerated Stress Test

Durability is a key property that determines the overall efficiency of PEMFC operation. It is possible for one to investigate the reliability and life cycle prediction of a PEMFC through series of steady-state lifetime tests. However, this kind of study is very time consuming and also expensive. Hence, to accelerate the life cycle test of the fuel cell, several studies have postulated various ways of inducing accelerated lifetime test, to enable efficient prediction of the performance, durability and reliability of the PEMFC [1-3]. An accelerated stress test (AST), usually involves the use of factors that significantly influence the performance of the PEMFC such as relative humidity, temperature, pressure and load as stressors. In PEMFC operations, high voltage and transient conditions coupled with improper cell temperature and water management can induce unexpected changes in system performance. Also, conditions such as fuel starvation, thermal and potential cycles or improper start and stop procedures can have damaging effect on the PEMFC if repeated over a long period. In order to carry out a prognostic test on the PEMFC's life cycle degradation mechanism, in-situ or ex-situ diagnostic methods can be used to examine the rate of component and performance degradation under specific working conditions.

Generally, most of the in-situ and ex-situ AST degradation tests are carried out on the MEA. It tries to isolate the extent the membrane, platinum catalyst, gas diffusion layers (GDL) and even the carbon support undergoes degradation or damage, and the effects of this degradation on the overall cell performance. For proper prognosis and diagnosis of various components degradation, there is a need to consider both the mechanical and chemical properties of each component and how they change under external AST procedures. In this study, the life cycle

response to degradation of both the Aquivion® and Nafion® MEA under induced AST techniques which target the overall MEA durability are investigated.

5.1 MEA Degradation

As earlier discussed, the MEA lies at the heart of the PEMFC. The MEA is made up of the membrane, GDLs and the catalyst layers. The membrane works in a two-way protocol acting as an electrolyte that enables proton conduction/transfer from the anode to the cathode and at the same time as an impermeable barrier for both gases and electrons between the anode and the cathode. The PFSA ionomers are added to the catalyst surface area in order to enhance proton conduction. In the right quantity they enhance the PEMFC performance and in excess proportion they stand the possibility of inhibiting the PEMFC's performance by blocking the Pt sites. In this work, we will be comparing both the widely used long-side chain (LSC) Nafion® and the short side chain (SSC) Aquivion® PFSA ionomer MEAs under exposure to same degradation techniques and conditions.

From various literature on membrane degradation mechanisms, it has been ascertained that typical membrane degradation in a PEMFC results from thermal, chemical and mechanical degradation. As earlier discussed in Section 2.10.4, the thermal degradation is as a result of dehydration of the membrane when operated under very low humidity or very high temperature conditions, thereby resulting in loss of proton conductivity [4]. Mechanical degradation occurs when there are cracks, tears, punctures, and pinholes formation in the membrane either due to the presence of foreign particles or fibres introduced during the MEA fabrication process hence perforating the membrane [5, 6]. On the other hand, chemical degradation originates from chemical attack by hydrogen peroxide radicals which is commonly associated with the presence of oxygen at the anode side. Thus, production of radicals is directly related to the gas crossover phenomena and accelerated by the above mentioned operating conditions. This

results in breaking the membrane's backbone and group's side-chain thereby causing subsequent loss of mechanical strength and proton conductivity. Eventually, this leads to an increase in resistance and declining cell performance [7-8].

Some common stress factors that have been discovered to affect the membrane's thermal and chemical stability includes high temperatures (HT) combined with low relative humidity (LRH) and high voltage (HV) conditions [8]. These conditions are considered in this work as the main stress factors related to the membrane degradation modes and used as accelerating variables. In this study, we employed the standard protocols – humidity drive cycle test for AST application in PEMFC domain as proposed by the U.S. Department of Energy (DOE) - [9]. The DOE protocols evaluate the durability of the MEA under load cycling conditions, at high and low humidity.

5.2 Analysis, Experiments and Results

Both the Nafion® and Aquivion® MEAs were prepared as earlier discussed in Section 4.4.2. The polarization curve analysis as well as EIS plot of the membranes were carried out, under the conditions established in Chapter 4. It was observed that the Aquivion® MEA performed better than the Nafion® MEA. However, using the AST protocol as presented in the DOE template for testing MEA durability, which involves a series of relative humility (R.H) cycling under both wet and dry conditions simultaneously with load cycling of the MEA under very low and high current loadings. Using this technique, the degradation process was accelerated to give results on irreversible degradation of the cell over a 24 hour cycle operation.

5.2.1 AST Degradation Protocol

The AST degradation test was carried out on the FuelCon Elevator–C test station. Both Aquivion® and Nafion® MEAs prepared in HySA Catalysis laboratory was used in the single cell AST experiment. The operating conditions were the optimized conditions for a 25cm^2

PEMFC hardware fixture as indicated in the DOE protocol shown in Table 5.1. The protocol incorporates operating conditions that are expected to occur during typical operation of PEMFC devices e.g. a PEMFC vehicle, but it excludes conditions associated with unmitigated start-ups and shutdowns, freeze operation, fuel starvation, and system fault conditions. The cell was operated at 80^{o}C and the bubbler humidifier temperature was cycled between wet condition at 80^{o}C at the cathode inlet and 75^{o}C at the anode inlet, while the dry conditions relative humidity was at 0^{o}C. The dry condition is achieved by switching off the bubbler humidifier completely. The cell was cycled between alternating loads of 1.2 and 0.02 A/cm^2 each for 5 cycles, and between 5 cycles of 0.1 and 0.02 A/cm^2 for the dry relative humidity cycle. Each relative humidity (RH) cycle between wet and dry conditions lasted for 10 minutes and the process was repeated over a 24 hour period. A 2 minutes transition time was allowed while operating the cell at 0.6 A/cm^2 current density to allow for some transition between the wet and dry RH cycle. The 5 minutes hold in step RH20 as observed in Table 5.1 was intended to represent a system idle point to represent the end of a complete cycle and set the pace for a new cycle. Figure 5.1 gives an overview of the load profile used in this work.

The cell was operated at atmospheric pressure of 1bar for the purpose of stability. The cathode and anode stoichiometry value was set at 2.0 and 1.5 respectively. The Teflon gasketed Nafion® membrane electrode assembly (MEA) was sandwiched between two AvCarb MB30 GDLs made from carbon fibre paper with a thickness of 0.175mm, a PTFE treatment, and micro-porous layer coating. The MEAs and GDLs were mounted on a 25 cm^2 Baltic PEMFC single cell test fixtures. The test fixture consists of gold plated copper current collector plates at the anode and cathode side, heating cartridges of diameter 6.5 mm, temperature sensing knobs and 2 voltage sensors. The cell fixture offers 5 multi-channel serpentine gas flow field (1 mm x 1mm) with robust aluminium end-plates and titanium monopolar plates.

Usually, the drive-cycle testing reflects only degradation losses associated with wet and dry cyclic operation. However, in this test, extra stress was placed on the MEA as a result of the load cycling. Other relevant stressors, including start-up/shutdown and freeze operation, are not included in this test. The same protocol was applied for both PFSA ionomers to give grounds for justifiable comparison. As an AST strategy, the load-cycling profile of a fuel cell has been found to affect the overall lifetime of the PEMFC significantly.

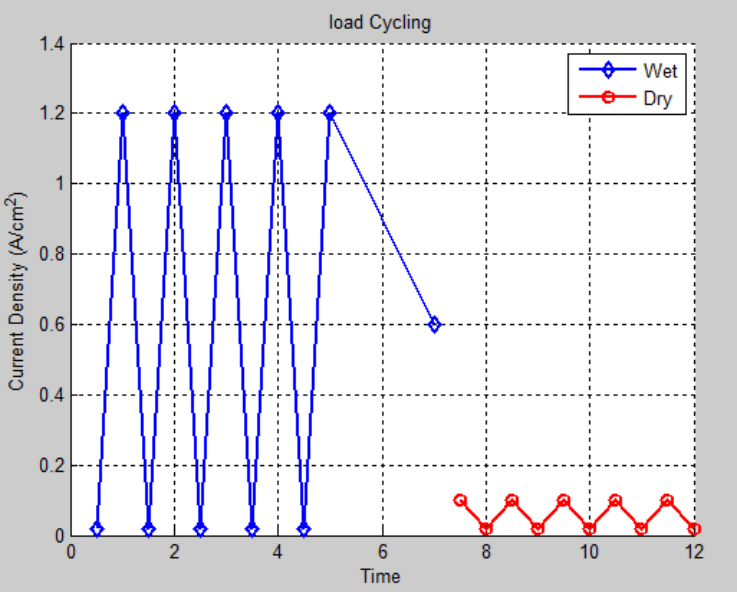

Figure 5.1: Load Profile used in the AST load cycling

As an AST strategy, the load-cycling profile of a fuel cell has been found to affect the overall lifetime of the PEMFC significantly. Figure.5.1 is an example of a dynamic loading effect used in this study. From literature, it is believed that the average value of current over the cycle has an impact over the degree of degradation that would be displayed by the cell. Under conditions of dramatic load changes as shown in Figure 5.1, carbon support corrosion of the Pt catalyst due to fuel starvation can also lead to the agglomeration of Pt catalyst particles, which will emanate in further durability loss and degradation of the PEMFC [11, 13]

Table 5.1: Drive-Cycle Durability Protocol [9]

Test Point #	**Current density(A/cm^2)**	**Anode Inlet Temp (^{o}C)**	**Cathode Inlet Temp (^{o}C)**	**Test Point Run Time (Minutes)**
Wet with Voltage Cycling				
RH1	0.02	75^o	80^o	0.5
RH2	1.2	75^o	80^o	0.5
RH3	0.02	75^o	80^o	0.5
RH4	1.2	75^o	80^o	0.5
RH5	0.02	75^o	80^o	0.5
RH6	1.2	75^o	80^o	0.5
RH7	0.02	75^o	80^o	0.5
RH8	1.2	75^o	80^o	0.5
RH9	0.02	75^o	80^o	0.5
RH10	1.2	75^o	80^o	0.5
Trans1	0.6	75^o	80^o	2.0
Dry With Load Cycling				
RH11	0.1	0^o	0^o	0.5
RH12	0.02	0^o	0^o	0.5
RH13	0.1	0^o	0^o	0.5
RH14	0.02	0^o	0^o	0.5
RH15	0.1	0^o	0^o	0.5
RH16	0.02	0^o	0^o	0.5
RH17	0.1	0^o	0^o	0.5
RH18	0.02	0^o	0^o	0.5
RH19	0.1	0^o	0^o	0.5
RH20	0.02	0^o	0^o	5.0

The aim of this study is to compare the Aquivion® and Nafion® ionomer MEAs when conducting ASTs in a more holistic manner rather than to investigate internal processes and chemical interaction or discrepancies occurring as a result of the AST ageing. However, previous work has shown that the cathode catalyst layer is more susceptible to agglomeration

than the anode side when undergoing the same load-cycling test, which implies that the catalyst particle size increases with increasing potential [10, 12].

The protocol, as explained above, was used to carry out an AST through simultaneous R.H cycling and load cycling of the Aquivion® and Nafion® MEAs under the same conditions. The following section details the comparative analysis through the use of both in-situ and ex-situ performance analysing techniques such as polarization curve and electrochemical impedance spectroscopy analysis.

5.2.2 Effect of Dry and Wet Cycle Durability Protocol on Aquivion® and Nafion® MEA Performance

Figures 5.2 shows the polarization curve analysis of the Aquivion® and Nafion® MEA after undergoing an AST procedure by cycling the R.H and load for 24 hours. Both MEAs were discovered to have undergone irreversible degradation as their performance had dropped drastically. First we compared the thickness of both MEAs to their initial values before the AST degradation procedure. It was observed that both the Aquivion® and Nafion® MEAs had undergone a slight decrease in weight as evident from the scanning electron microscope image of both membranes before and after AST (see appendix C). This reduction in MEA could be attributed to the compression effect of the cell and also as a result of membrane thinning. The membrane thinning is a good method for observing membrane degradation since the degradation occurs when the membrane is consumed.

The combined effect of the R.H and load cycling significantly degraded the PEMFC in 24 hours over a 40 cycle period of wet and dry inlet conditions. From previous studies, R.H cycling has been discovered to have many complex effects on the PEMFC membrane durability since both flooding and drying are well-known factors in PEMFC performance loss [14]. Cycling the cell at the zero humidification condition is detrimental to the membrane, causing higher

chemical degradation of the membrane and the lack of water makes the membrane brittle and fragile. Excessive humidification, however, under the low current density condition can lead to excess water percolation during the fuel cell operation causing flooding of the membrane and blockage of active reactant diffusion sites.

Figure 5.2 shows the potential-plot for the wet load cycle. The potential was recorded at the lower current density of 0.02 A/cm^2, each R.H cycle has 5 cyclic load loops between 0.02 A/cm^2 and 1.2 A/cm^2, and hence, there are 5 voltage data points for each R.H cycle loop. The voltage response was found to increase down the loops, with the fifth loop point being the largest of the 5 voltages.

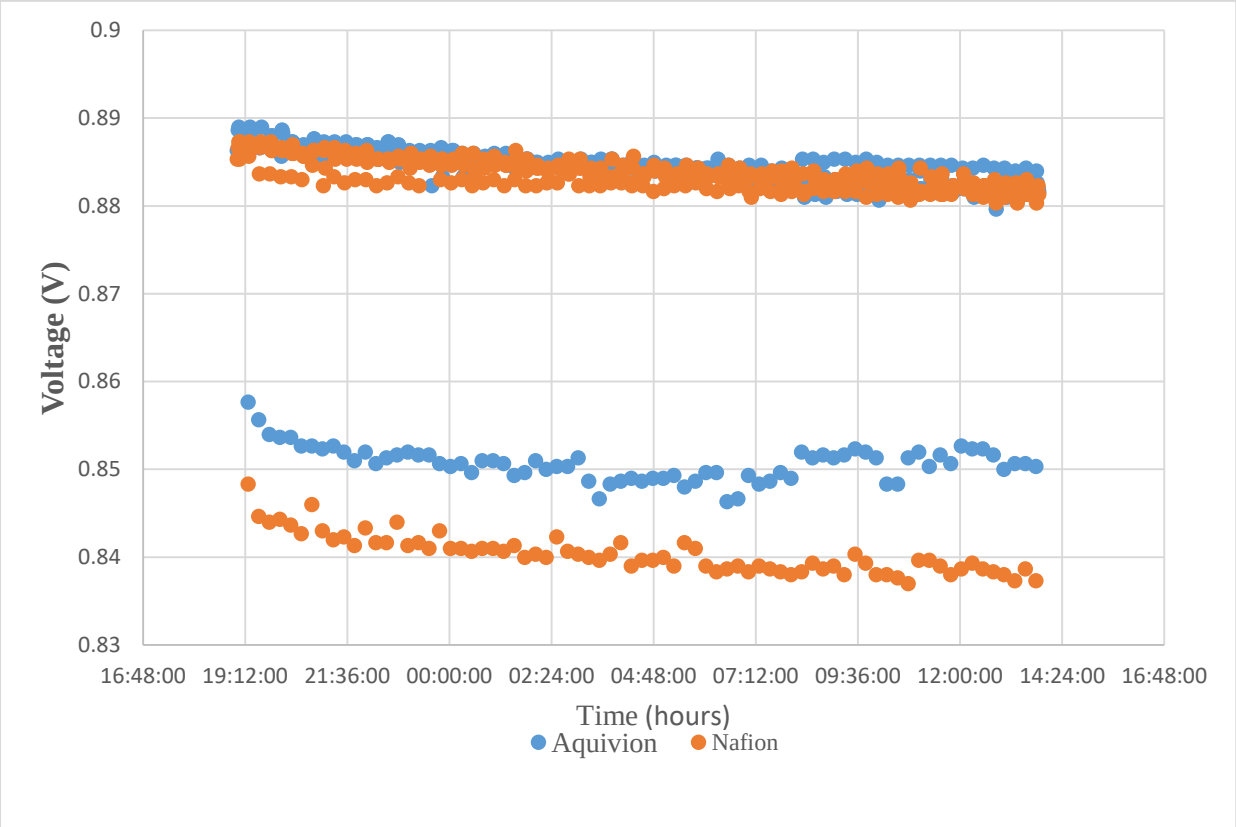

Figure 5.2: Wet Load Cycling Voltage-Time Response on the Aquivion® and Nafion® based MEAs

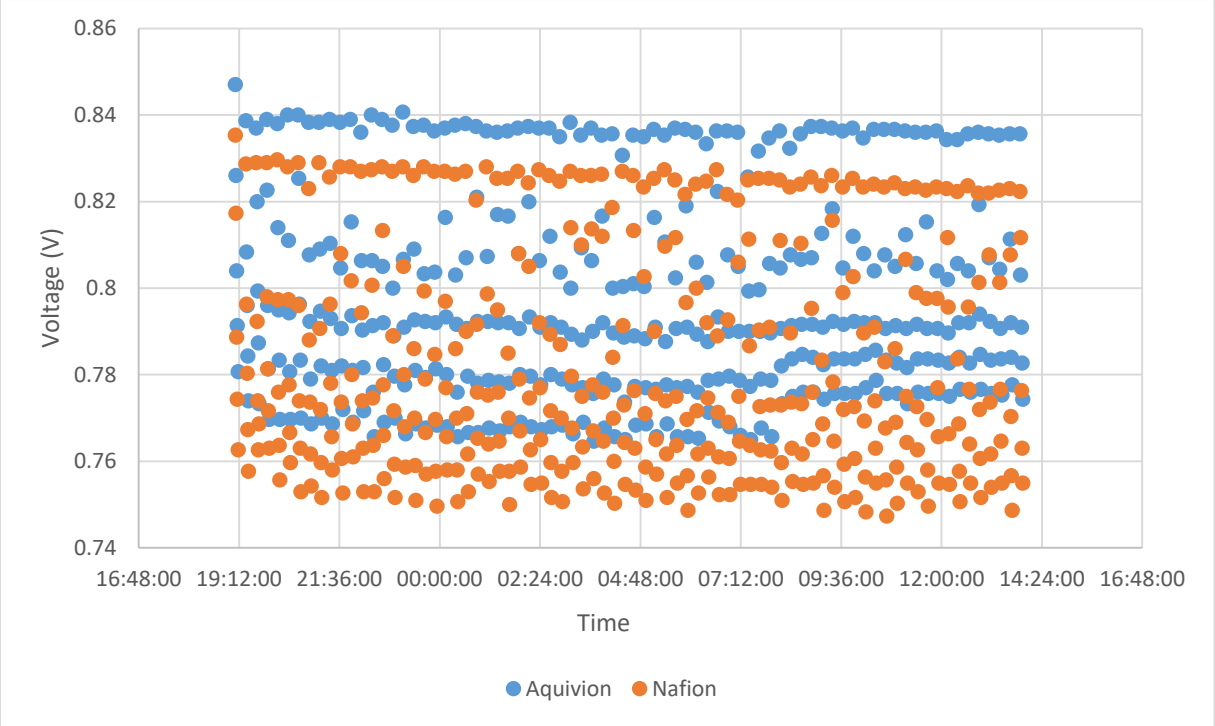

Figure 5.3: Dry Load Cycling Voltage-Time Response on the Aquivion® and Nafion® based MEAs

Figure 5.3 shows the potential - time plot for the dry load cycle. Immediately after the wet cycle, the test station switches off its gas relative humidity bubbler mimicking the condition for 0% R.H or unhumidified gas inlet. The voltage points corresponding to the 0.1 A/cm^2. Unlike the wet load cycle, the voltage reduces, with the first point being the highest. During the wet load cycle, the membrane is getting sufficient water during the course of its operation, the voltage increases as the membrane is more humidified and allows for easier proton conduction and better performance. During the dry load cycle, the first load cycle is still somewhat humid as the membrane may have retained some water carried over from the wet load cycle operation. With continual operation in the dry condition, the membrane loses humidity which will result in reduced proton conduction, and poorer performance with time. From Figure 5.2 and Figure 5.3, it is observed that the Aquivion® MEA outperformed the Nafion® MEA both in the wet load cycle and dry load cycle conditions. The polarization curve

plot shown in Figure 5.4 shows that the Aquivion® MEAs is more durable than the Nafion® MEA after being exposed to AST conditions. To further analyse the polarization curve, Figure 5.5 shows an overview of percentage degradation per voltage point of both membranes when compared before and after the AST protocol.

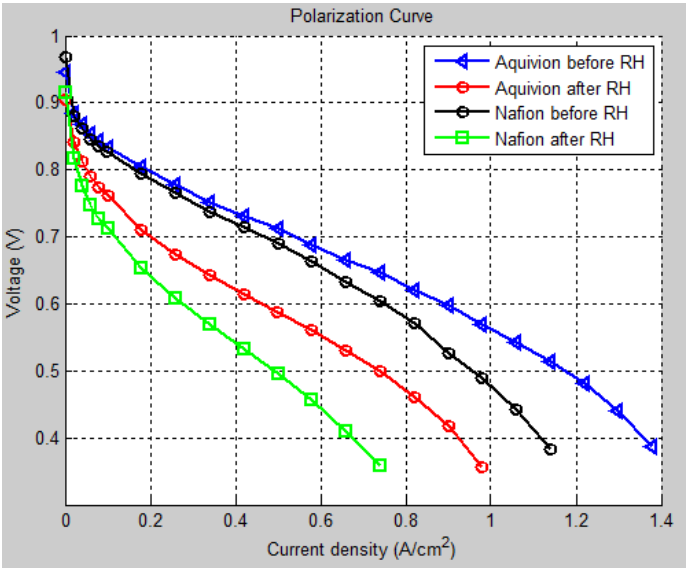

Figure 5.4: Polarization curve analysis of Aquivion® and Nafion® membrane before and after the AST test completed after 24 hrs.

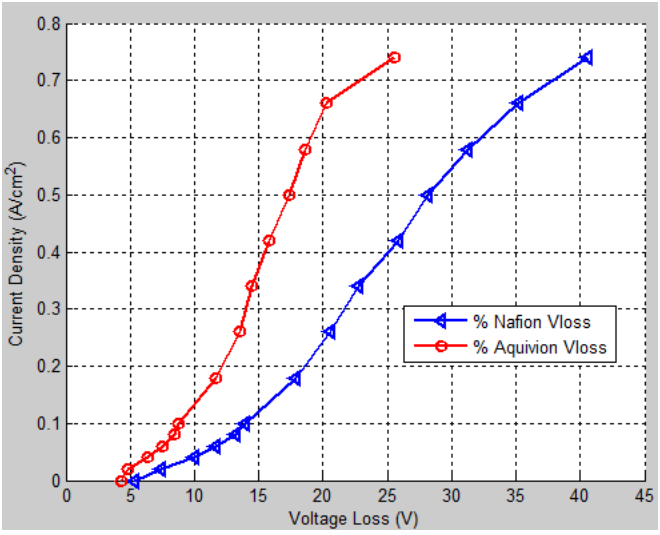

Figure 5.5: Percentage voltage loss after AST at each current density point.

From Figure 5.5, it is clear that at each current density point, the Nafion® membrane underwent more degradation than the Aquivion® membrane, supporting the observed results for the polarization curves analysis of the MEAs in Figure 5.2. The rate of degradation is very likely related to the fact that the gas cross-over is significantly larger in the presence of Nafion® as observed from the low OCV in the polarization curve. The Aquivion® ionomer has higher water retention capacity, higher crystallinity and a higher glass transition temperature (*Tg*) compared to the Nafion® ionomer MEAs.

Attack on the per-fluorocarbon backbone side chain of the ionomer membranes is the core of the membrane degradation. This loss of sulfonic acid sites leads to a reduction in membrane conductivity [15]. The easier this side chain is broken, the more severe and faster the rate of degradation. From the above comparative analysis, it can be inferred that the short-side chain Aquivion® ionomer membrane has a stronger bond with its per-fluorocarbon backbone, higher water retention as well as higher *Tg* as compared with the long-side chain Nafion® ionomer membrane, the reason for an extended lifecycle after undergoing the R.H-load cycling AST.

5.2.3 EIS – ECM Modelling for MEA Characterization

To further investigate the performance of both membranes under stress, a comparative analysis was carried out between the Aquivion® and Nafion® MEA using the electrochemical impedance spectroscopy (EIS) technique. The electrical aspect of the MEA were characterized with the use of equivalent circuit model (ECM) as discussed in Chapter 3. The EIS measurement was repeated for current density values of 100m A/cm^2 and 300m A/cm^2 for both Aquivion® and Nafion® membranes. The acquired data was then fitted to the equivalent circuit model (ECM) described in Section 3.3.1 using the EC-Lab software which uses a combination of Randomize and Simplex least-square nonlinear fitting algorithm to determine the path of best fits for different data points.

Figures 5.6 and 5.7 shows the Nyquist plots of both the Nafion® and Aquivion® MEA taken after the AST. Analogous to what was observed in Section 4, Tables 5.4 and 5.5 shows the fitted parameters for the ECM, and it is observed that that ohmic resistance (R_{Ω}) decreases with increasing load from 4 A (100 m A/cm^2 Current density) to 12 A (300 m A/cm^2 Current density) across both membranes.

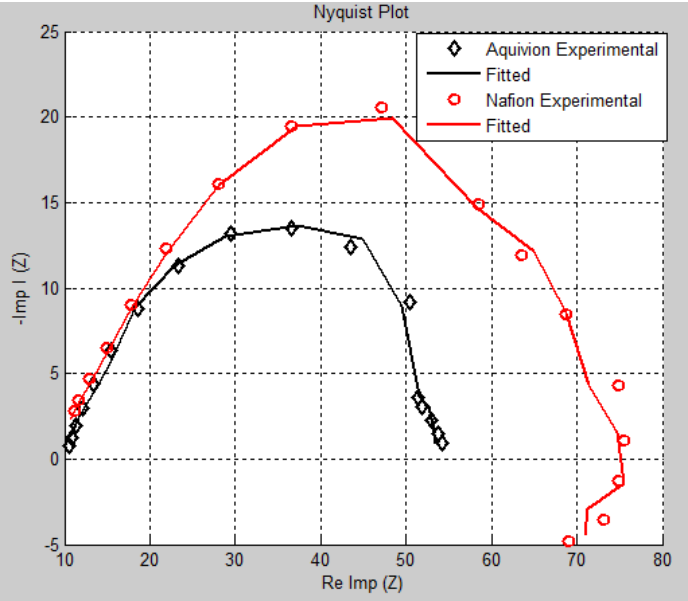

Figure 5.6: Nyquist plot of EIS measurement at 100m A/cm2 for both Aquivion® and Nafion® after AST

Table 5.4: Fitted values for the 100m A/cm^2 EIS – ECM data

Parameter	R_m	$R_{ct,\ A}$	$R_{ct,\ C}$	$C_{dl,\ A}$ (mF)	$C_{dl,\ C}$ (mF)	L(H)	Z_w
Aquivion	8.254	11.06	32.44	21.55e-3	76.06e-3	0.314 2	3.657
Nafion	9.454	15.25	47.4	26.58e-3	1.033	0.483 4	12.43

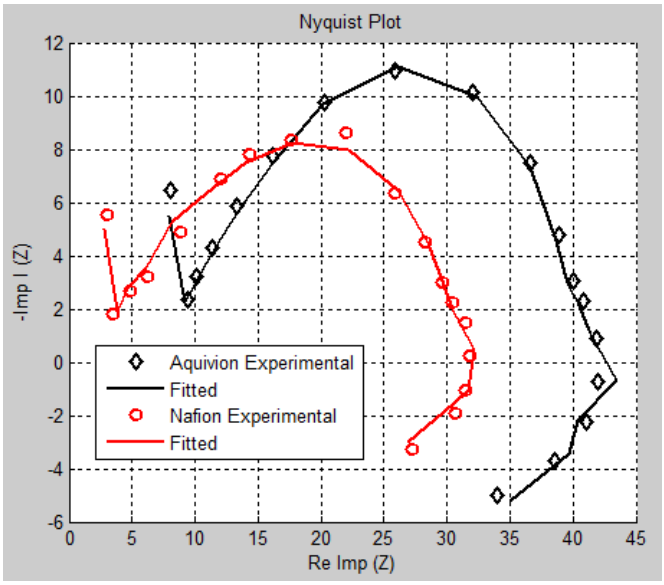

Table 5.7: Nyquist plot of EIS measurement at 300m A/cm2 for both Aquivion® and Nafion® after AST

Table 5.5: Fitted values for the 300m A/cm^2 EIS – ECM data

Parameter	R_m	$R_{ct,\,A}$	$R_{ct,\,C}$	$C_{dl,\,A}$ (mF)	$C_{dl,\,C}$ (mF)	L(H)	Z_w
Aquivion	2.652	13.51	14.27	11.81e-6	0.106	0.318 6	3.101
Nafion	7.355	8.437	25.18	8.602e-6	36.97e-3	0.325	24.12

After exposure to AST through RH and load cycling of the cell, the Aquivion® MEA has a lower ohmic resistance compared to the Nafion® MEA, hence indicating that the Aquivion membrane overall has a higher conductivity than the Nafion® MEA. From the extracted parameter values summarized in Tables 5.4 – 5.5, it was observed that $R_{ct,A}$ is small compared to $R_{ct,C}$ for the entire load current range. From the merged cathode and anode impedance arcs, the effective fuel cell charge transfer resistance (R_{ct}) is the sum of both, i.e. $R_{ct} = R_{ct,A} + R_{ct,C}$. After undergoing degradation, the Nafion® MEA has a larger charge transfer resistance compared to the Aquivion®, thus indicating that the Aquivion® membrane is more durable and can withstand more stressors than the Nafion®, hence indicating a longer lifecycle under continuous operation.

Besides the lower ohmic resistance, a better electro-catalytic activity was observed for the Aquivion® due to its lower Z_w values. Thus, we can infer that there is a higher rate of catalyst utilization by the Aquivion® compared to the Nafion® PFSA ionomer MEA.

References:

[1] Ye S, Hall M, Cao H, He P. "Degradation resistant cathodes in polymer electrolyte membrane fuel cells." *ECS Trans* 2006; 3(1):657–66.

[2] Knights SD, Colbow KM, St-Pierre J, Wilkinson DP. "Aging mechanisms and lifetime of PEFC and DMFC." J Power Sources 2004; 127 (1–2):127–34.

[3] Pierpont D, Hicks M, Watschke T, Turner P. "Accelerated testing and lifetime modeling for the develop of durable fuel cell MEAs". ECS Trans 2006;1 (8):229–37.

[4] T. Okada, in: W. Vielstich, A. Lamm, H.A. Gasteiger (Eds.), "Handbook of Fuel Cells." vol. 3, Wiley, Chichester, 2003, pp. 627–646.

[5] A.B. LaConti, M. Hamdan, R.C. McDonald, in: W. Vielstich, A. Lamm, H.A. Gasteiger (Eds.)," Handbook of Fuel Cells," vol. 3, Wiley, Chichester, 2003, p. 647.

[6] G. Escobedo, K. Raiford, G. Nagarajan, K. Schwiebert, ECS Trans. 1 (2006) 303–311

[7] E. Endoh, 2005 "Fuel Cell Seminar Abstracts, Courtesy Associates" Palm Springs, 2005.

[8] Borup R, Meyers J, Pivovar B, Kim YS, Mukundan R, Garland N, et al. "Scientific aspects of polymer electrolyte fuel cell durability and degradation". Am Chem Soc 2007;107:3904e51

[9] DOE Fuel Cell Technologies Office, Fuel Cells Technology "Multi-Year Research, Development, and Demonstration Plan" 2016.

[10] Borup RL, Davey JR, Garzon FH, Wood DL, Welch PM, More K. "PEM fuel cell durability with transportation transient operation." ECS Trans 2006;3(1):879–86.

[11] Wahdame B, Candusso D, Francois X, Harel F, Pe ´ra M-C, Hissel D, et al. "Comparison between two PEM fuel cell durability tests performed at constant current and under solicitations linked to transport mission profile." Int J Hydrogen Energy 2007; 32(17):4523–36.

[12] Liu D, Case S. "Durability study of proton exchange membrane fuel cells under dynamic testing conditions with cyclic current profile." J Power Sources 2006; 162(1):521–31.

[13] Harel F, Francois X, Candusso D, Pe ´ra M-C, Hissel D, Kauffmann J-M. “PEMFC durability test under specific dynamic current solicitation, linked to a vehicle road cycle.” Fuel cells 2007; 7(2):142–52.

[14] Liu W, Cleghorn S. “Effects of relative humidity on membrane durability in PEM fuel cells.” ECS Trans 2006;1(8): 263–73.

[15] Marianne P. Rodgers*, Leonard J. Bonville, H. Russell Kunz, Darlene K. Slattery, and James M. Fenton “Fuel Cell Perfluorinated Sulfonic Acid Membrane Degradation Correlating Accelerated Stress Testing and Lifetime” Chem. Rev. 112, 11, 6075-6103

6. Effect of High Shear Dispersion (HSD) catalyst ink mixing on PEM Performance

From the previous Section, we have established that the Aquivion® MEA showed better beginning of life performance and was also more durable than the Nafion® MEA under the same operating and design conditions. In this Section we shall be considering the effect of the preparation method of the catalytic inks on the performance as well as durability of both the Nafion® and Aquivion® MEAs and, thus, on the performance of polymer electrolyte membrane fuel cells (PEMFC).

The electrochemical reaction in a PEMFC occurs within a triple phase boundary where there is interactions among the electrolyte, the electrodes, and the gaseous fuel. The boundary is such that the reactant, H_2 or O_2 in this case, and the electrically connected catalyst particles are in contact within a membrane electrode assembly (MEA) [1]. From literature, it has been ascertained that the triple-phase-boundary area is largely dependent on the fabrication procedure of the MEA as well as other parameters such as fabrication method of the catalytic ink [2], catalyst loading [3] and ionomer loading [4]. Two MEA fabrication methods have been described in literature, including - the GDL based method where the catalyst ink is sprayed directly on the GDL and the membrane based method where the catalyst ink is sprayed directly onto a dry, blank, hot and fixed membrane followed by a hot pressing step [5-8]. In this study, the Aquivion® and Nafion® based inks were coated into membranes.

Figure 6.1 shows a complete outline of the different stages involved in the membrane electrode assembly fabrication process. In this study, the ink mixing process will be considered.

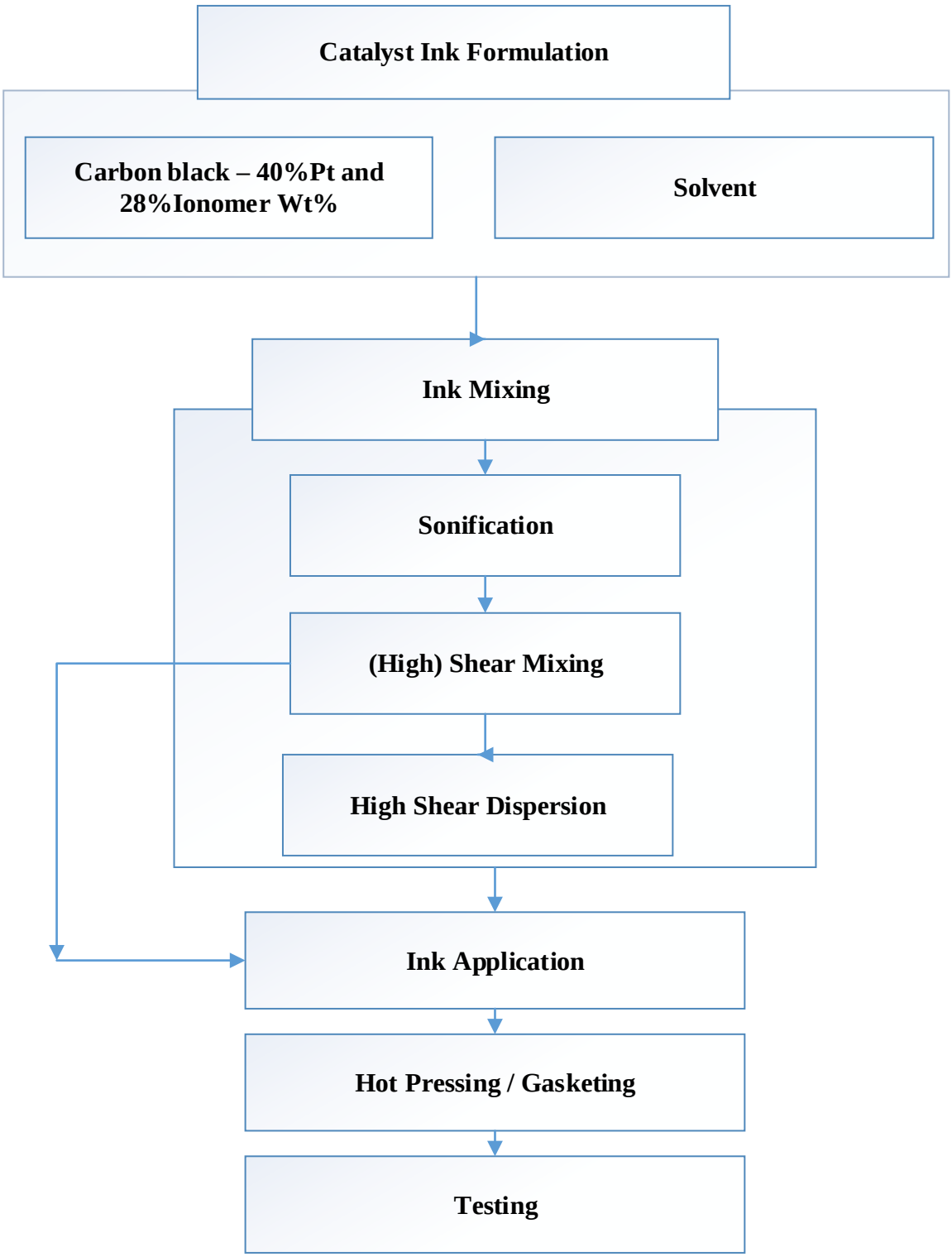

Figure 6.1: MEA Preparation outline for both Nafion® and Aquivion® MEAs.

The ink application and hot pressing process are discussed in detail in [11] as the same process and laboratory equipment was used in this work.

6.1 Catalyst Ink Formulation

Pt/C catalyst consisting of 40% Pt as illustrated in Figure 6.1, both the Aquivion® and Nafion® ionomer used with a 28wt% was used for the ink formation. Initial state of the Carbon-black/Platinum (Pt) was provided in granular (immiscible state), however it is required to be in a miscible state to enable formation of the ink. To achieve this, the catalyst was hydrated by adding 10ml of H_2O dropwise to 0.9g of the catalyst powder in a 100ml beaker such that the catalyst is fully submerged in water. 10ml of isopropanol and 10ml of n-propanol was added to the water submerged catalyst. The entire mixture was then whirled thoroughly to ensure proper mixing. Finally, 3.63ml of Nafion® was added for the Nafion® MEA catalyst ink and 3.63ml of Aquivion® was added for the Aquivion® membrane catalyst ink.

6.2 Ink Mixing

The mixing of the ink goes through a series of processes before application. After the mixing process, the catalytic inks, which are a mixture of Pt/C powders, solvent, and ionomers, changes into either a solution of colloids or precipitates, depending on the interaction between the solvents and ionomers.

6.2.1 High Shear Mixing

A Silversons LST LST high shear mixer is used in dispersing one phase or ingredient (liquid, solid, gas), into a main continuous phase (liquid), with which in most cases would be immiscible. The high shear mixer is often used for emulsification, particle size reduction and homogenization purposes. It consists of an inner rotor and an outer stationary stator, which are used in a tank containing the solution to be mixed or in a pipe through which the solution passes, to create shear [9]. Upon adding the prepared catalyst ink to the beaker (tank), the solution was placed at the centre of the stirrer and 10cm above the beaker's base. To prevent spillage during the course of its high revolution spinning, it was sealed using parafilm.

6.2.2 Sonication

In this thesis, a Grant sonicating device set to 100% sonication was used to carry out the sonication process. The sample was submerged in a tub of water, afterwhich the device sends a sonicator through the water. The sonication process uses sound waves to agitate particles in the submerged sample. It converts electrical signals into a physical vibrator to break substances apart. It uses an ultrasonic horn to cause the disruptions which is then used to mix the catalyst ink solution and also used to remove dissolved gas from the catalyst ink.

6.2.3 High Shear Dispersion

The High Shear Disperser works based on the principle of energy transfer. It is used to incorporate powders into liquid and break down particle agglomerates to produce a fine dispersion. Conventionally, the catalyst ink is taken through a process of high shear mixing, then passed on through a stage of sonication, and finally we apply the high shear dispersion process which concludes the mixing process. In this Section we shall analyse the effect of high shear dispersion, which is a very expensive and intensive process, on how it impacts the performance and durability of both Nafion® and Aquivion® ionomer MEA. We contrasted the performance of the catalyst ink made by bypassing this process with the conventional one which includes it. The result of this comparison helped in determining the magnitude of the high shear dispersion effect on the overall performance and durability of the PEMFC.

6.3 Analysis, Experiments and Results

Both the Nafion® and Aquivion® MEAs were prepared in the same way as earlier discussed in Section 4.4.2. However, the catalyst ink was made slightly differently with the omission of the high shear dispersion (HSD) mixing process. The polarization curve analysis as well as EIS plot of the membranes were carried out, under the conditions established in Chapter 4. Also, the durability of the membranes under this condition was investigated using the accelerated

stress testing (AST) protocol presented in Chapter 5 which involves cycling both the relative humidity (RH) and the load relative to each other for a 24 hour period. After the AST process, the polarization curve and EIS analysis was performed on the degraded/stressed membrane to determine its performance. This analysis was repeated using 3 MEAs made without HSD.

The performance of the membranes is discussed in this session, (i.e. membranes whose ink was made without the high shear dispersion process) was then compared with the performance of the membranes discussed in earlier Section of this work (i.e. membranes whose ink were made in the conventional way – involving high shear dispersion process). The AST cycle, polarization curve and EIS analysis formed the basis of our comparison and the result are presented herein.

6.3.1 Comparative Analysis of Aquivion® Membrane Performance

As depicted in Figures 6.5 – 6.8, from the polarization curve analysis of the Aquivion® MEA, it performed better when its ink was made without undergoing the high shear dispersion (HSD) process. The beginning of life (BOL) (Figure 6.5) performance was similar for the Aquivion® MEA made with and without the HSD. The Aquivion® without HSD slightly outperformed the one made in the conventional way (i.e. with HSD) at the activation and ohmic region while the reverse was the case at the mass transfer region.

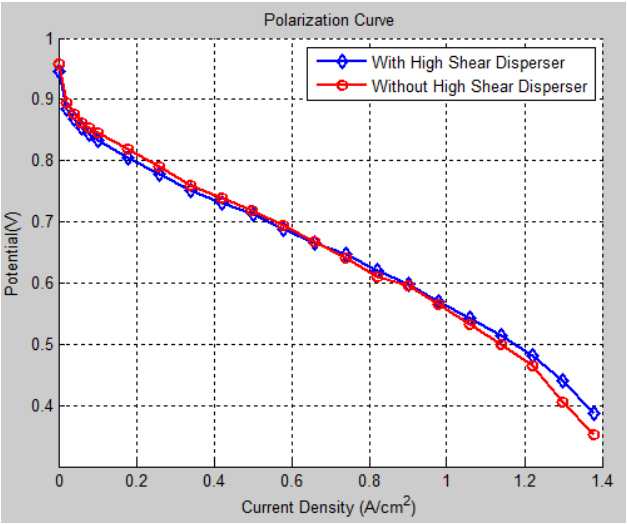

Figure 6.2: Polarization Curve analysis of Aquivion® based MEA before AST

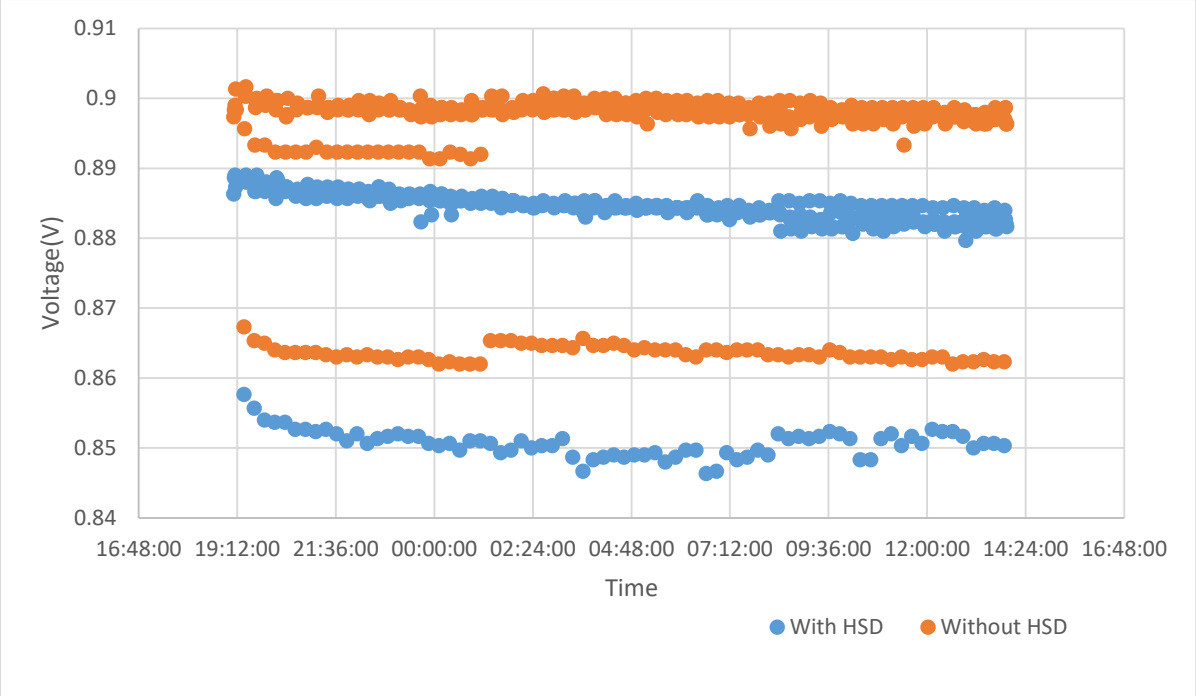

Figure 6.3: Wet load cycling Voltage-Time response for Aquivion® based MEA

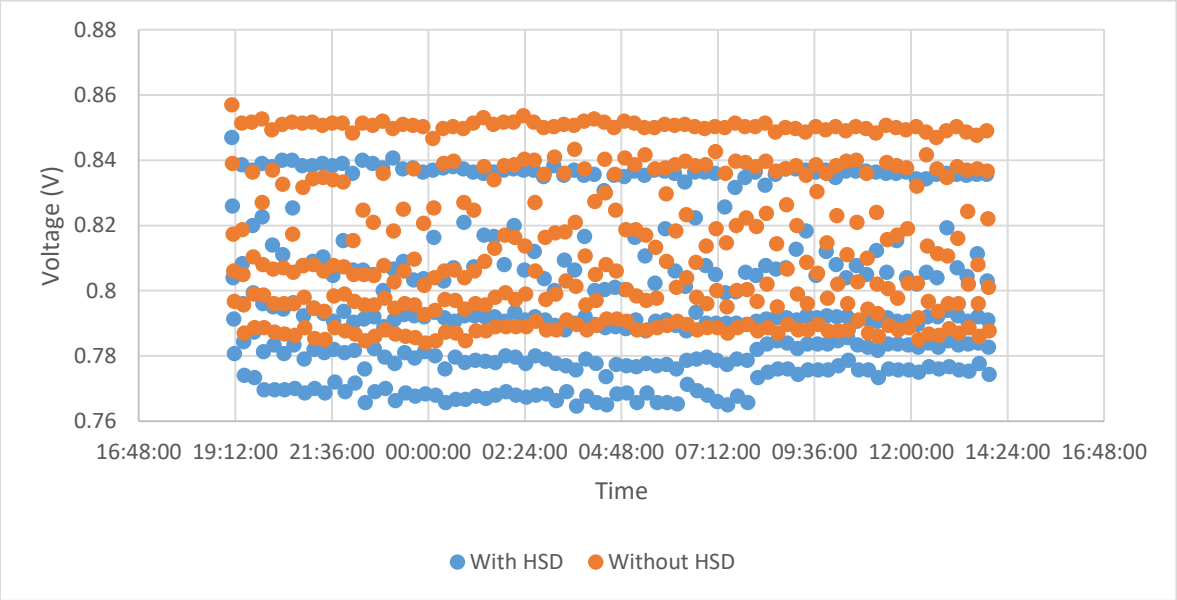

Figure 6.4: Dry load cycling Voltage-Time response for Aquivion® based MEA

After the membrane were stressed using the AST test, Figure 6.3 and 6.4 clearly shows that the HSD process negatively impacted on the durability of the Aquivion® MEA. Figure 6.5 shows

the polarization curve analysis of the membrane after the AST protocol, it is clearly observed that the HSD process negatively impacts the performance of the Aquivion® membrane.

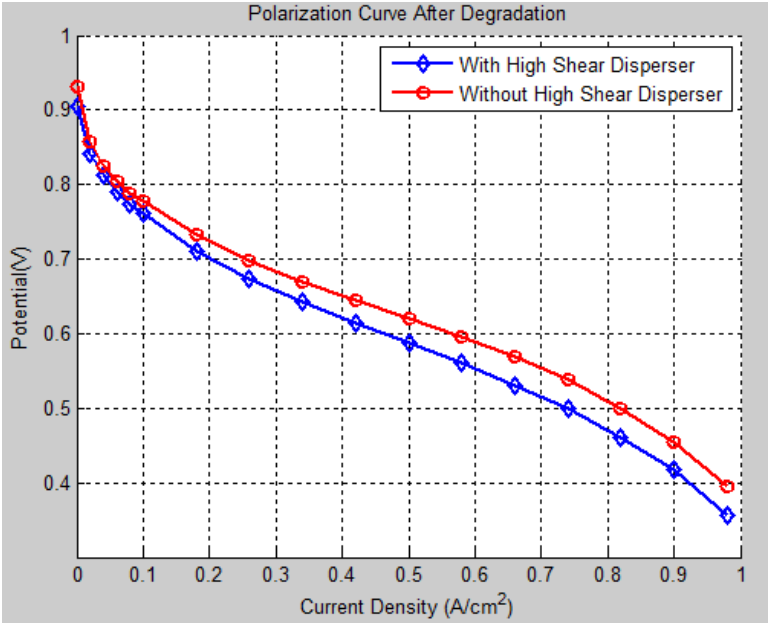

Figure 6.5: Polarization Curve Analysis of Aquivion® MEA with and without HSD after AST

To quantify the discrepancy in performance and the influence of HSD process on the Aquivion® MEA, the EIS was used to further analyse the performance and the result fitted to an equivalent circuit model as earlier discussed in Chapter 4. Figure 6.6 and Table 6.1 shows the result of the EIS analysis before AST while Figure 6.7 and Table 6.2 shows the EIS analysis after the AST process.

Table 6.1 shows the BOL performance of the Aquivion® MEA. The table indicated there was an increase in the membrane resistance R_m and a slight increase in the charge transfer resistance R_{ct} when the MEA ionomer ink was made without HSD. However, upon application of AST, from table 6.2, it is observed that there was an increase in membrane resistance R_m upon application of the HSD process. The HSD gave rise to an increase in charge transfer resistance (R_{ct}) of the membrane, the Warburg impedance which is an indication of mass transfer also increases with the application of the HSD process. It has been shown that the double-layer

capacitance *(C_{dl})* has a great influence on the fuel cell dynamic performance [12]. The C_{dl} is linked directly to the cell's space charge which is formed by H^+ or H_3O^+ appearing on the electrode-electrolyte interface [4], and an increases in its value leads to a corresponding increase in the area of the double layer. In other words, the area of double-layer forming on the platinum surface becomes larger, resulting in a larger capacitance and thus indicating better cell performance [12-15]. C. Song et al. [16] as well as other researchers [17-21] have shown that the level interaction of the ionomer and the Pt/C double layer is highly dependent on the relative humidity (RH). Hence, in a more humid cell, there is an increase in the double layer capacitance which is an indication that there is a high Pt/C in contact with the ionomer. From these studies, it can be concluded from Tables 6.1 and 6.2, that there is a clear correlation between increased double layer capacitance and improved fuel cell performance. The HSD process results in a reduction of the charge transfer capacitance, and therefore a reduction in the proton conductivity of the oxidised carbon surface, which according to M. Wesselmark et al. [23], is the reason for the reduction in performance of the Aquivion® MEA.

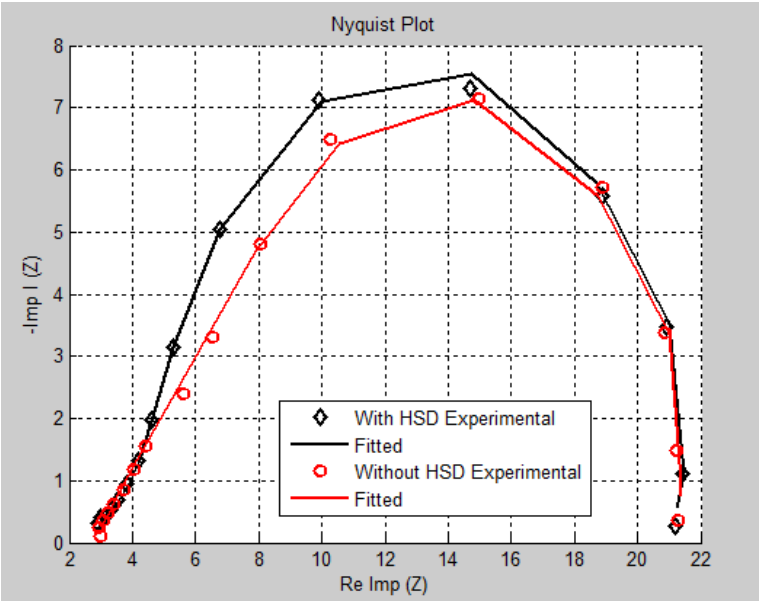

Figure 6.6: Nyquist plot of EIS at 100m A/cm^2 –Aquivion® MEA before AST

Table 6.1: Fitted values for the 100m A/cm^2 EIS – ECM Aquivion® before AST (n=3)

Parameter	R_m	$R_{ct,A}$	$R_{ct,C}$	$\boldsymbol{R_{ct,tot}}$	$C_{dl,A}$ (mF)	$C_{dl,C}$ (mF)	$\boldsymbol{C_{dl,C}}$ **(mF)**	L(H)	Z_w
With HSD	2.619	7.198	11.250	**18.45**	0.161	1.213	**1.374**	0.081	1.340
Without HSD	2.829	8.225	10.77	**19.00**	0.699	2.167	**2.866**	0.098	1.181

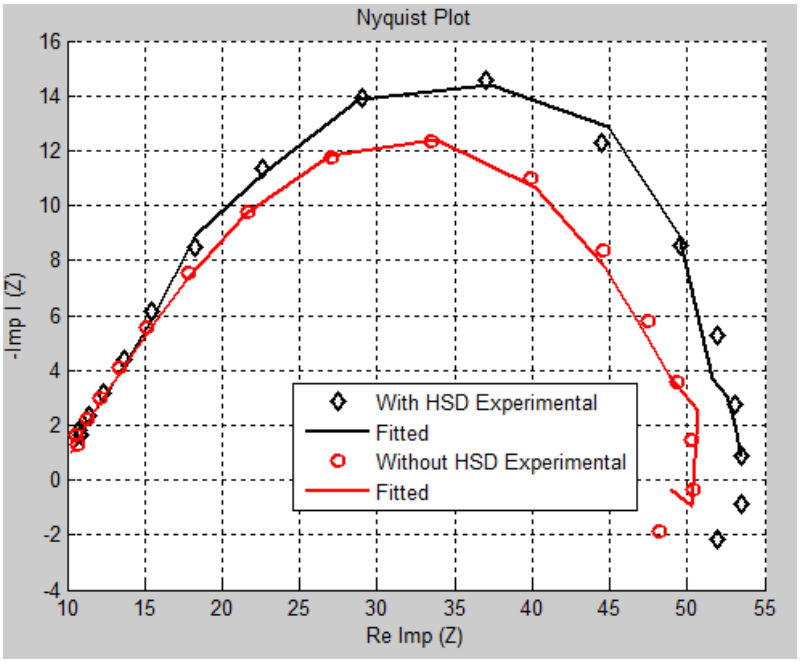

Figure 6.7: Nyquist plot of EIS at 100m A/cm^2 –Aquivion® MEA after AST

Table 6.2: Fitted values for the 100m A/cm^2 EIS – ECM Aquivion® data after AST

Parameter	R_m	$R_{ct,A}$	$R_{ct,C}$	$\boldsymbol{R_{ct,tot}}$	$C_{dl,A}$ (mF)	$C_{dl,C}$ (mF)	$\boldsymbol{C_{dl,C}}$ **(mF)**	L(H)	Z_w
With HSD	8.254	11.06	32.44	**43.50**	21.55e-3	76.06e-3	**97.61e-3**	0.314	3.657
Without HSD	8.142	9.87	29.39	**39.26**	28.65e-3	96.05e-3	**131.58e-3**	0.113	1.099

From The results presented in Table 6.2 it is evident that for the Aquivion® MEA, the application of the HSD procedure lead to a decrease in the C_{dl} value, which indicates a decrease in the Pt/C active site that is in contact with the ionomer, and thus a reduction in cell performance and durability.

6.3.2 Comparative Analysis of Nafion® MEA Performance

The Nafion® MEA performance and durability was investigated, comparing as we did for the Aquivion® MEA above, with or without the high shear dispersion (HSD) process. As depicted by the polarization curve analysis in Figure 6.8, it can be observed that unlike in the case of the Aquivion® MEA, the Nafion® MEA performed slightly better when its catalyst ink underwent a high shear dispersion (HSD) process. In Figure 6.8, its beginning of life (BOL) performance was similar for the two conditions, as the activation region shows the same performance with or without the HSD process. However, as the current increased, the ohmic and mass transfer losses increased for the case without HSD, which was dissimilar to Aquivion® MEA.

The AST process was the performed on the Nafion® MEA with and without HSD, as discussed earlier. Figure 6.9 and 6.10 clearly shows that the HSD process had a positive impact on the durability of the Nafion® membrane, showing better durability under stress/ continuous usage. Figure 6.11 shows the polarization curve analysis of the membrane after the AST protocol, it is clearly observed that the HSD process positively impacts the performance of the Nafion® MEA, contrary to what was observed for the Aquivion® MEAs.

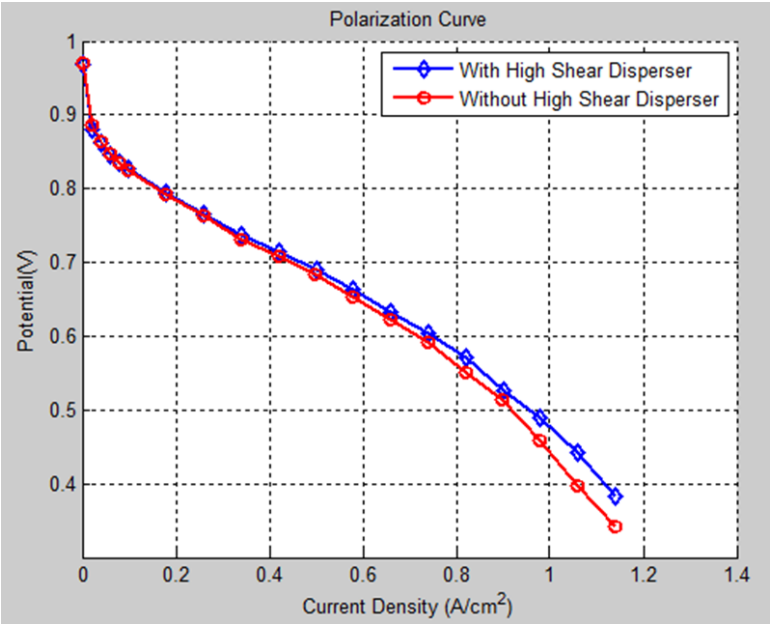

Figure 6.8: Polarization Curve analysis of Nafion® with and without HSD before AST

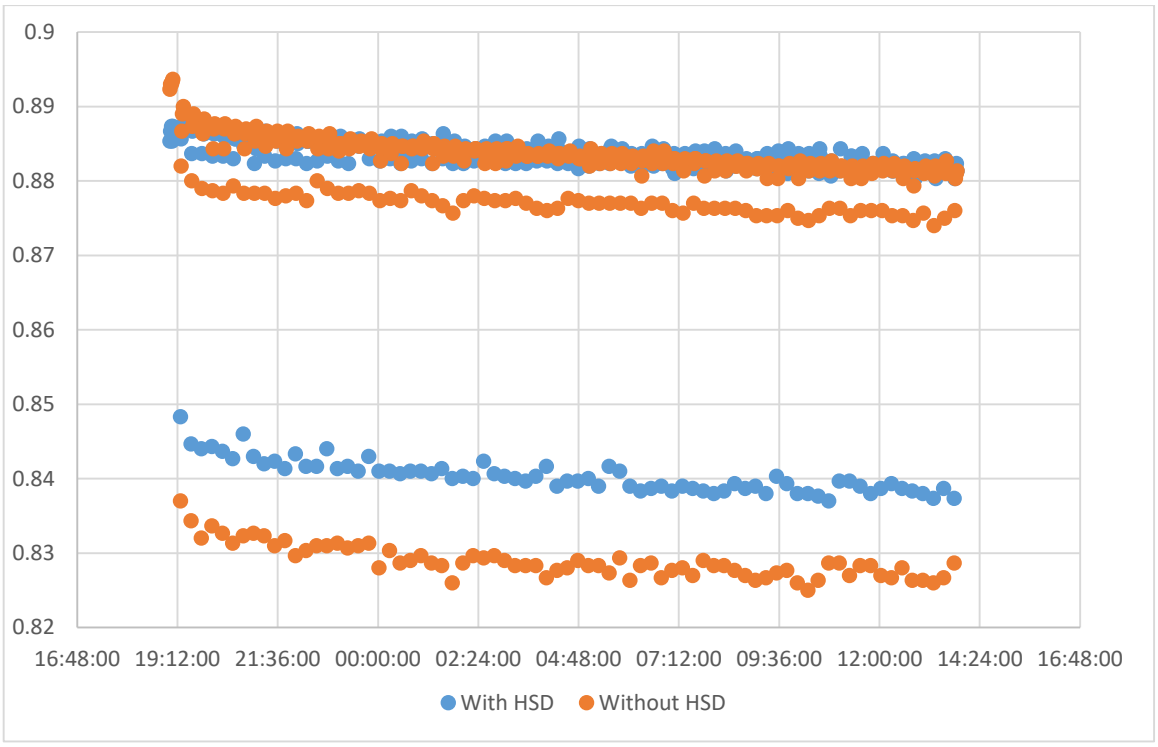

Figure 6.9 Wet load cycling Voltage-Time response for Nafion® membrane

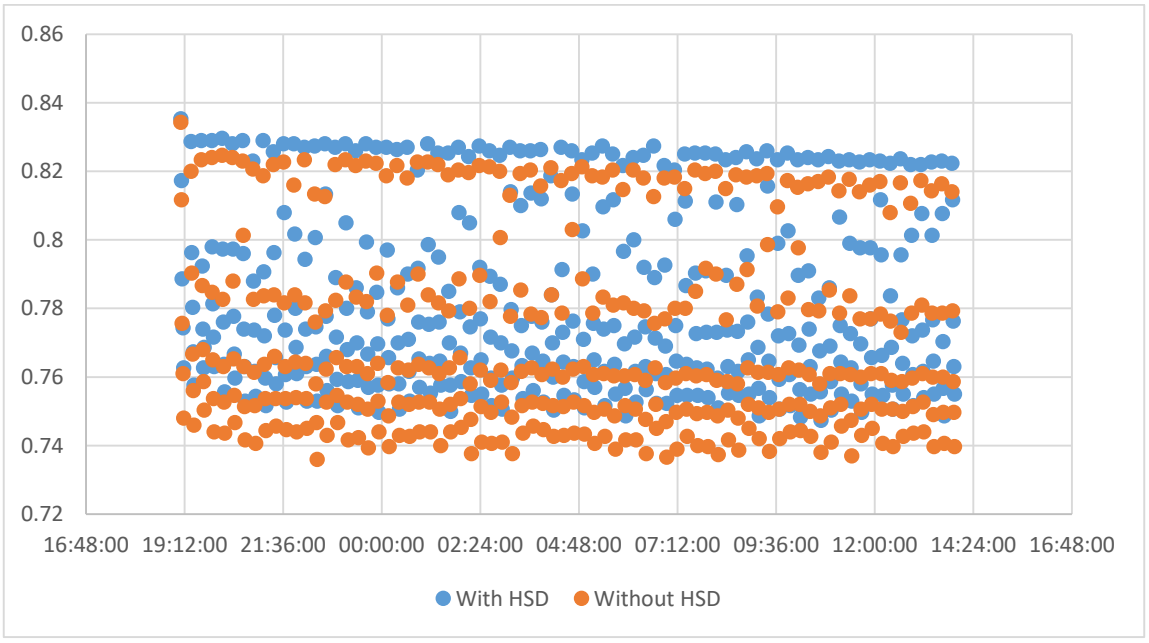

Figure 6.10: Dry load cycling Voltage-Time response for Nafion® MEA

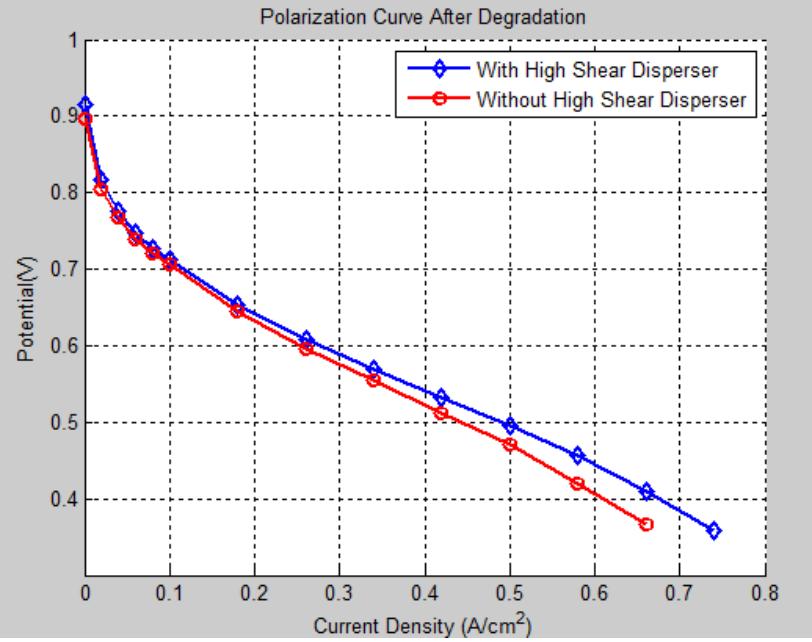

Figure 6.11: Polarization Curve analysis of Nafion® with and without HSD after AST

To understand the difference in performance and the influence of HSD process on the Aquivion® MEA, the EIS was used to further analyse the performance and the result fitted to an equivalent circuit model as earlier described in Chapter 4. Figures 6.12 and Table 6.3 shows the result of the EIS analysis before AST while Figure 6.13 and Table 6.4 shows the EIS analysis after the AST process.

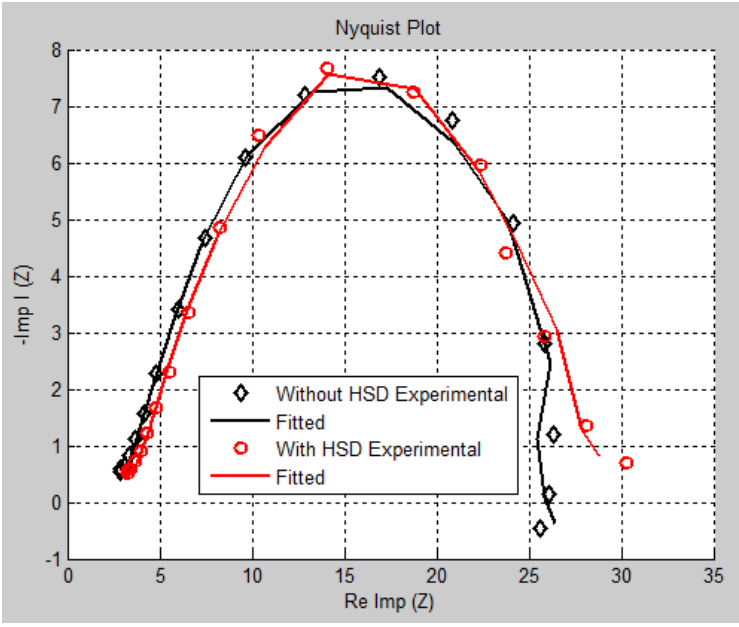

Figure 6.12: Nyquist plot of EIS at 100m A/cm^2 –Nafion® MEA before AST

Table 6.3: Fitted values for the 100m A/cm^2 EIS – ECM Nafion® data before AST (n=3)

Parameter	R_m	$R_{ct,A}$	$R_{ct,C}$	$\boldsymbol{R_{ct,tot}}$	$C_{dl,A}$ (mF)	$C_{dl,C}$ (mF)	$\boldsymbol{C_{dl,C}}$ **(mF)**	L(H)	Z_w
Without HSD	1.082	11.56	19.44	**31.0**	0.435	3.564	**3.999**	3.249	0.174
With HSD	2.645	12.00	18.41	**30.41**	1.148	3.599	**4.747**	0.059	5.162

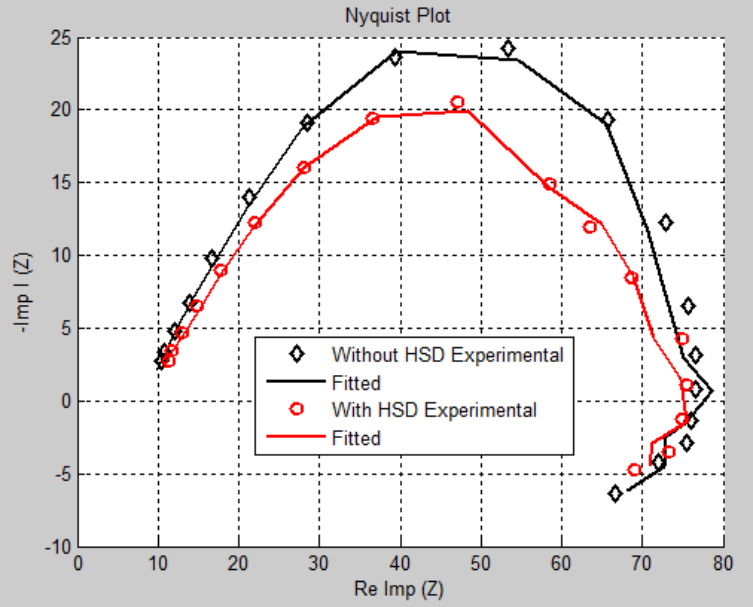

Figure 6.13: Nyquist plot of EIS at 100m A/cm^2 –Nafion® MEA after AST

Table 6.4: Fitted values for the 100m A/cm^2 EIS – ECM Nafion® data after AST

Parameter	R_m	$R_{ct,A}$	$R_{ct,C}$	$\boldsymbol{R_{ct,tot}}$	$C_{dl,A}$ (mF)	$C_{dl,C}$ (mF)	$\boldsymbol{C_{dl,C}}$ **(mF)**	L(H)	Z_w
Without HSD	9.303	19.5	49.29	**68.79**	8.16e-3	25.13e-3	**33.29e-3**	0.3906	12.43
With HSD	9.454	15.25	47.4	**62.65**	26.58e-3	1.033	**1.034**	0.4834	10.02

From the EIS analysis of the Nafion® MEAs before undergoing AST, it was observed that there was an increase in membrane resistance R_m upon application of the HSD process similarly to what was observed in the Aquivion® MEA. However, unlike the Aquivion® membrane, the Nafion® MEA behaviour under the HSD process is such that there was a decrease in charge transfer resistance (R_{ct}) of the membrane, the Warburg impedance which is an indication of mass transfer also decreases with the application of the HSD process.

For the Nafion® membrane, the application of the HSD process in the making of its ink gave rise to an increase in the double layer capacitance since the particles are more homogenous after undergoing this process, and the ink is better dispersed over the Pt/C active, thereby causing an increase in the number of active site that is in contact with the ionomer. It is safe to conclude that the HSD process positively enhances the performance and durability of the Nafion® MEA and on the other hand, negatively impacts and reduces the durability as well as performance of the Aquivion® MEA PEMFC.

References

[1] Thompson SD, Jordan LR, Forsyth M. "Platinum electrodeposition for polymer electrolyte membrane fuel cells." *Electrochimica Acta* 2001; 46:1657–1663.

[2] Shin, S.-J & Lee, J.-K & Ha, Heung Yong & Hong, SA & Chun, Hai-Soo & Oh, Il-Hoan. (2002). "Effect of the catalytic ink preparation method on the performance of polymer electrolyte membrane fuel cells". *Journal of Power Sources*. 106. 146-152. 10.1016/S0378-7753(01)01045-X.

[3] Gode P, Jaouen F, Lindbergh G, Lundblad A, Sundholm G. "Influence of the composition on the structure and electrochemical characteristics of the PEFC cathode." Electrochimica Acta 2003; 48:4175–4187

[4] Antolini E, Giorgi L, Pozio A, Passalacqua E. "Influence of Nafion loading in the catalyst layer of gas-diffusion electrodes for PEFC." *Journal of Power Sources* 1999; 77:136–142.

[5] R.D. Mussel, T.J. Regh, "Active Layer for Membrane Electrode Assembly," The Dow Chemical Company, US Patent 5,882,810 (1999).

[6] A.T. Hunt, "Materials and Processes for Providing Fuel Cells and Active Membranes," Microcoating Technologies Inc., WO Patent 00/72391 (2000).

[7] S.R. Narayanan, B.J. Nakamura, W. Chun, R.P. Ruiz, T.I. Valdez, "Sputter-deposited Fuel Cell Membranes and Electrodes" CIT, US Patent 6,171,721 (2001).

[8] Ren X, Zelenay P, Thomas S, Davey J, Gottesfeld S. "Recent advances in direct methanol fuel cells at Los Alamos National Laboratory." *Journal of Power 2000*; 86:111–116

[9] C Banaszek "Ultra High Shear Mixing Technology" 2009-12-27

[10] http://www.ehow.com/how-does_5171302_sonication-work_.html accessed 12/05/2018

[11] C.Jeffery “Influence of catalyst ink mixing procedures on catalyst layer properties and in-situ PEMFC performance” MS.c. thesis, University of Cape town, 2016.

[12] M. Eikerling, A.A. Kornyshev, J. Electroanal. Chem. 475 (2) (1999) 107e123

[13] I. Sadli, M. Urbain, M. Hinaje, J.P. Martin, S. Raël, B. Davat, *Energ. Convers. Manage*. 51 (12) (2010) 2993e2999.

[14] J. Kim, H. Lee, S. Hong, H.Y. Ha, *J. Electrochem. Soc*. 152 (12) (2005) A2345eA2351.

[15] Z. Siroma, T. Sasakura, K. Yasuda, M. Azuma, Y. Miyazaki, *J. Electroanal*. Chem. 546 (0) (2003) 73e78.

[16] F. A. Uribe, T. E. Springer, S. Gottesfeld, J. Electrochem. Soc., 139 (3) (1992).

[17] J. Chlistunoff, F. Uribe, B. Pivovar, ECS Trans., 1(6) (2006) 137–146

[18] J. Chlistunoff, B. Pivovar, ECS Trans., 11 (1) (2007) 1115–1125.

[19] S. Ma, Q. Chen, F. H. Jøgensen, P.C. Stein, E. M. Skou, Solid State Ionics 178 (2007) 1568– 1575.

[20] D. L. Wood III, J. Chlistunoff, J. Majewski, R. L. Borup, J. Am. Chem. Soc., 131 (2009) 18096–18104.

[21] M. A. Modestino, A. Kusoglu, A. Hexemer, A. Z. Weber, R. A. Segalman, Macromolecules, 45 (2012) 4681−4688.

[22] M. Wesselmark, C. Lagergren, G. Lindbergh, ECS Trans., 25 (1) (2009) 1241-1250.

7. Major Findings and Observations

7.1 Operating and Design Parameters

This study considered the effect of design conditions on the PEMFC performance and considered ways to optimize its performance. It was determined that the clamping torque has a crucial effect on the performance of the PEMFC and it is dependent on the active area of the membrane electrode assembly (MEA), and the type of bolt and nuts used. For the 25cm^2 PEMFC single cell fixture used in this study, the optimal clamping torque that effectively compresses the PEMFC uniformly and does not impede the flow of reactant was 17.5lbfin (1.98Nm), above or below this clamping torque value, the performance of the PEMFC decreases.

Another design parameter that has a major influence on the performance of the PEMFC is the gas diffusion layer (GDL). For optimal performance, the GDL must have very high proton conductivity, chemically stable, and it must have ability to withstand the temperatures and compression forces of the fuel cell fixture. It was determined that of the two types of GDLs, the Freudenberg H23C9 GDL with thickness of 0.218mm and the AvCarb MB30 GDL with thickness of 0.175mm, that the thinner GDL (i.e. AvCarb MB30) performed better than the thicker GDL (Freudenberg) for this particular cell design. The AvCarb GDL being thinner has a higher porosity, making it possible for reactants to easily transit to the catalyst layer, with minimal impedance to gas flow. Hence, it was concluded, that for this cell design, thinner GDLs gives an enhanced performance of the PEMFC.

From analysis of the operating parameters, it was discovered that the performance of the PEMFC is highly influenced by relative humidity (R.H) gradient and pressure gradient between the anode and cathode. It was observed that R.H gradient between the anode and cathode has

significant impact on the fuel cell performance especially at high current densities. After considering series of R.H gradient values between both electrodes, it was determined that the PEMFC performance is inversely proportional to the R.H gradient, the smaller the R.H gradient, the better the PEMFC performance. For the 25cm^2 single PEMFC cell fixture used in this study, the optimized R.H for both the anode and cathode was set at 80^{o}C and 75^{o}C respectively corresponding to 100% humidity level at the anode and 81% humidity level at the cathode.

Increasing the pressure at both the anode and cathode would lead to an increase in cell performance due to an increase in concentration of reactant. However, creating a pressure gradient in the cathode to anode direction results in a lower current density and the cell performance drops at low R.H with increasing pressure. A higher current density, the cell performance increases with increasing cell pressure as a result of convective water flux which causes an increase in the level of hydration (water level) of the membrane at the anode. At high R.H values, the cell performance reduces with increase in cathode pressure. The pressure gradient in the anode to cathode side has a negative influence on cell performance at both low and high R.H values.

Lastly, the findings presented in literature concerning the influence of temperature on PEMFC performance was supported in this study. The cell performance was observed to increase with an increase in operating temperature up to 80^{o}C, above this temperature the PEMFC performance reduced significantly.

7.2 Comparative Analysis of Nafion® and Aquivion® MEAs

The Aquivion® SSC MEA shows higher ionic conductivity at the point of cyclic conditioning break-in voltage of 0.3V compared to the Nafion® long-side chain MEA. This is as a result of the easy mobility of hydrated ions move around in the Aquivion® ionomer MEA due to its

short side chain. Both polarization curve and EIS analysis of the MEAs showed that the Aquivion® ionomer MEA performs better and is also more durable than the Nafion® MEA. The Aquivion® MEA has a lower ohmic resistance compared to the Nafion® MEA, hence indicating that the Aquivion® membrane overall has a higher conductivity. The Nafion® MEA has a larger charge transfer resistance compared to the Aquivion®, indicating that the Aquivion® membrane boasts faster reaction kinetics and lower charge transfer losses.

The effect of degradation was more pronounced on the Nafion® MEA compared to the Aquivion® MEA. This disparity in rate of membrane degradation is an indication that the Aquivion® based MEA is more durable, having lower ionomer and membrane dry-out characteristics as and also possessing better mechanical properties and higher thermal stability than the Nafion® based MEA.

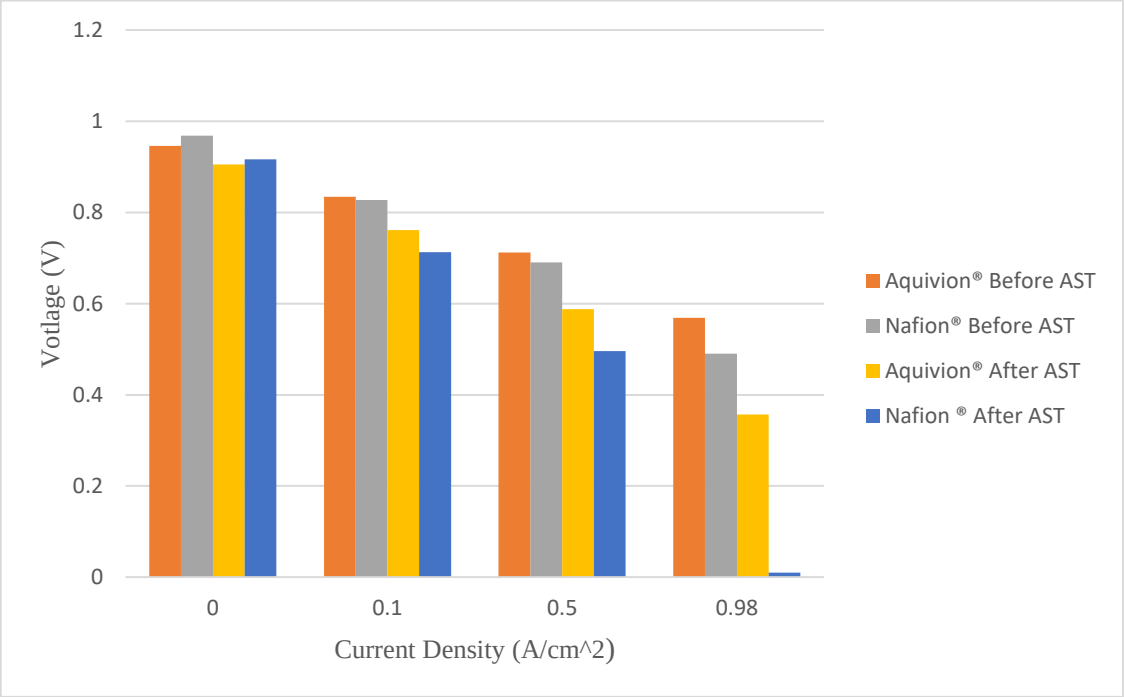

Figure 7.1: Overview of Aquivion and Nafion MEA Performance Before and After AST

Figure 7.1 gives an overview of the comparative analysis of the performance of both the Nafion® and Aquivion® ionomer MEA at different point on the polarization curve, with 0 A/cm^2 representing the OCV behaviour, 0.1 A/cm^2, 0.5 A/cm^2 and 0.98 A/cm^2 representing the activation, ohmic and mass transfer point on the polarization curve.

7.3 Effect of HSD Catalyst ink mixing

The High Shear Dispersion (HSD) process negatively affects the Aquivion® MEA, as the performance of the Aquivion® ionomer PEMFC reduces upon the application of the process. The adverse effect of this process is more pronounced over the life cycle of the membrane as the HSD process lead to a higher degradation rate and lower the durability of the membrane. The EIS – ECM investigation of this HSD effect showed that the application of the HSD procedure lead to a decrease in the C_{dl} value, which is a direct indication that there is a decrease in the Pt/C active site that is in contact with the ionomer, and thus the reason for the reduction in cell performance and durability.

However, for the Nafion® ionomer MEA, the HSD process resulted in a slightly higher beginning of life (BOL) performance. During the life cycle of the Nafion® ionomer MEA, the HSD process resulted in a more Nafion® ionomer membrane PEMFC as the application of the HSD process in the making of its ink gave rise to an increase in the double layer capacitance since the particles are more homogenous after undergoing this process, and the ink is better dispersed over the Pt/C active sites, thereby causing an increase in the number of active site that is in contact with the ionomer.

Figures 7.2 and 7.3 clearly shows the effect of HSD process on the Aquivion® and Nafion® ionomer membrane performance at both the beginning if life and after the AST process respectively

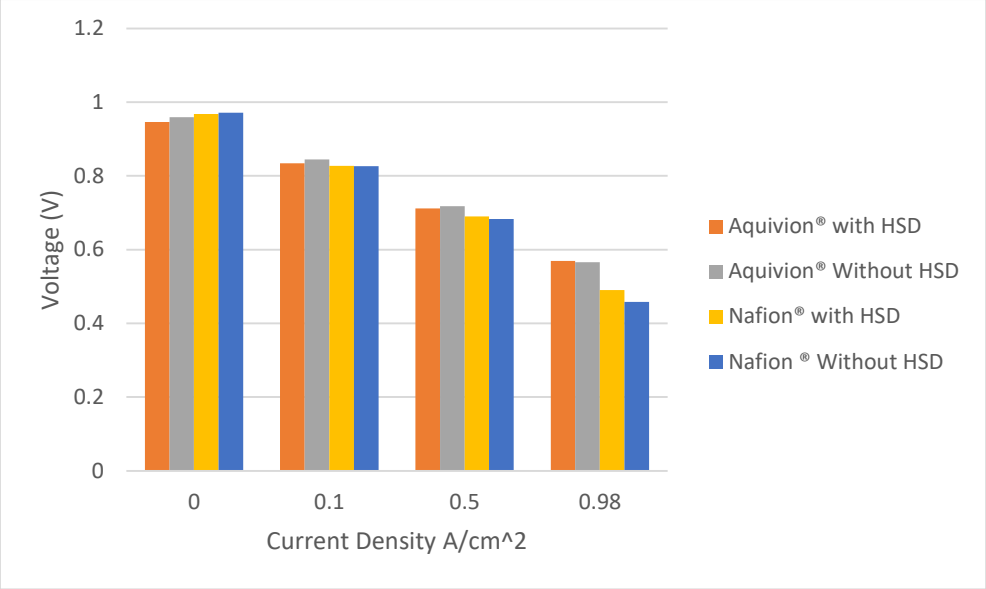

Figure 7.2: Overview of MEA Performance at the beginning of life (Before AST).

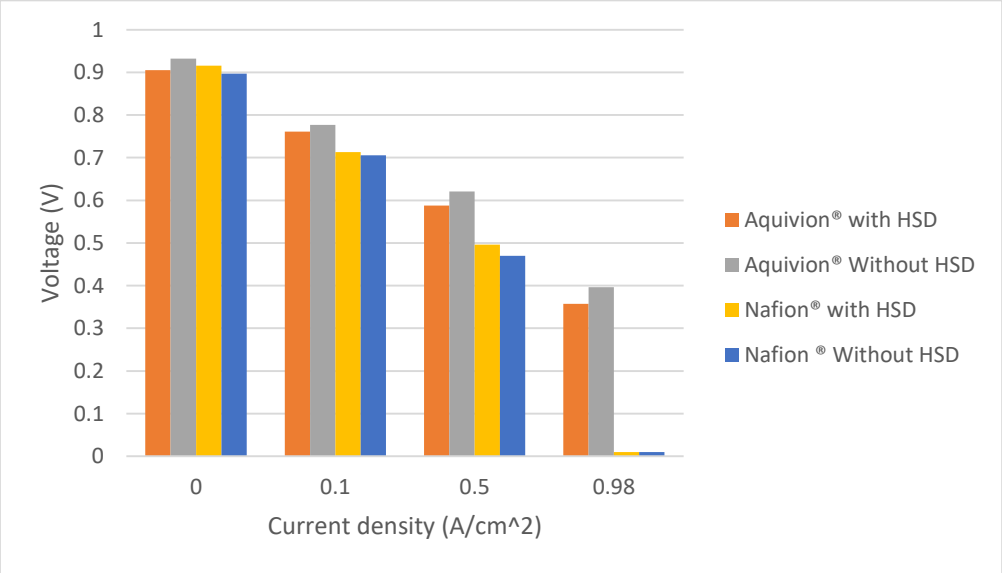

Figure 7.3: Overview of MEA Performance after AST

From the analysis of the experimental results presented herein, this thesis has been able to present a detailed analysis of PEMFC hardware and MEA components optimization as well as provide a comparative study of the long side chain ionomer (Nafion®) and short side chain ionomer (Aquivion®) along the line on its performance and durability which as earlier discussed in the beginning of this thesis are the main aims of this study.

8. Conclusion and Future Work

Much more research is still required to ensure increased adoption for PEMFC technology as a competitive energy generation source for both portable and industrial application. This thesis presented a comparative analysis of the long side chain (LSC) Nafion® ionomer MEA and the short side chain (SSC) Aquivion® ionomer membrane PEMFC using several electrochemical analysis tools with focus on performance and durability.

A literature review was conducted, which describes the function of the fuel cell and identifies different types of fuel cells available. The PEMFC was adopted based on its low operating temperature, absence of harmful by-product, high energy efficiency, high power density and low start-up time hence making it the most viable option for most portable power application. The PEMFC was then introduced in detail, looking at its working principle, components, process parameters, degradations process as well as diagnostics wherein various diagnostics such as polarization curve and electrochemical impedance spectroscopy were introduced.

Experimental analysis was then carried out to ensure optimized the operating and design parameters with which the PEMFC was to be operated. Detailed review of both the long side chain Nafion® and short side chain Aquivion® ionomer membrane was then presented. Both ionomer membranes were subjected to the same design and process parameters and upon analysing the result of each experiment, it was discovered that the short side chain Aquivion® ionomer MEA performed better and also more durable than the long side chain Nafion® ionomer MEA.

Further work was performed on the MEA, as we investigated the effect of high shear dispersion (HSD) catalyst ink mixing process on both Aquivion® and Nafion® ionomer membranes. From experimental analysis, it determined that the HSD process negatively affects the

performance and durability of the Aquivion® MEA. However, the performance and durability of the Nafion® ionomer MEA was enhanced by the HSD process. From the various analysis carried out in this thesis, it can be conclude that the short side chain Aquivion® ionomer MEA is the best option to use in determining the which MEA to use in an PEMFC application, and the making of the catalyst ink of the Aquivion® ionomer MEA should not include the HSD process as it inhibits the overall performance and durability of the MEA.

The experiments were all carried using standard protocols as observed in literature, most of the data collected were repeated three to ensure reproducibility, and the margin for error was reduced by taking the mean of these values. Going forward, it would be nice to see how the EIS data would compare with an external device say an Autolab potentiostat, and compare the results.

8.1 Further Research

It was presented in this thesis that the on applying the HSD process to the catalyst ink Nafion® ionomer MEA the performance as well as durability if the Nafion® ionomer MEA increases. However, from our analysis the difference performance without and with the HSD process was not significant. Further research can be conducted in this regard in quantifying the improvement in performance and durability by applying the HSD process and compare this to the financial and technical cost of applying this process, giving a form of cost-benefit analysis.

Another aspect that can be considered for further investigation is the interaction between the ionomer membranes and the catalyst layer upon carrying out AST. During the course of carrying out the accelerated stress testing (AST) of the PEMFC, we isolated the MEA and focused on the performance of the MEA per cycle. The interaction between the catalyst layer (CL) and the MEA under this AST conditions may present some interesting behaviours which

may provide us with more detailed information about how the membrane degrades and why the Nafion® ionomer MEA degraded faster than the Aquivion® ionomer MEA.

9. Appendix

Appendix A: MATLAB Codes

A.1: MATLAB code for Kim's model - Polarization curve fitting

```
function [fitresult, gof] = createFit(I, V)
%CREATEFIT(I,V)
%  Create a fit.
%  Data for 'Kim's Model' fit:
%      X Input : I
%      Y Output: V
%  Output:
%      fitresult : a fit object representing the fit.
%      gof : structure with goodness-of fit info.
%  See also FIT, CFIT, SFIT.
 %  Auto-generated by MATLAB on 25-May-2018 16:53:04
%% Fit: 'Kim's Model'.
[xData, yData] = prepareCurveData( I, V );
% Set up fittype and options.
ft = fittype( '1.299 - b*log(x) - R*x - (m*exp(n*x))', 'independent', 'x',
'dependent', 'y' );
opts = fitoptions( 'Method', 'NonlinearLeastSquares' );
opts.Algorithm = 'Levenberg-Marquardt';
opts.Display = 'Off';
opts.Lower = [0 0 0 0];
opts.Robust = 'Bisquare';
opts.StartPoint = [0.278498218867048 0.309425683031331 0.63235924622541
0.0975404049994095];
opts.Upper = [1 1 1 1];

% Fit model to data.
[fitresult, gof] = fit( xData, yData, ft, opts );

% Plot fit with data.
figure( 'Name', 'Kim''s Model' );
h = plot( fitresult, xData, yData );
legend( h, 'V vs. I', 'Kim''s Model', 'Location', 'NorthEast' );
% Label axes
xlabel( 'I' );
ylabel( 'V' );
grid on
```

A.2: MATLAB code for Yutaro's model - Polarization curve fitting

```
function [fitresult, gof] = createFit(I, V)
%CREATEFIT(I,V)
%  Create a fit.
%  Data for 'Yutaro's Model' fit:
%      X Input : I
%      Y Output: V
%  Output:
%      fitresult : a fit object representing the fit.
%% Fit: ' Yutaro's Model'.
[xData, yData] = prepareCurveData( I, V );
% Set up fittype and options.
ft = fittype( ' 1.299  - (298.15*(b + a*log(x)))-(b * (237.2 /8.314))*x - R*x
- m*exp(n*i) ', 'independent', 'x', 'dependent', 'y' );
opts = fitoptions( 'Method', 'NonlinearLeastSquares' );
opts.Algorithm = 'Levenberg-Marquardt';opts.Display = 'Off';
opts.Lower = [0 0 0 0];
opts.Robust = 'Bisquare';
opts.StartPoint = [0.278498218867048 0.309425683031331 0.63235924622541
0.0975404049994095];
opts.Upper = [1 1 1 1];

% Fit model to data.
[fitresult, gof] = fit( xData, yData, ft, opts );

% Plot fit with data.
figure( 'Name', ' Yutaro's Model' );
h = plot( fitresult, xData, yData );
legend( h, 'V vs. I', ' Yutaro's Model', 'Location', 'NorthEast' );
% Label axes
xlabel( 'I' );
ylabel( 'V' );
grid on
```

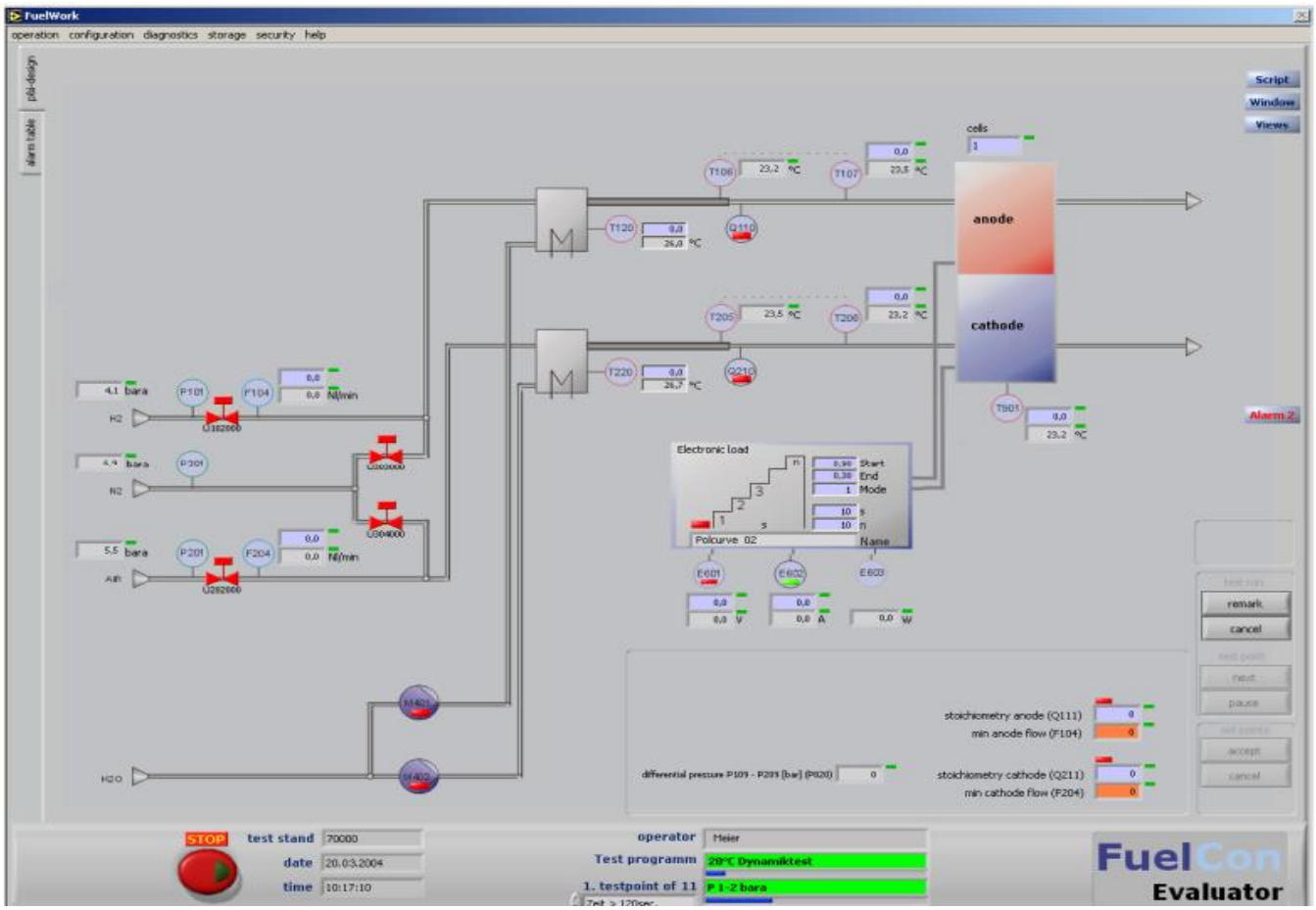

Figure A.1: Depiction of the FuelCon Elevator–C 70342 test station Main View.

Table A.1: Overview of the FuelCon Elevator-C screen function.

Detail	Description
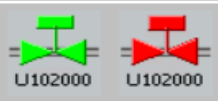	**Valve** Valves to close off mediums. They can be activated by clicking with the mouse. green = „open", red = "closed"
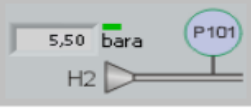	**Panel pressure** Pressure values at the Connector Panel on the test stand. Indicated only.
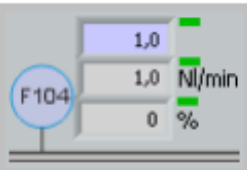	**Flow** Indication of the actual flow rates of gases as well as preset tolerances. The tolerances can be set either as absolute values or – depending on the extent of functions available – as relative settings relating to the flow of hydrogen.
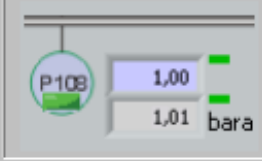	**Pressure of medium** Indication of the current value as well as setting of the set points.
	**Temperature** Temperature of the supplied mediums. Indication of actual value as well a possibility to enter a set point.
	**Heated hoses / tubes** The temperature of the jacket of the heated tubes. Indicated only.
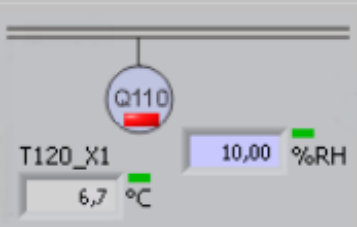	**Relative humidity** The relative humidity content of supplied gases prior to entering the fuel cell. Entry of set point only. Independent of the set point adding humidification can be switched on or off in the circle named Q110/Q210 above the beam. This must be done manually While choosing the humidification level please attend to a possible temperature difference between supplied gas and testing hardware.

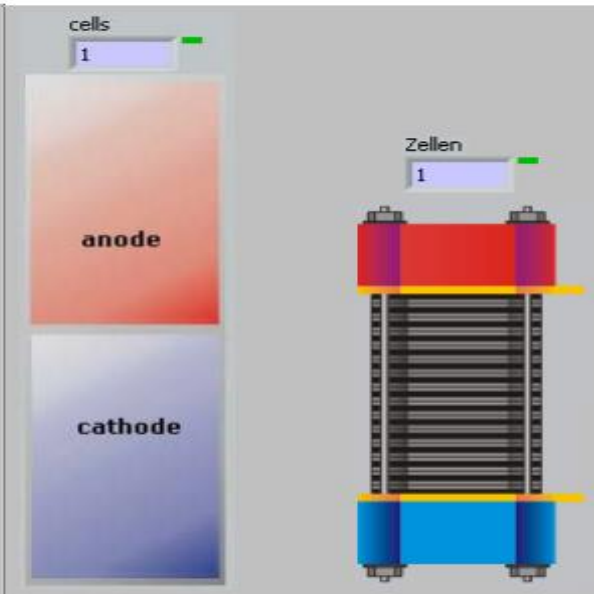

Test item

Place to enter the number of individual cells of the test item.

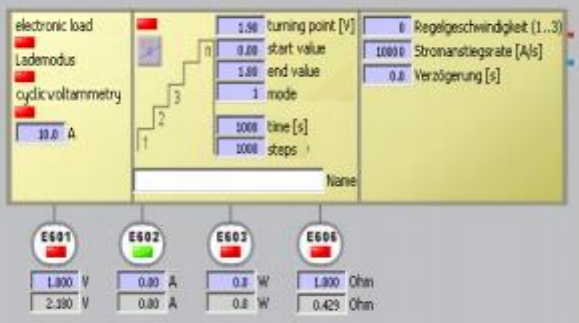

Electronic load

Indication of voltage, current and performance values as well as set points for voltage and current.
The step function can be activated on the button at the beginning of the steps. It is possible to specify the total time period of the ramp in seconds, the number of steps, the mode of the load as well as the start and end value and the turning point:
Mode 1 = voltage-guided
Mode 2 = current-guided
Mode 3 = power-guided.
In the field "Name" it's possible to name the ramp. For more informations about the ramp function see chapter *8.7.3. Polarization curve as automatic ramp function*.
: Calls „SaveChartPoint" (see *3.1.2. Additional functions*) and records a pol-curve point.
The load can be turned on and off with the button under the title "Electronic Load".

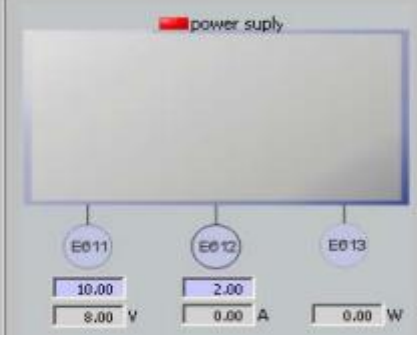

Power supply

Indication of voltage, current and performance values as well as set points for voltage and current.

The load can be turned on and off over the bar to the left next to the title "Power-supply".

Appendix B: True-Data EIS

Figure B.1: TrueData-EIS hardware

The electrical connection of the TreuData-EIS, the test item (fuel cell) and the electronic load is displayed below. (The second sense line of the TreuData-EIS shos the impedance meansurement of a single cell in a stack.

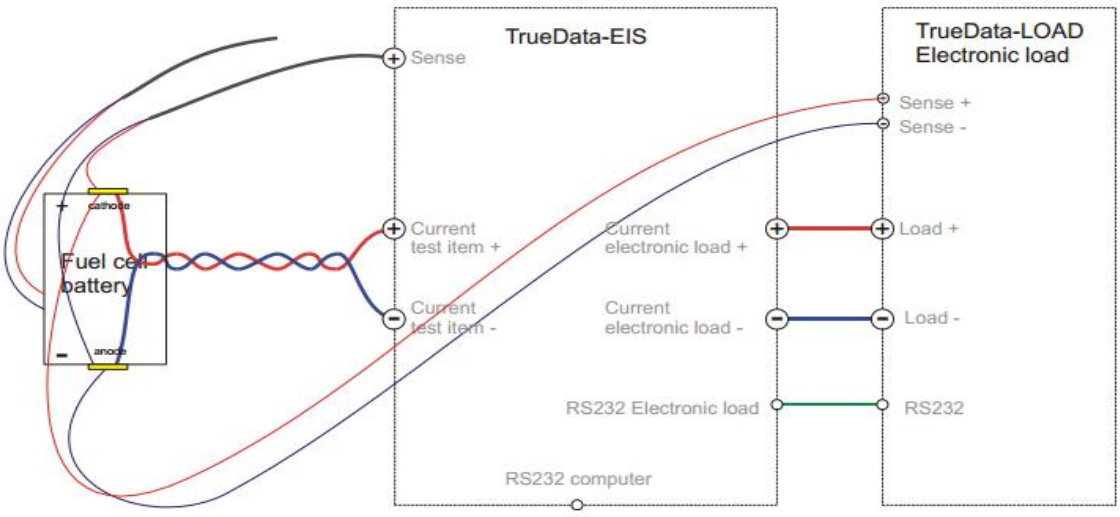

Figure B.2 Electrical connection of the TrueData-EIS.

Table B.1: TrueData-EIS Technical Parameter

	TrueData-EIS
Impedance range	0.1 mΩ to 15 Ω
Waveform	Sinus
Frequency range	200 µHz to 10 kHz, 200 µHz to 50 kHz, 200 µHz to 100 kHz
Frequency accuracy	± 1 %
AC current amplitude	up to 2500 mA
AC voltage accuracy	± 1 %
DC voltage maximum	10 V, 35 V, 100V
DC current maximum	100 Amp, 250 Amp, 500 Amp, 1000 Amp
Load mode	Current (Galvanostate), Voltage (Potentiostate), Power, Resistance
Phase angle accuracy	± 1 °
Impedance accuracy	± 1 %
Online-Nyquist plot	Option
Frequency Sweep with FuelWork	✓
Frequency Sweep	✓
DC drift compensation	✓
RS232-Interface	✓
Ethernet-Interface (Telnet)	Option
Color TFT-Display	✓
Power supply	110 / 230 VAC, 100 W
Housing	19" housing, 3 HE
Dimensions (W x H x D)	485 mm x 135 mm x 440 mm (19 " x 5.3 " x 17.3 ")
Weight	13.2 kg

Appendix C: SCANNING ELECTRON MICROSCOPE (SEM) VIEW

C.1: Scanning Electron Microscope (SEM) View of the Aquivion® & Nafion® ionomer MEA consisting of the high shear dispersion (HSD) process

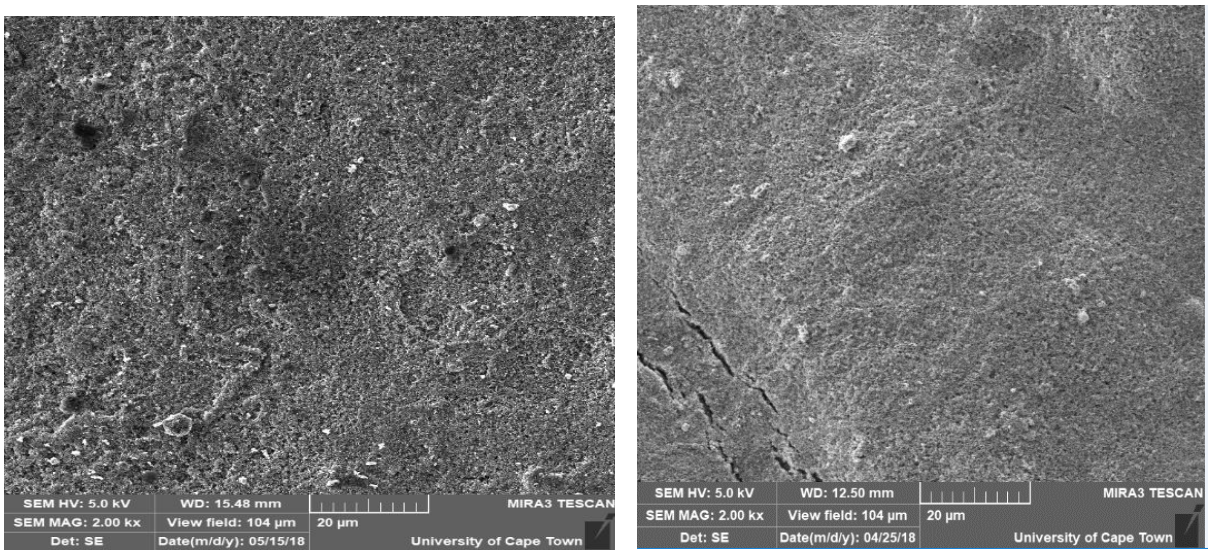

Figure C.1: Surface of the Aquivion® ionomer (a) before and (b) after durability test.

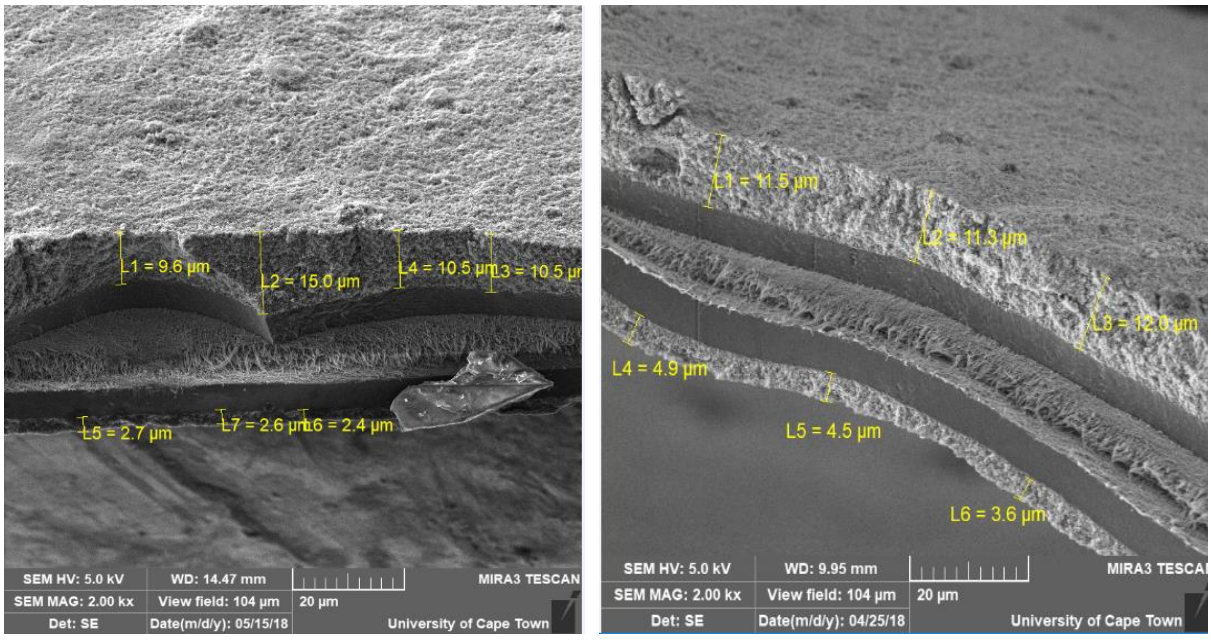

Figure C.2: Dimensions of the Aquivion® ionomer (a) before and (b) after durability test.

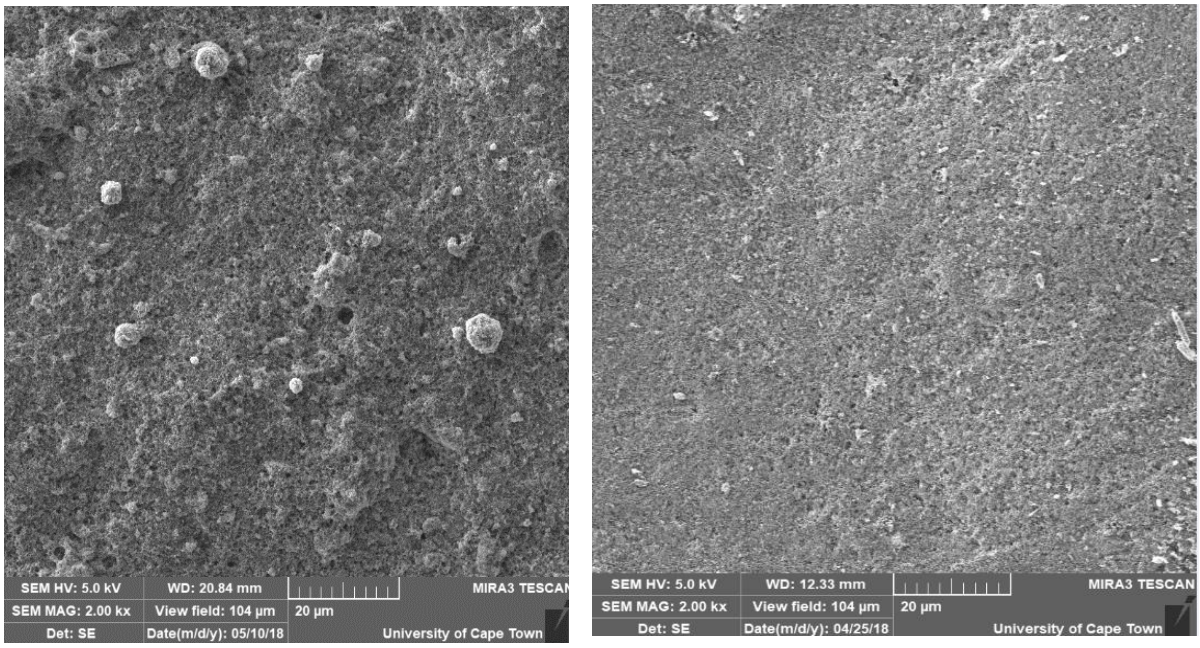

Figure C.3: Surface of the Nafion® ionomer (a) before and (b) after durability test.

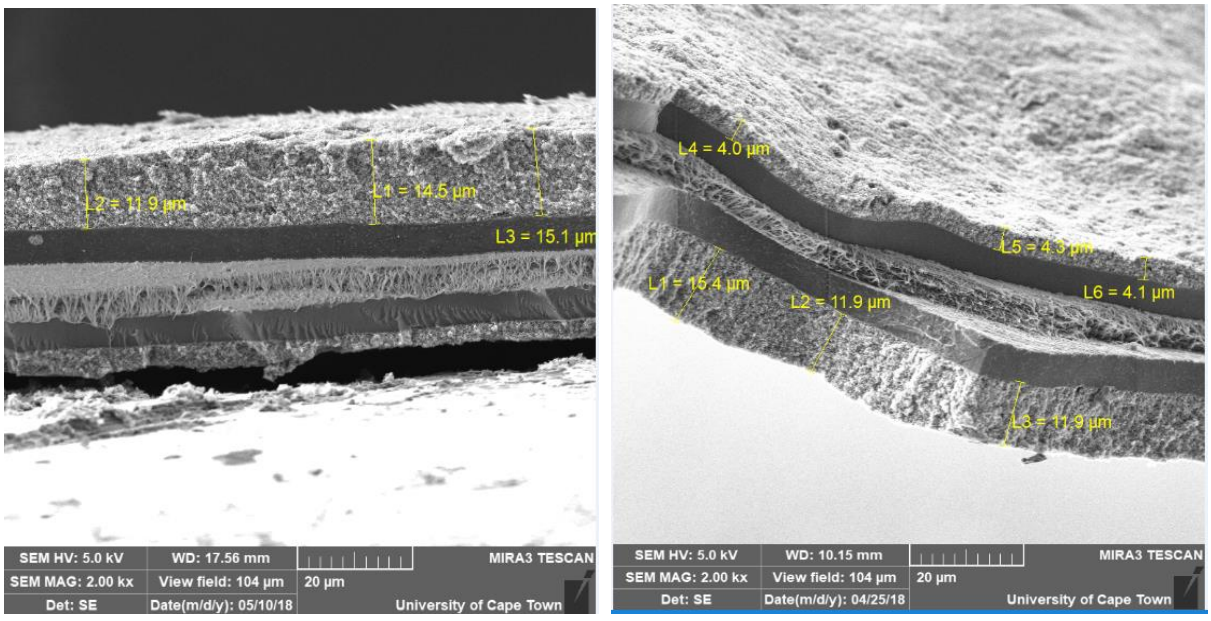

Figure C.4: Dimensions of the Nafion® ionomer (a) before and (b) after durability test.

C.2: Scanning Electron Microscope (SEM) View of the Aquivion® & Nafion® ionomer MEA without the high shear dispersion (HSD) process

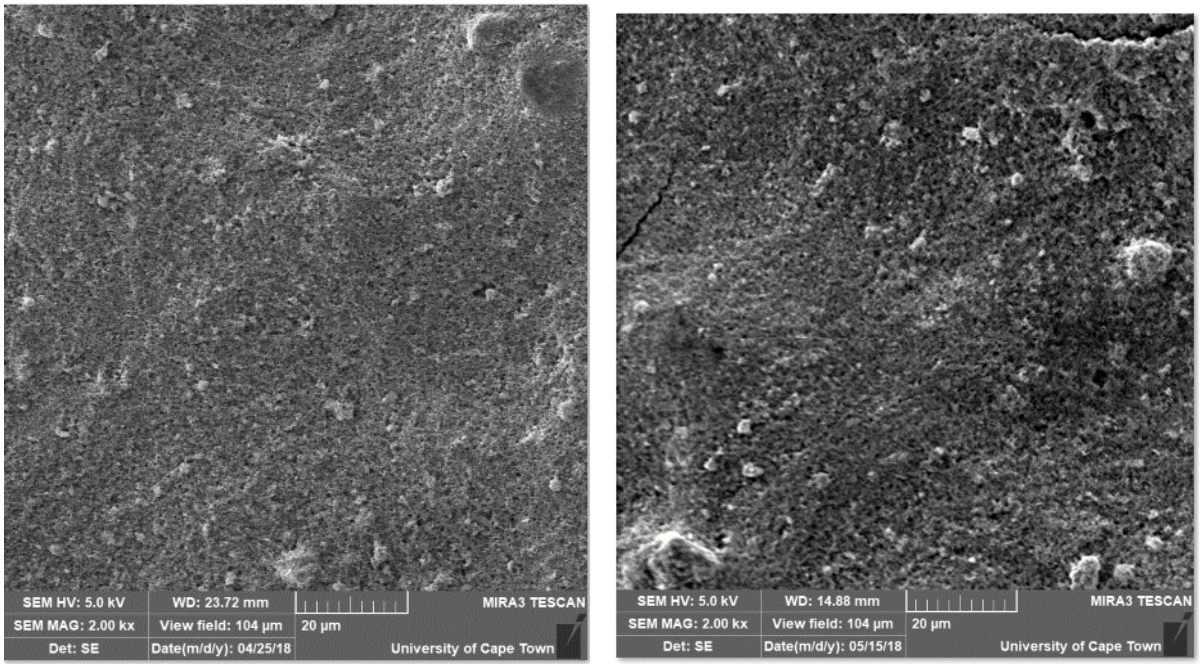

Figure C.5: Surface of the Aquivion® ionomer (a) before and (b) after durability test.

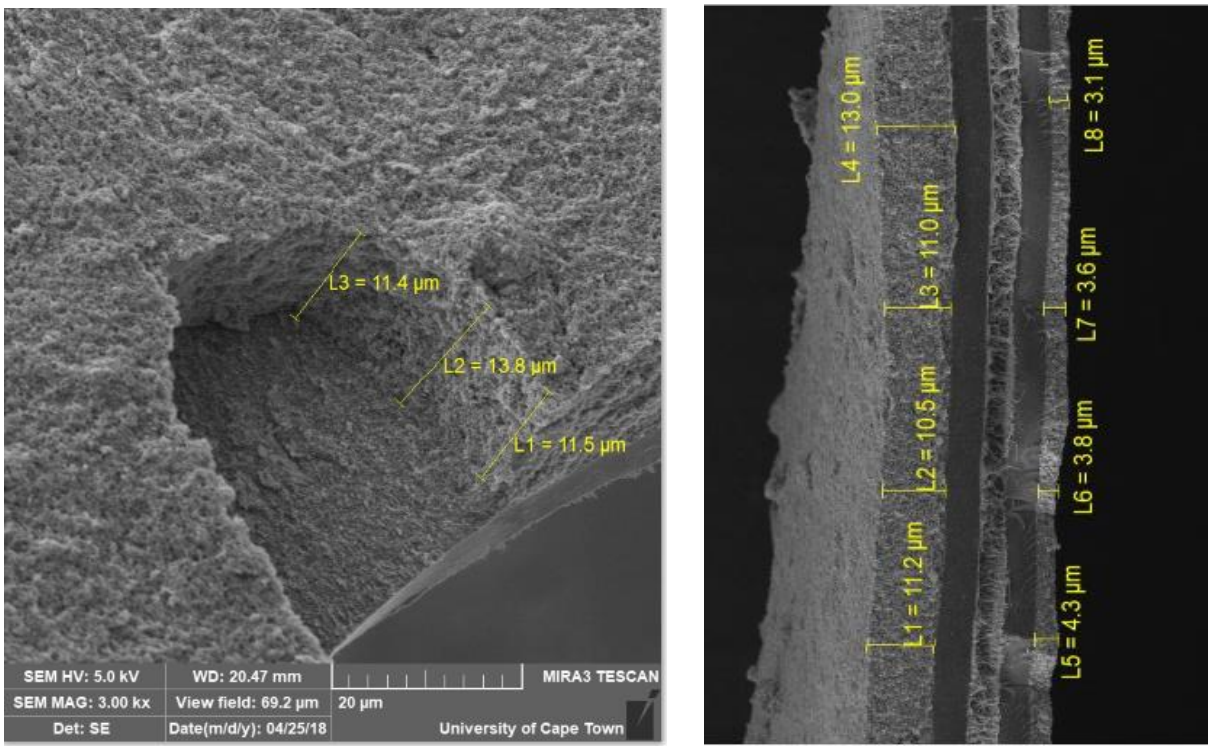

Figure C.6: Dimensions of the Aquivion® ionomer (a) before and (b) after durability test.

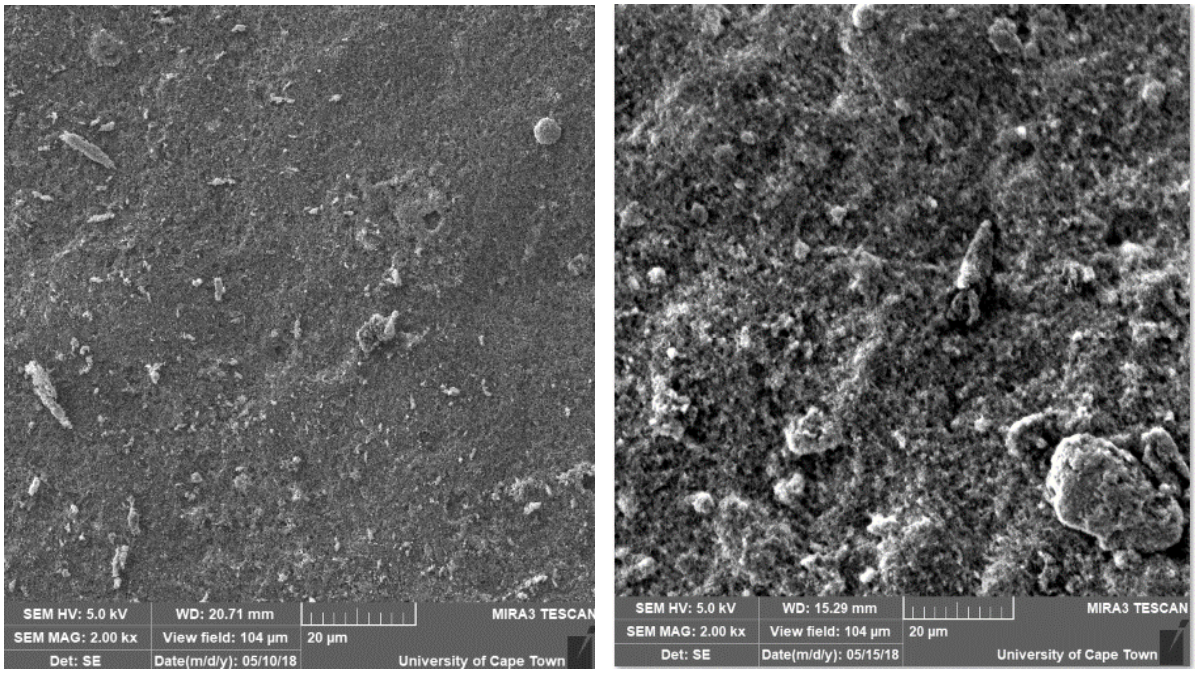

Figure C.7: Surface of the Nafion® ionomer (a) before and (b) after durability test.

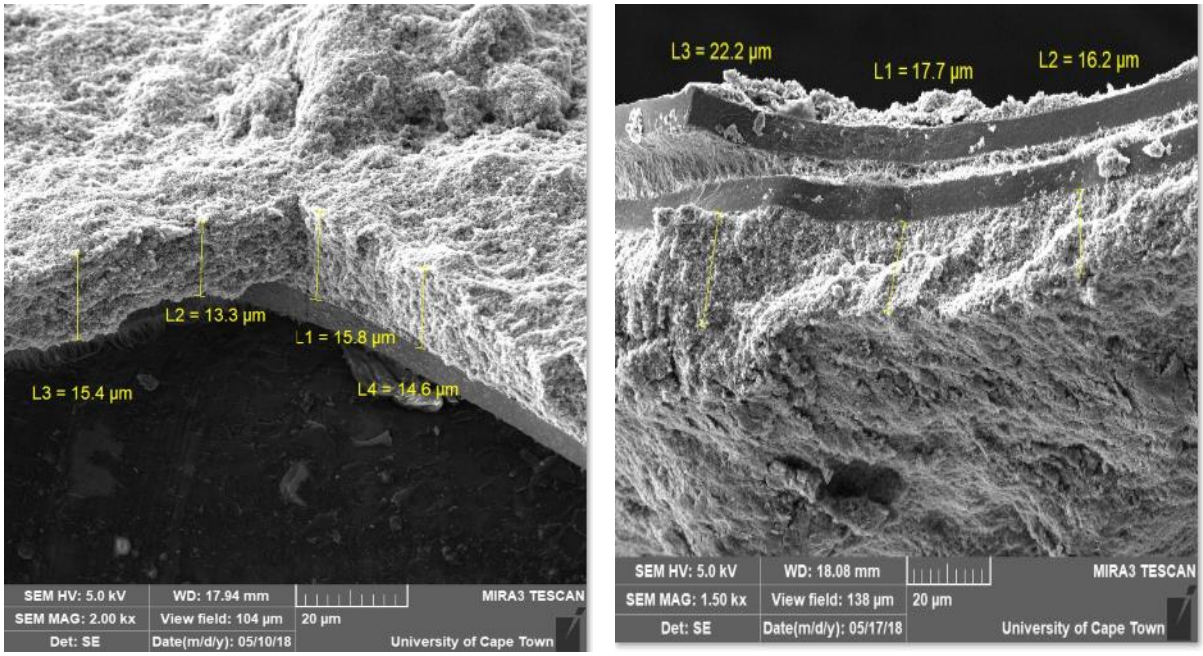

Figure C.8: Dimensions of the Nafion® ionomer (a) before and (b) after durability test.